

GROUND PROVING SEISMIC REFRACTION TOMOGRAPHY (SRT) IN LATERALLY
VARIABLE KARSTIC LIMESTONE TERRAIN

By

TIMOTHY PATRICK QUIGLEY

A THESIS PRESENTED TO THE GRADUATE SCHOOL
OF THE UNIVERSITY OF FLORIDA IN PARTIAL FULFILLMENT
OF THE REQUIREMENTS FOR THE DEGREE OF
MASTER OF ENGINEERING

UNIVERSITY OF FLORIDA

2006

Copyright 2006

by

Timothy Patrick Quigley

To my grandfather, John Link, whose lifetime of hard work has made mine immeasurably easier

ACKNOWLEDGMENTS

First of all, I thank Dr. Dennis Hiltunen for serving as my advisor. His continued support, encouragement, and availability during my research and studies were what made this possible. I thank the other members of my thesis committee, Dr. Frank Townsend for his guidance, advice, and real world perspective on academic problems during my graduate studies, as well as Dr. Nick Hudyma for his guidance and input during this research. Acknowledgements must also be given to the remaining University of Florida faculty, and to current and former graduate students from whom I learned an immense amount from both academically and personally.

Any acknowledgements made would be incomplete without thanking those who helped get me to this point. I thank my mother who was seemingly able to do it all, without ever tiring or complaining, and my father for his tireless work ethic. I thank the remaining members of my family for their support, as well as all of my friends who treated me like family. Lastly, special gratitude goes out to my girlfriend Rosanne Lee, who has been supportive of all my decisions and the results of those decisions for the past three years.

TABLE OF CONTENTS

	<u>page</u>
ACKNOWLEDGMENTS	4
LIST OF TABLES	8
LIST OF FIGURES	9
ABSTRACT	12
CHAPTER	
1 INTRODUCTION	14
1.1 Problem Statement	14
1.2 Objective	15
1.3 Scope	15
2 BACKGROUND	17
2.1 Location	17
2.2 Geological Setting	17
2.2.1 Characteristics of Karstic Limestone	18
2.3 Seismic Refraction Method	19
2.3.1 Previous Studies in Karst using Seismic Refraction Tomography (SRT) Programs	21
2.3.2 Overview of Seismic Refraction Tomography Programs	23
2.3.2.1 Rayfract (version 2.64)	23
2.3.2.2 SeisImager (version 2.67)	25
2.3.2.3 SeisOpt Pro (version 3.0)	25
3 SEISMIC REFRACTION TOMOGRAPHY (SRT) PROGRAMS ON FIELD DATA	28
3.1 Seismic Refraction Testing Site Layout	28
3.1.1 Field Testing Procedure	28
3.1.2 Testing Limitations and Potential Sources of Error	29
3.2 Analyzing and Processing Field Data	30
3.2.1 Selection of First Arrivals from Time Records	30
3.2.2 Travel Time Curve Generation	30
3.3 Seismic Refraction Tomography Program Processing Flow	31
3.3.1 Rayfract (Version 2.64)	31

3.3.2 SeisImager (version 2.67)	34
3.3.3 SeisOpt Pro (version 3.0).....	37
3.4 Comparison of the (SRT) Programs	40
3.4.1 Creation of Tomograms using Surfer (version 8.04).....	40
3.4.2 General Visual Observations of Tomograms.....	41
3.4.4 Specific Visual Observations of Tomograms	42
3.4.5 Quantitative Comparison of Calculated Travel Times	43
3.4.5 Processing Time.....	44
3.5 General Assessment of Performance of the SRT Programs Evaluated	45
4 COMPARISON OF SRT PROGRAM RESULTS AND INTRUSIVE TESTING DATA ...	53
4.1 Selection of Intrusive Test Locations	53
4.2 Types of Intrusive Testing Performed	53
4.2.1 Cone Penetration Test (CPT) Procedure.....	54
4.2.2 Standard Penetration Test (SPT) Procedure	54
4.2.3 Rock Coring Procedure.....	55
4.3 General Results of Intrusive Testing.....	55
4.3.1 A Line Intrusive Testing Results	56
4.3.2 F Line Intrusive Testing Results	56
4.3.3 U Line Intrusive Testing Results	57
4.3.4 Z Line Intrusive Testing Results.....	57
4.4 Comparison of Intrusive Testing to the SRT Tomograms.....	58
4.4.1 Comparison of A Line Tomograms to Intrusive Test Results	59
4.4.1.1 Sinkhole Observations Along the A Line	63
4.4.2 Comparison of F Line Tomograms to Intrusive Test Results.....	63
4.4.3 Comparison of U Line Tomograms to Intrusive Test Results	65
4.4.4 Comparison of Z Line Tomograms to Intrusive Test Results.....	66
4.5 Geological Explanations for Variability in P-wave Velocity	68
4.6 CPT Tip Penetration and P-Wave Velocity	68
4.7 Comparison of the SRT Raytracing Models to Intrusive Test Results.....	69
4.7.1 A line 0-36.6 m SRT Raytracing Models to Intrusive Test Results	69
4.7.2 Comparison of A Line 36.6-73.2 m Raytracing Models to Intrusive Test Results	70
4.7.3 General Observations for each of the Three SRT Programs Ray Path Diagram Comparisons to the Intrusive Test Data.....	71
5 CLOSURE	82
5.1 Summary of Findings.....	82
5.1.1 Summary of Findings from the SRT Programs	82
5.1.2 Summary of Findings from the Comparison of the SRT Programs to the Intrusive Testing Data.....	83
5.2 Conclusions.....	84
5.3 Research Recommendations	84

APPENDIX

A P-WAVE VELOCITY TOMOGRAMS86

B INTRUSIVE TESTING FIELD DATA96

C COMPARISON OF P-WAVE VELOCITY TOMOGRAMS TO TOP OF BEDROCK
DEPTHS ENCOUNTERED THROUGH INTRUSIVE TESTING128

D CLOSE CONTOUR P-WAVE TOMOGRAM INTRUSIVE DATA COMPARISON.....132

E RAYTRACING DIAGRAMS FOR TOMOGRAMS136

LIST OF REFERENCES140

BIOGRAPHICAL SKETCH143

LIST OF TABLES

<u>Table</u>	<u>page</u>
3-1 Comparison of Calculated Travel Time Differences Between Programs for A Line Station 0-36.6 m.....	45
3-2 Comparison of Calculated Travel Time Differences Between Programs for A Line Station 36.6-73.2 m.....	45
4-1 P-wave velocities from tomograms at top of bedrock depths determined by intrusive test data for the A line	73
4-2 Comparison of depth to bedrock determined from intrusive testing and visually inferred from close contour interval, 10 m/s, tomograms for the A line.....	73
4-3 P-wave velocities from tomograms at top of bedrock depths determined by intrusive test data for the F line.	73
4-4 P-wave velocities from tomograms at top of bedrock depths determined by intrusive test data for the U line.	73
4-5 P-wave velocities from tomograms at top of bedrock depths determined by intrusive test data for the Z line.....	74

LIST OF FIGURES

<u>Figure</u>	<u>page</u>
2-1 Location of geophysical/ground proving test site and zones within the site.	26
2-2 Dissolution of carbonate rock	27
2-3 Karstic limestone features	27
3-1 Example of PickWin95 time record along survey line A from stations 0-36.6 m for source location 0 m.	46
3-2 PlotRefa travel time curves, A line, station 0-36.6 m.....	47
3-3 PlotRefa travel time curves, A line, station 36.6-73.2 m.....	47
3-4 PlotRefa outside source location travel time curves, A line, station 0-36.6 m.....	48
3-5 P-wave Tomograms, A line, Station 0 – 36.6 m.	49
3-6 P-wave Tomograms, A line, Station 36.6-73.2 m.	50
3-7 Measured vs. predicted travel time curves, A Line, station 0 – 36.6 m.	51
3-8 Measured vs. predicted travel time curves, A Line, station 36.6-73.2 m.	52
4-1 Estimated top of bedrock from intrusive testing overlain onto tomograms produced for A line station 0-36.6 m.	75
4-2 Estimated top of bedrock from intrusive testing overlain onto tomograms produced for A line station 36-73.2 m.	76
4-3 Estimated top of bedrock from intrusive testing overlain onto 10 m/s contour interval tomograms produced for the A line 0-36.6 m.	77
4-4 Estimated top of bedrock from intrusive testing overlain onto 50 m/s contour interval tomograms produced for the A line 0-36.6 m.	78
4-5 Estimated top of bedrock from intrusive testing overlain onto 10 m/s contour interval tomograms produced for the A line 36.6-73.2 m.	79
4-6 Raytracing diagrams from each of the three SRT programs for A line 0-36.6 m.	80
4-7 Raytracing diagrams from each of the three SRT programs for A line 36.6-73.2 m.	81
A-1 P-wave tomograms, F line, station 0 – 36.6 m.	86

A-2	P-wave tomograms, F line, station 36.6 – 73.2 m.	87
A-3	P-wave tomograms, K line, station 0-36.6 m.	88
A-4	P-wave tomograms, K line, station 36.6-73.2 m.	89
A-5	P-wave tomograms, P line, station 0 – 36.6 m.	90
A-6	P-wave tomograms, P line, station 36.6-73.2 m.	91
A-7	P-wave tomograms, U line, station 0 – 36.6 m.	92
A-8	P-wave tomograms, U line, station 36.6-73.2 m.	93
A-9	P-wave tomograms, Z line, station 0 – 38.4 m.	94
A-10	P-wave tomograms, Z line, station 36.6-73.2 m.	86
B-1	Intrusive testing data from A Line, station 19.8 m	96
B-2	Intrusive testing data from A Line, station 36.6 m	99
B-3	Intrusive testing data from A Line, station 39.6 m	102
B-4	Intrusive testing data from A Line, station 44.2 m	103
B-5	Intrusive testing data from A Line, station 66.5 m	104
B-6	Intrusive testing data from A Line, station 66.5 m	105
B-7	Intrusive Testing Data from F Line, Station 3.0 m.....	107
B-8	Intrusive testing data from F Line, station 13.7 m.....	110
B-9	Intrusive testing data from U Line, station 8.5 m	113
B-10	Intrusive testing data from U Line, station 24.4 m	114
B-11	Intrusive testing data from U Line, station 36.6	117
B-12	Intrusive testing data from U Line, station 73.2 m	118
B-13	Intrusive testing data from Z Line, station 21.9 m.....	119
B-14	Intrusive testing data from Z Line, station 35.0 m.....	123
B-15	Intrusive testing data from Z Line, station 64.0 m.....	126
C-1	Top of bedrock location from intrusive testing for F Line, station 0-36.6 m.	128

C-2	Top of bedrock location from intrusive testing for U Line, station 0-36.6 m.	129
C-3	Top of bedrock location from intrusive testing for Z Line, station 0-38.4 m.	130
C-4	Top of bedrock location from intrusive testing for Z Line, station 36.6-73.2 m.	131
D-1	Estimated top of bedrock from intrusive testing overlain onto 10 m/s contour interval tomograms produced for the F line 36.6-73.2 m.	132
D-2	Estimated top of bedrock from intrusive testing overlain onto 10 m/s contour interval tomograms produced for the U line 0-36.6 m.	133
D-3	Estimated top of bedrock from intrusive testing overlain onto 10 m/s contour interval tomograms produced for the Z line 0-38.4 m.	134
D-4	Estimated top of bedrock from intrusive testing overlain onto 10 m/s contour interval tomograms produced for the Z line 36.6-73.2 m.	135
E-1	Raytracing diagram for F Line, station 0-36.6 m.	136
E-2	Raytracing diagram for U Line, station 0-36.6 m.	137
E-3	Raytracing diagram for Z Line, station 0-38.4 m.	138
E-4	Raytracing diagram for Z Line, station 36.6-73.2 m.	139

Abstract of Thesis Presented to the Graduate School
of the University of Florida in Partial Fulfillment of the
Requirements for the Degree of Master of Engineering

GROUND PROVING SEISMIC REFRACTION TOMOGRAPHY (SRT) IN LATERALLY
VARIABLE KARSTIC LIMESTONE TERRAIN

By

Timothy Patrick Quigley

May 2007

Chair: Dennis Hiltunen

Major Department: Civil and Coastal Engineering

The ability to characterize the subsurface of a site containing a laterally variable top of bedrock surface that is also prone to sinkhole development is extremely limited through the sole use of traditional, physically intrusive geotechnical exploration techniques, such as soil borings and rock coring. These types of tests provide information regarding the subsurface only at the specific location performed and cannot be used reliably to interpret the surrounding conditions at sites with significant lateral variability. Seismic refraction testing serves as a well established geophysical tool that can help provide more complete detail of the subsurface over a much larger area.

The Florida Department of Transportation (FDOT) constructs retention basins in order to provide effective return of surface water runoff to the subsurface aquifer. This runoff water frequently contains contaminants which are naturally filtered by the overburden soil above the aquifer. However, many of these retention basins are located in areas with karstic limestone as the bedrock at shallow depths. The increased flow of water into these basins may lead to the increased development of sinkholes, which provide an open conduit for the contaminated runoff

to return directly into the aquifer. As a result the FDOT is interested in methods of early detection.

The capabilities of three commercially available seismic refraction tomography (SRT) programs, specifically Rayfract, SeisImager, and SeisOpt Pro, to image the subsurface were evaluated. The resulting tomograms were then compared to traditional, intrusive geotechnical test methods such as: CPT soundings, SPT soundings, and rock coring data. The results of these comparisons suggest that SRT is capable of accurately imaging the laterally-variable top of bedrock typical of karst terrain.

CHAPTER 1 INTRODUCTION

1.1 Problem Statement

The ability to characterize the subsurface of a site containing a laterally variable top of bedrock surface that is also prone to sinkhole development is extremely limited through the sole use of traditional physically intrusive geotechnical exploration techniques, such as soil borings and rock coring. These types of tests provide information regarding the subsurface only at the specific location performed and cannot be used reliably to interpret the surrounding conditions at sites with lateral variability. Seismic refraction testing serves as a well-established geophysical tool that can help provide more complete detail of the subsurface over a much larger area. Commercially available seismic refraction tomography (SRT) software has only had limited use on sites with these types of complex conditions. The purpose of my study was to provide ground-truthing for three different commercially available SRT programs on a site whose top of bedrock elevation varies laterally and was prone to sinkhole formation.

The seismic refraction testing presented herein was performed on a storm water retention basin site with variable top of bedrock elevation in the subsurface and with known previous sinkhole activity with the hope of being able to detect subsurface features associated with sinkhole formation. Testing on these types of sites is of interest because of the potential environmental concerns associated with sinkhole formation, which provide an open conduit for contaminated storm water runoff to enter the subsurface aquifer rather than flowing slowly down through the overburden soil, which effectively filters pollutants out of the water. The ability to detect subsurface features associated with early sinkhole formation can be used to remediate a site, and, if desired, make the site suitable for future construction. The ability to map the

changing top of bedrock surface is also of interest for foundation and numerous other geotechnical engineering designs.

1.2 Objective

This study will provide additional confidence in the ability of SRT programs to provide accurate subsurface imaging on a site with karstic terrain containing variable top of bedrock elevations and sinkhole potential, as very little field study has been done on these types of sites.

Three commercially available SRT programs: Rayfract, SeisImager, and SeisOpt Pro were chosen to develop tomograms of the site's subsurface. To accomplish this objective:

- 1 P-wave velocity tomograms were produced along each line for each of the three SRT programs and the features generated by each program were then compared against one another.
- 2 Next, these final P-wave tomograms were compared against results obtained from physically intrusive traditional geotechnical techniques (Cone Penetration Tests (CPT), Standard Penetration Tests (SPT), and rock coring).
- 3 Finally, the tomograms produced by the SRT programs were evaluated for accuracy based on visual observations between the tomograms and intrusive testing results, as well as quantitative calculations between the measured and calculated travel times.

These comparisons will demonstrate the ability of SRT programs to map laterally variable top of bedrock surfaces as well as features indicative of sinkhole formation.

1.3 Scope

The data presented in this paper comes from seismic refraction testing performed on a single Florida Department of Transportation (FDOT) storm water runoff retention basin, located in Alachua County off of State Road 26 in Newberry, Florida. The physical layout of the seismic refraction test performed consisted of six lines, each of which was 73.2 meters in length, and spaced 3 m apart from one another. This study was conducted in order to see how well three commercially available SRT programs were able to model the subsurface features of this particular site.

The testing performed was intended to serve as the first step in building a database from multiple sites to demonstrate the viability of using SRT programs on sites with laterally variable top of bedrock in sinkhole prone karstic terrain. It is not intended to serve as the final answer regarding the abilities or inabilities of them to do so. The conclusions drawn from the performance of the three SRT programs evaluated for this site are only intended to present how each of the programs performed when used on this particular site using this particular test procedure and layout.

CHAPTER 2 BACKGROUND

2.1 Location

The University of Florida (UF) and the University of North Florida (UNF) have developed a Florida Department of Transportation (FDOT) dry retention pond into a karstic limestone geophysical ground proving test site. The test site is located just outside of Newberry, Florida on State Road 26 in Alachua County, approximately 29 kilometers to the west of Gainesville. The location of the test site within the state and Alachua County is shown in Figure 2.1(a). The test site is approximately 1.6 hectares in size and contains a number of survey lines and 5 PVC-cased boreholes extending to approximately 15 meters below the surface elevation so that future geophysical testing may be conducted.

What makes this test site ideal for study is that the northern portion of the retention pond commonly experiences sinkhole activity due to the increased accumulation of surface water runoff, whereas the southern portion rarely experiences sinkhole activity. Numerous sinkholes have formed in the northern portion of the site, requiring repair. However, the southern portion has been relatively free of sinkholes and is an ideal location for characterizing a karstic limestone site, as the subsurface has yet to be modified from the repairing process. This portion of the site is roughly 113 m x 78 m in size. The two zones within the test site are shown in Figure 2.1(b).

2.2 Geological Setting

The area of study is located just outside of Newberry, Florida which is located in the western portion of Alachua County, more specifically identified geologically as the Western Valley (Newberry Limestone Plain). The Western Valley is generally flat in nature with sinkholes, quarries, and low hills composed of erosional remnants of the Northern Highlands providing the greatest topographic relief in the area. It is a subdued limestone plain composed of

the upper unit of the Ocala Group, the Crystal River Formation which is Upper Eocene in age. It consists of nearly pure limestone and dolostones (Scott, 2001). Numerous terrestrial vertebrate fossil deposits preserved in sinkholes formed in the Crystal River Formation indicate that it has undergone karstification periodically since the Late Oligocene (Williams et al. [1977]).

Karstification is a geological term that refers to the formation of the features of karst topography by the chemical and sometimes mechanical, action of the water in a region of limestone. As a result of this karstification, along with erosion, the top of the limestone surface is extremely variable.

The Crystal River Formation is overlain by a thin or variable soil cover and occasional residual hills composed of sediments of the Hawthorne Formation, which is Miocene to early Plio-Pliocene in age. This thin layer of sand and soil cover commonly includes residual boulders of silicified limestone ranging in size from 0.3 to 4.6 m in diameter as well as interbedded and intermixed carbonate and siliclastics containing varying percentages of phosphate grains. Residual sediments occur most frequently as sinkhole fillings and tend to mask the great irregularities of the limestone surface (Williams et al. [1977] and Campbell and Scott [1991]).

2.2.1 Characteristics of Karstic Limestone

Karstic terrain forms primarily from the solution of soluble bedrock, such as limestone, by natural waters. In general, the solution process begins as rainwater absorbs carbon dioxide from the atmosphere and as it percolates downward through the soil, which is high in CO₂, generated from the decay of organic matter. This absorbed carbon dioxide makes the recharge water weakly acidic (carbonic acid), and this acidic water then dissolves the limestone (CaCO₃).

When the slightly acidic water reaches the limestone it continues moving downward through any interconnected pores or fractures, dissolving and enlarging any pores or cracks

through which it flows, as shown in Figure 2.2. The most favored vertical path dissolves more rapidly than the surrounding areas, because it is now larger and can transmit more water in ever greater quantities. This "self accelerating" process results in few greatly enlarged tubes or pipes permeating down through the limestone, with little dissolved rock in between (Tihansky [1999]).

Over time, chemical weathering within the limestone enlarge the vertical discontinuities forming slots. These slots may remain narrow or they may enlarge to form “valleys” or “bowls” depending on whether or not additional chemical weathering occurs. As the limestone weathers from its massive structure it transitions through the block structures to pinnacles (Hudyma et al. [2007]). This transition is shown in Figure 2.3 from left to right. The surface of the soluble rock may be erratic indicating that chemical weathering/dissolution is occurring or had occurred before the overburden soil was deposited, in which case it is termed as a karstic limestone. Features of karstic terrain may include horizontal bedding planes delineating the different times of deposition as well as near vertical fissures/fractures/joints, depending on their geological formation.

2.3 Seismic Refraction Method

The seismic refraction test method consists of measuring the travel times, at known points along the surface, of seismic compression (P) waves generated by an energy source. The energy source is usually generated by a small explosive charge or accelerated weight drop, such as a sledgehammer (Redpath [1973]). Energy that radiates out from the source, or shot point, either travels directly through the upper layer, known as a direct arrival, or travels down to and laterally along a lower high velocity layer, known as a refracted arrival. This energy is detected on the surface using receivers (geophones) arranged in a linear array and travel times are recorded via seismograph (Geo-Services International Limited, [1999]). The recorded travel time information is then used to generate a velocity profile of the subsurface along the length of

the refraction profile relying upon the assumption that the velocity of the subsurface material increases with depth.

Conventional processing of refraction data falls short of showing the true strength of seismic refraction testing because it uses oversimplified geometry and media (Zhang and Toksoz [1998]). Whereas conventional methods divide the model into continuous layers of constant velocity, SRT divides the model into a large number of smaller constant velocity grid cells or nodes. The model is then inverted by performing ray tracing, or by other techniques, through the initial model, with the grid cells adjusted after each iteration in attempt to match the calculated travel times with the measured as closely as possible. This is repeated until the number of pre-defined iterations within the program has been completed, with the resulting subsurface velocity model, known as a tomogram, being produced upon completion.

It is because of these techniques that seismic refraction tomography is able to resolve velocity gradients and lateral velocity changes within the subsurface with greater ability than conventional methods. As such, SRT may be applied in settings where conventional refraction methods fail, such as areas of compaction, karst, and zone faults (Zhang and Toksoz, [1998]). These enhanced capabilities seem to make it ideal for this study because of the karstic terrain and the lateral variability of the overburden material present.

However, some drawbacks do exist when choosing to use SRT techniques over conventional methods. SRT requires that more shots and receivers be used than conventional techniques. This allows for denser data collection, which, when coupled with increased available computing power, allows for a much more detailed interpretation of the subsurface.

This increase in field data collected significantly increases the amount of time necessary to perform the field testing. The time required to prepare and process this data, i.e., make first

arrival picks, before it is ready to be imported into the SRT programs for inversion is also significantly increased. An experienced operator using a similar test procedure as this study should be able to perform field testing on one 36.6 m long survey line, process the field data, make first arrival picks, and generate a reasonable tomogram using one of the SRT programs in one full working day.

2.3.1 Previous Studies in Karst using Seismic Refraction Tomography (SRT) Programs

The use of SRT programs in karstic field applications is relatively new and as such few published accounts document their performance. However, several synthetic model studies coupled with field investigations have been undertaken that demonstrate the capabilities of SRT programs. Carpenter et al. (2003) used SRT programs, among them SeisOpt Pro, on sites known to be karstic in Illinois and Kentucky, to determine their accuracy by comparing with known subsurface geology from outcrops, borehole logs, other geophysical methods, and synthetic travel time data. The tomograms seemed to indicate consistency with known geology and borehole information. However, the authors mention problems when using the SeisOpt Pro program with model instability, and with artifacts appearing such as pinnacles or cutters in the lower third of the model when too many velocity elements are used. This is important to note when looking at the model produced because these types of artifacts are consistent with actual karstic features and may actually not be present in the subsurface.

Cramer and Hiltunen (2004) used SRT to characterize the subsurface at Pennsylvania bridge sites in mantled karst terrain. They found the method can produce valuable information for subsurface profiles that include dropping and pinnacle interfaces. Refraction profiles generated by SeisImager were found to match the basic layer structure gathered from the intrusive testing data, particularly the top of rock profile.

In an on-going study dating back prior to 2003, Sheehan et al. have been evaluating the use of different SRT programs, including Rayfract and SeisImager, with the long term goal being to assess the performance of these codes for karst terrains. In Sheehan et al. (2003), synthetic models were used with gradational velocity change and lateral velocity variation with the final models produced found to be reliable. However, the codes did have difficulty modeling sharp boundaries, instead modeling them as areas of higher gradient.

In Sheehan et al. (2005a), the ability of SRT programs to detect cavities in karst terrains was explored. They found SRT to have the potential to be an effective tool in cavity detection. This study did indicate false positives and negatives were possible, and that further study would be needed to determine the ability of SRT programs to detect cavities in karst. After several years of using synthetic and field data to investigate the effectiveness of commercially available SRT codes, Sheehan et al. (2005b) indicated that refraction tomography is able to resolve many of the features observed in a karst environment.

Through the use of synthetic models and field data these authors were able to test the capabilities of the programs while at the same time learning the programs limitations. All previous studies have demonstrated the ability of SRT to generally, determine the top of bedrock elevations at sites with complex subsurface conditions. Very little if any investigation has been done to examine the capabilities of SRT programs on karstic sites located in Florida. Florida's karstic limestone presents some very unique conditions for SRT programs to resolve, such as variation of the material properties within the limestone due to different degrees of weathering and times of deposition, as well as differing top of bedrock elevation due this weathering and subsequent sinkhole related activity. This study will expand the use of SRT programs into karstic terrains and the subsurface features associated with them.

2.3.2 Overview of Seismic Refraction Tomography Programs

In this study, three commercially available programs were used to produce P-wave velocity tomograms from travel time data sets collected in the field. The three programs, Rayfract, SeisImager, and SeisOpt Pro, are described in great detail by their authors and in publications by users of these programs. The following is intended to serve as a brief overview, with references noted for the reader if more detail is desired. While each of the three programs uses different methods to arrive at the final velocity tomogram, they each contain the same three important components. Each use a forward model for calculating source to receiver first arrival times based upon the current velocity model. Each has an inversion routine that adjusts the calculated and measured first arrival travel times. Finally, each updates the velocity model until an acceptable match is found for a preset number of iterations, and each has a way to generate an initial velocity model. With respect to cost, the list price for Rayfract was \$2200 plus the cost of Surfer by Golden Software, Inc., \$599, to display the final tomograms, SeisImager was \$1800, and SeisOpt Pro cost \$3200.

2.3.2.1 Rayfract (version 2.64)

Rayfract uses the wavepath eikonal traveltimes (WET) inversion method in its tomography processing, as presented by Schuster and Quintus-Bosz (1993). WET inversion computes wavepaths by using finite-difference solutions to the eikonal equation (Qin et al. [1992]). Woodward (1992) showed that a wavepath similar to a “fat” ray defines the propagation path of band limited seismic energy from the source to the receiver point.

WET inversion uses the Fresnel volume approach as an alternative to the ray path approach used by most programs. The Fresnel volume approach takes into account the effects that the real waves have on the adjacent parts of the model in the vicinity of the ray paths. It accomplishes this by taking into account ray paths with slightly longer travel times (Sheehan et

al. [2005b]). These effects are unaccounted for by simple ray tracing methods, however the WET inversion method is able to account for effects such as shadow zones and multi-pathing effects (Schuster et al. [1993]).

Rayfract provides the user with two different methods to generate an initial model: 1) the Delta t-v inversion method, or 2) the “smooth inversion” method. The Delta t-v method is useful in identifying small features and velocity inversions. The disadvantage of using the Delta t-v for the initial output is that there may be artifacts in the Delta t-v output that are not completely removed by the subsequent WET inversion (Sheehan et al. [2005b]). As a result, the final tomogram produced after using the Delta t-v method to generate the initial model often contains artifacts.

The “smooth inversion” method is recommended by the Rayfract users manual as the fail-safe method to generate the initial model. This method eliminates artifacts in the initial model in areas of strong refractor curvature and lateral variation that the Delta t-v method would produce. If these artifacts are eliminated in the initial model generation the subsequent WET inversions are more likely to generate a final tomogram that accurately models the features of the subsurface.

However, with the “smooth inversion” the ability to detect and image velocity inversions as well as vertical velocity resolution is somewhat decreased (Intelligent Resources Inc., [2006]). Because of this the Rayfract users manual still recommends that the Delta t-v method at least be tried in order to generate an initial model. Once the initial model has been generated the WET inversion is performed with user defined input parameters and number of iterations set to generate the final velocity tomogram model.

2.3.2.2 SeisImager (version 2.67)

SeisImager uses nonlinear traveltime tomography consisting of ray tracing for forward modeling and simultaneous iterative reconstruction technique (SIRT) for inversion. The main features of the algorithm are: 1) an initial model is constructed so that the velocity is layered and increasing with depth, 2) first arrival travel times and ray paths are calculated by the ray tracing method based on shortest path calculation, as described by Moser (1991), and a travel time between a source and a receiver is defined as the fastest traveltime of all ray paths, 3) the model is updated by SIRT and the velocity of each cell is updated during the iterations (Hayashi and Takahashi [2001]). The SeisImager users manual describes two methods for creating an initial model.

In the first method the user may create a simple “layer-cake” initial model by assigning layers manually to the travel time curve and performing a time-term inversion. The second method makes use of tomographic inversion and creates the initial model based on a user defined velocity range, depth to top of lowest layer, and number of layers to divide the model into. There is no user control of the grid spacing in SeisImager, and the code creates a variable cell size with the width equal to the geophone spacing and the height varying with shorter cells at the surface and taller cells deeper in the model. This is presumably to decrease processing time and avoid artifacts caused by low ray coverage at deeper depths (Sheehan et al. [2005b]). Upon completion of the initial model the inversion takes place which generates the final velocity tomogram.

2.3.2.3 SeisOpt Pro (version 3.0)

SeisOpt Pro uses a Monte Carlo-based optimization scheme called generalized simulated annealing to invert first arrival times for velocities, as described by Pullammanappallil and Louie (1994). For the forward model it employs a fast finite-difference scheme based on a solution to

the eikonal equation which computes first arrival travel times through the velocity model (Vidale [1988]). Travel time inversions that use linearized inversions do not take into account changes in the velocity field due to ray paths, making them initial model dependent, which could cause them to converge at an incorrect solution.

SeisOpt Pro avoids ray tracing and uses nonlinear optimization, namely generalized simulated annealing, to invert first arrival travel times for shallow velocities making it independent of the initial model. This accounts for curved rays and all types of primary arrivals (Pullammanappallil and Louie [1994]). The user must specify the vertical and horizontal resolution spatial resolution (cell size) and velocity range of the initial model. This may be accomplished by using the autocal setting and allowing the program to choose the resolution parameters and velocity range or by manually entering these parameters based on results from previous runs. With this information defined the program begins the inversion routine and outputs a final velocity tomogram.

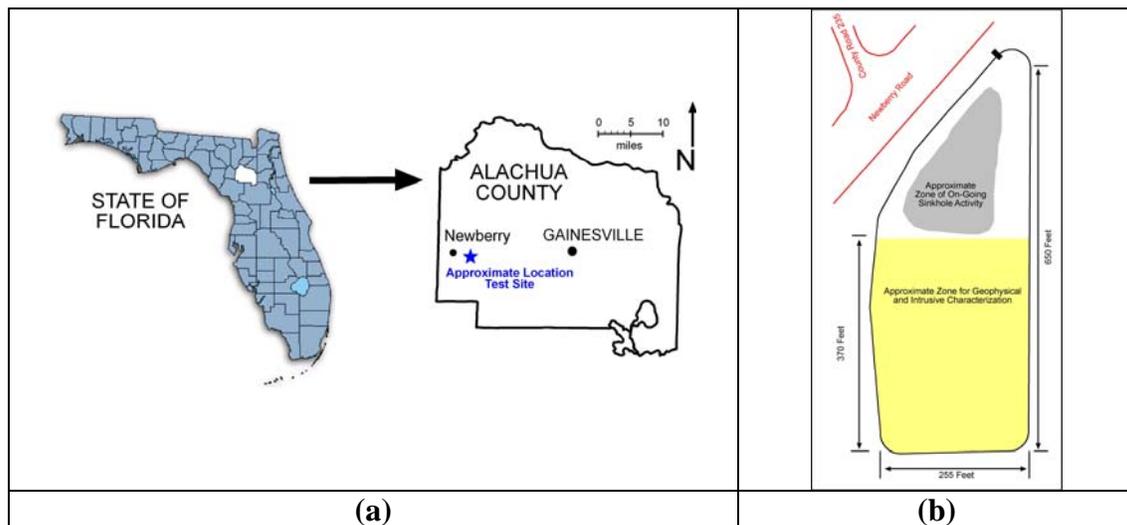


Figure 2-1 Location of geophysical/ground proving test site and zones within the site (from Hudyma, N., Hiltunen, D.R., and Samakur, C. (2007), “Variability of Karstic Limestone Quantified Through Compressional Wave Velocity Measurements,” (Accepted for Publication), *Proceedings of GeoDenver 2007, New Peaks in Geotechnics*, American Society of Civil Engineers, Denver, CO, February 18-21.

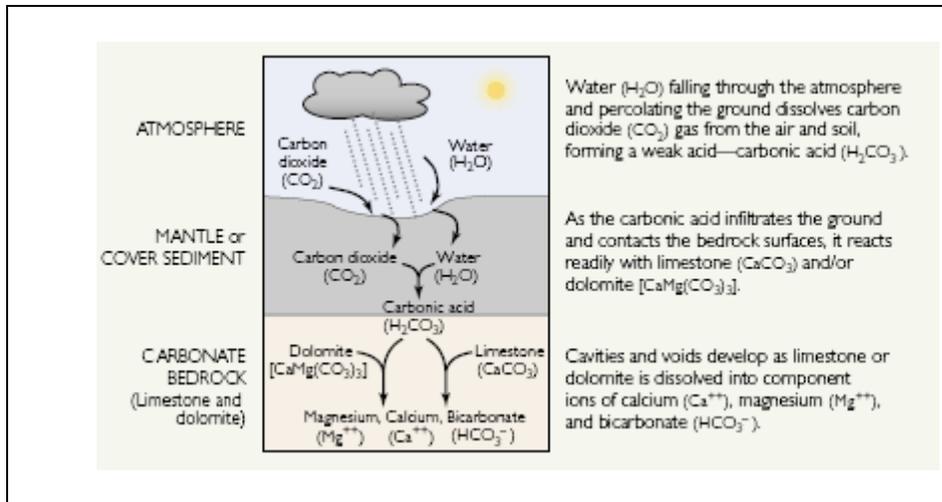


Figure 2-2 Dissolution of carbonate rock (from Tihansky, A.B. (1999), “Sinkholes, West-Central Florida: A link between surface water and ground water,” *U.S. Geological Survey Circular 1182*, pp. 126.)

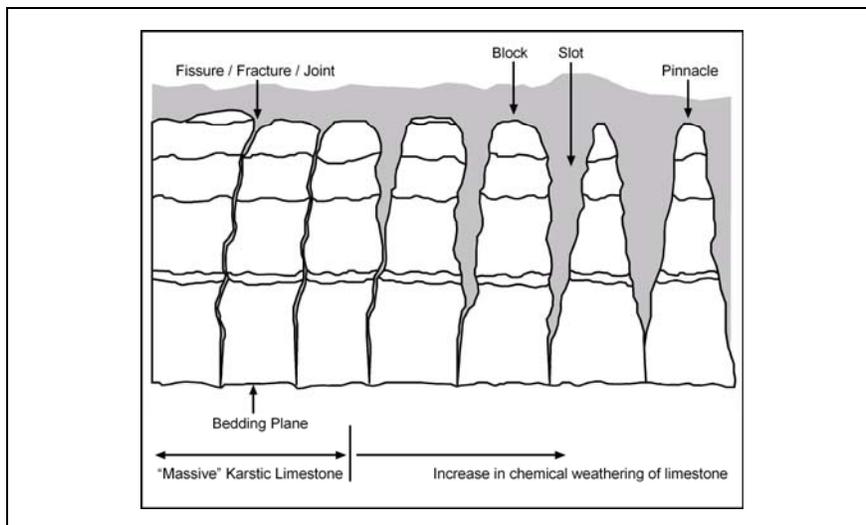


Figure 2-3 Karstic limestone features (from Hudyma, N., Hiltunen, D.R., and Samakur, C. (2007), “Variability of Karstic Limestone Quantified Through Compressional Wave Velocity Measurements,” (Accepted for Publication), *Proceedings of GeoDenver 2007, New Peaks in Geotechnics*, American Society of Civil Engineers, Denver, CO, February 18-21.)

CHAPTER 3
SEISMIC REFRACTION TOMOGRAPHY (SRT) PROGRAMS ON FIELD DATA

3.1 Seismic Refraction Testing Site Layout

Seismic refraction testing was conducted during the summer of 2005 in the southern portion of the test site, as shown in Figure 2.1(b). This area was subdivided into 26 north-south survey lines, A through Z, going from west to east across the site, and spaced at a distance of 3.0 m apart from one another. Each line was 85.3 m in length with station 0 m located at the southern end of the line. For this study, testing was performed along six of the lettered survey lines: A, F, K, P, U, and Z, which are each 15.2 m apart from one another. Along each of these six lettered survey lines two 36.6 m long refraction surveys were conducted end to end beginning at station 0 m and ending at station 73.2 m, for a total of 12 refraction lines tested.

3.1.1 Field Testing Procedure

The twelve 36.6 m long refraction lines chosen were each tested individually. Vertical geophones were used as receivers and spaced equally at 0.61 m apart from one another other along the line, for a total of 61 geophones along each 36.6 m length of line. The geophones used were 4.5 Hz and were manufactured by Geophysical Instrument and Supply Company, Inc. (GISCO). The seismic energy to produce the compression, or (P), wave first arrivals was induced by striking a metal plate on the ground with an 89 N sledgehammer, with a geophone placed at the source location in order to record the zero-time of wave propagation. Shots were spaced at 3.0 m intervals starting at 0 m along each of the 36.6 m refraction lines, for a total of 13 shots along each of the twelve refraction lines.

The time records measured in the field by the geophones were recorded by a Data Physics Mobilizer II 32-channel dynamic signal analyzer with Signal Calc software and saved on a Dell Inspiron 8600 laptop computer. Because each of the twelve lines contained 61 geophones and

the dynamic signal analyzer only had 32-channels to collect the time records, each of the twelve lines had to be further subdivided into two parts. For example, a line going from 0-36.6 m would be subdivided into test sections from 0-18.3 m and from 18.3-36.6 m. However, even though a line of geophones only went from 0-18.3 m, source locations were still visited at 3.0 m intervals from 0 to 36.6 m. As a result each of the 13 shot locations for each of the twelve 36.6 m survey lines had to be visited twice.

3.1.2 Testing Limitations and Potential Sources of Error

The length of the refraction lines tested in the field were limited to a length of 36.6 m, as Hiltunen and Cramer (2005) had found this distance to be a limiting refraction line length using a similar testing layout and testing procedure. Once lengths were increased beyond this, using the same falling weight sledgehammer source, first arrival times became difficult to pick from the far receivers when the source location was at the opposite end of the refraction line. This was due primarily to the fact that traffic and other environmental noise energy levels became so close to the dissipated seismic compression (P) wave energy imparted that it was difficult, if not impossible, to make a first arrival pick at the far geophone locations. Similar observations were noted during the field testing at this site.

This limiting length also served as a limiting factor with respect to the depth to which the subsurface could be explored due to the geometry of the layout. However, the first arrival P-waves recorded traveled to sufficient depths to delineate the soil/bedrock interface and lateral variability of the overburden soil in the subsurface for this site. In order to image the subsurface at greater depths it would be necessary to increase the length of the line while at the same time imparting a greater amount of source energy. Another possible source of error that may have occurred as a result of having to visit each shot location twice due to limitations of the number of channels on the dynamic signal analyzer. However this error is thought to be random and small.

Traffic and other environmental noises recorded on the travel time records also made choosing first arrival times at geophone locations far from the source location difficult and sometimes impossible.

3.2 Analyzing and Processing Field Data

After the field portion of the seismic refraction testing was completed, the next step was to begin processing the data collected. The first step in this process was to determine the first arrival times, which was accomplished using SeisImager's first arrival picking module PickWin95. It should be noted that all three of the SRT programs had first arrival picking capability and that PickWin95 was chosen simply because of previous experience and familiarity.

3.2.1 Selection of First Arrivals from Time Records

The data files for each of the twelve refraction survey lines tested were imported into SeisImager's PickWin95 module where first arrival times were determined manually through visual inspection from the collected time records and were then saved, see Figure 3.1 for a typical time record with first arrivals chosen manually. This was done for each of the twelve survey lines for each of the thirteen source locations for each line. The first arrival data files were then saved for subsequent analysis by each of the three different SRT programs.

3.2.2 Travel Time Curve Generation

After PickWin95 was used to determine the first arrivals PlotRefa, the interpretation module of SeisImager, was used to append the thirteen source first arrival time records for each refraction line into one file, as well as to generate travel time curves. In order to do this each of the first arrival data files along a refraction line for the 13 source locations were appended to a single graph and then saved to one file. Typical travel time curves generated by PlotRefa for the A line are shown in Figures 3.2 and 3.3. This data contains the first arrival times for each of the

13 shot locations at each of the 61 geophone locations along a given refraction line. It is this file that will be imported into each of the three SRT programs for inversion into a final velocity model so that each of the programs would start off with the same initial set of first arrival times.

3.3 Seismic Refraction Tomography Program Processing Flow

While each of the three SRT programs use different inversion methods they each have the same basic components in processing flow in order to generate the final velocity model, as described previously in section 2.5. First the complete appended first arrival file saved in PlotRefa was imported into each of the SRT programs. Each of the programs generates initial models, and then use inversion methods to produce improved velocity models. The user may also make changes to the inversion parameters to improve the final velocity model.

3.3.1 Rayfract (Version 2.64)

The first step in using Rayfract is to create a profile for the refraction survey line to be analyzed. Once the profile is created the user may enter information such as Line ID, Job ID, station spacing, and station offset information. The next step is to import the complete travel time data file, previously created in PlotRefa, into Rayfract. However, Rayfract requires the travel time file imported be in a “station number” format, which requires the shot and receiver locations be assigned station numbers instead of their position in meters along the survey line. For example, a receiver at location 0.6 m along the refraction line would be renamed as receiver station 1 and the next receiver at 1.2 m would be receiver station 2, and so on until the final receiver located at 36.6m is renamed as station number 60. Likewise the source or “shot” locations needed to be assigned shot numbers as well as shot station numbers, so a shot at source location 0 m would be identified as shot number 1 at shot station 0, the second shot at 3.0 m would be shot number 2 at shot station number 5.

Rayfract also required some relatively minor formatting changes be made to the travel time data file produced by PlotRefa. In order to make these formatting changes most efficiently an Excel macro program was created which allowed the user to make these changes with minimal manipulation and then save as an ASCII text file. Rayfract also has a first arrival picking module within the program which, if utilized, may have lessened the amount of time and effort to get the data ready to be imported.

Since all the shot and receiver locations are identified as station numbers, Rayfract requires that a station coordinate file be created to give the location in meters of these station numbers along the refraction line. This file contains four columns: 1) Station Number, 2) x coordinate, 3) y coordinate, and 4) elevation. The x coordinate column simply gives the location in meters of the station number assigned to the receiver and shot locations, while columns 3 and 4 remained zero for this set of data because the testing was assumed to have been done in a straight line at a constant elevation. Only two of these files needed to be created for all twelve refraction survey lines, one from 0-36.6 m and the other from 36.6-73.2 m, and the appropriate one chosen for each refraction line imported because the geometry of the test layout remained the same throughout the testing. This coordinate file was then imported into Rayfract and the modified travel time data file was now ready to be imported into Rayfract for inversion.

The Rayfract users manual recommends that the initial velocity model be determined using the “smooth inversion” method, which produces a simple “layer cake” model with one-dimensional variation in velocity with depth. Once complete, the wavepath eikonal travelttime (WET) inversion method was used with the velocity smoothing set to “full” for 10 iterations to generate the velocity tomogram using the default WET tomography parameters, as recommended by the Rayfract users manual. The purpose of smoothing, as it relates to velocity inversion, is to

take into account the velocity of neighboring cells when assigning a cell a velocity to keep it from deviating too much from neighboring cells, as the actual velocities of neighboring cells in most subsurfaces should be similar to one another. By doing so the final velocity model should be less effected by changes in velocity for a single cell, and therefore be more representative of the actual subsurface velocity profile.

Rayfract sets the maximum velocity to 6000 m/s as a default, which was observed to be well above the maximum velocities encountered and was left unchanged as lowering it did not show any decrease in error calculation in the runs. The final velocity tomogram and ray path model produced were automatically outputted by Rayfract for viewing to Surfer, a mapping program by Golden Software, Inc. They were then reviewed looking at how complete the ray coverage was throughout the model and if any artifacts or unusual features existed within the final velocity tomogram.

Based on observations from the first tomogram produced, additional runs at full smoothing were made to see if adjusting the wavepath width parameter up from the default of 3.0%, as recommended in the Rayfract users manual to smooth out gaps or anomalies, produced a better tomogram. While this often helped remove anomalies and gaps in ray coverage, the downside to increasing the wavepath width was that some features became blurred. Rayfract also has a few other parameters related to the wavepath that may also be adjusted, however no recommendations were made regarding adjustments to these parameters and the few that were tried yielded little change in the final tomogram. So the tomogram chosen to go forward with was the one that had the lowest wavepath width, while still providing adequate ray path coverage and velocity model lacking artifacts.

Once the best velocity models were chosen, they were specified as the initial models and an additional 10 iterations, for a total of 20 iterations, were run using the full velocity smoothing option to further refine the tomogram, as suggested by the Rayfract users manual. The Rayfract manual then suggests using the minimal smoothing setting for the second run of 10 iterations. However this produced models with velocity features appearing sharp and jagged, which were deemed not representative of the even these highly variable geologic conditions.

With several models now complete for a line, it became necessary to evaluate them in order to determine the best overall model produced. The criteria looked at were: 1) how complete the ray path coverage was, 2) if any anomalies occurred in the velocity model, and 3) how the final error compared with the other models. Upon completion of the inversion process Rayfract displayed the results of three error calculations: 1) mean unsigned error (ms), 2) maximum unsigned error (ms), and 3) the relative misfit function, calculated by squaring the error over all of the traces modeled and dividing that by twice the modeled trace count (Schuster [1993]). In cases where ray path coverage was complete and no anomalies existed in several models, the velocity model with the smallest wavepath width was usually selected as it often showed the most detail and had the lowest error. The final P-wave velocity tomograms for the A line stations 0-36.6 m and 36.6-73.2 are shown in Figures 3.5 (a) and 3.6 (a), respectively, with the remaining final tomograms shown in Appendix A.

3.3.2 SeisImager (version 2.67)

SeisImager uses PlotRefa to develop P-wave velocity tomograms. The first step in using PlotRefa is to open the previously saved appended travel time data file. Next the initial model needs to be generated, using user specified parameters such as velocity range, depth to top of lowest layer, and the number of layers. The SeisImager users manual notes that the most important parameters to correctly identify are the minimum and maximum velocities, and if

unsure of actual velocities to be conservative in choosing them as the inversion will not converge if the actual velocities are not bracketed.

Since no information existed regarding the actual P-wave velocities for the subsurface at this site, it was necessary to employ a method to help bracket them, as well as the depth to the top of the lowest layer. Cramer and Hiltunen (2003) determined these parameters by generating simple “layer-cake” initial models consisting of two or three layers in SeisImager which were generated by manually assigning layers to the travel time curves from the two outside source locations, stations 0 and 36.6 m. Since the SeisImager manual offers minimal guidance to the user in determining these initial model parameters, this method was used as a first attempt to bracket these parameters. Figure 3.4 shows the two end source travel time curves for the A line 0-36.6 m with three layers assigned to each: red, green, and blue.

After the assignment of layers the inversion was run and a simple two or three layer velocity model was produced. The minimum velocity initial model parameter was determined from the velocity of the first layer, the maximum velocity from the deepest layer, and the depth to the top of the lowest layer from that interface. Cramer and Hiltunen (2003) found that the best velocity models could be generated by decreasing the minimum velocity found by 25%, and increasing the maximum velocity and depth to top of lowest layer by 25%. This same method was attempted for this particular set of data, however it was unable to bracket the actual velocity range and depth to top of lowest layer.

Thus, in order to develop an initial model, a wide velocity range was assigned to the parameters based on values well outside of what was expected. With that the minimum velocity was initially set as 300 m/s, and the maximum velocity to 4500 m/s, with the depth to the top of the lowest layer assigned based on the depth of the lowest ray from the velocity model produced

using the method of Cramer and Hiltunen (2003). The velocity model inversion was run setting the number of layers equal to twenty, and producing the best final velocity model became an iterative process in which the previously run final velocity model was evaluated in order to see what changes were necessary to make in the initial model parameters to produce a better velocity model. The velocity parameters were the first that needed to be bracketed, so the minimum velocity was reduced if the model was within 100 m/s of the 300 m/s minimum velocity, and the maximum velocity was reduced from 4500 m/s if the maximum value found was less than 3500 m/s, approximately 25% less than 4500 m/s. Usually any velocity changes were minimal and were made only after the first model inversion.

With the velocity range now bracketed, determining the top of the lowest layer parameter for the initial model was an iterative process in which the velocity range inputs were held constant and the depth was changed. This depth was then adjusted incrementally several times to progressively lower depths to make sure the lowest ray paths were at depths sufficiently less than the lowest layer depth specified in the initial model. This was done to ensure the depths that the ray paths traveled were not being constrained by the initial model parameters.

After this was complete, the final velocity model was chosen based on having: 1) a lack of artifacts, 2) a low RMS error, but not necessarily the lowest, and 3) a depth to top of lowest layer depth sufficiently large enough to allow ray path travel not to be constrained. The runs were each made using the default number of iterations of 10. Additional runs made using 20 iterations and were found to produce models looking virtually identical with a minimal reduction in error, so final models were generated using 10 iterations. The final P-wave velocity tomograms for the A line stations 0-36.6 m and 36.6-73.2 m are shown in Figures 3.5(b) and 3.6(b), and the final tomograms for the remaining lines are shown in Appendix A.

3.3.3 SeisOpt Pro (version 3.0)

SeisOpt Pro requires that the input files used for inversion of the final velocity model consist of 3 ASCII (text) files. The first file contains source location information, the second receiver location information, and the third first-arrival pick times (Optim LLC, [2004]). In order to accomplish this, SeisOpt Pro has several conversion programs built in to take the first arrival information from travel time data files created using other first-arrival picking programs and converts them into the required ASCII format. Since this version of SeisOpt Pro did not have a conversion program to convert first arrival files created in PickWin95, customer support at Optim Software, the program's manufacturer, was contacted and a conversion program was written and sent electronically. This is a service offered to the user in the SeisOpt Pro users manual.

The next step was to set the input parameters for the initial model. SeisOpt offers five different preset resolutions that determine the cell width (hx) and cell height (hz) to be used in the model. The higher the resolution the smaller the cell size used in the inversion and, consequentially, the more detailed the final velocity model becomes. The SeisOpt manual recommends running the inversion at the "Medium", "High", and "Highest" settings to determine which resolution will provide the best solution without any artifacts, but suggests that the Highest or sometimes the High resolution setting for geotechnical type applications usually performs the best. Runs were made for each of these three different resolutions using the autocal option, which automatically determines the cell width (hx), cell height (hz), number of cells in the x direction (nx), and number of cells in the z direction (nz) to be used in the velocity model inversion based on receiver spacing, for each refraction line.

The velocity models from each of the three resolutions were compared against one another, and it was observed that the high and medium resolution settings produced models with fewer

artifacts and better ray coverage than the highest. Carpenter et al. (2003) also noted in their study of SeisOpt Pro that using the highest resolution developed severe modeling artifacts and could not be used to infer subsurface geology. With this observation, it was decided to no longer make runs using the highest resolution setting because of the inadequacy of the models, and the lengthy computational time necessary to produce them, approximately 9 hours. The high and medium resolution models use larger cell sizes which, when a ray passes through it, will cover a larger area of the model. While some detail in the model may be lost due to the increased size of the cell, ray coverage should be greater with fewer artifacts present due to a lack of ray coverage.

The output from high and medium initial autocal runs included the default n_x , n_z , h_x , h_z , and maximum and minimum velocity used to produce the velocity model. With these values determined, 10 additional runs were made with 10 different values of n_z , changing it by increments of 1, with 5 of them above the default n_z value and 5 below, as recommended by the SeisOpt Pro users manual. The other output parameters determined in the initial autocal run were held constant. The reason for changing only the number of cells in the vertical direction (n_z) is that the depth of penetration of the first arrival rays is a nonlinear function of source-receiver offset and subsurface velocities, as a result the depth of the model is the biggest unknown (Optim LLC, [2004]).

The resulting 10 velocity models produced from the medium and high resolutions were then compared against one another. The best velocity model was determined for each resolution based on: 1) displaying a lack of artifacts, 2) having adequate ray path coverage, and 3) having comparatively low least square error. The best tomogram of the high and medium resolution models were compared against one another using this criteria and it was found that the medium resolution setting produced the best overall velocity models.

Carpenter et al. (2003) also found for their data sets that the medium resolution models produced velocity tomograms consistent with the geology and provided a reasonable solution that resembled the best high-resolution models. Thus, it was decided to proceed forward with the remaining lines using primarily only the medium resolution setting. However, to be certain a better velocity model had not been overlooked, a few runs were conducted at the high and highest resolutions.

After reviewing the 10 initial runs using different n_z values it was noted that the best models often occurred at or near the lowest and highest n_z values run. In order to help ensure that a better model did not exist outside these initial ten runs, and to effectively bracket the best model with several inferior models of both higher and lower n_z values, the number of runs was expanded to between 20 and 25 different n_z values. This process was accelerated by using the “batch processing” feature which allows the user to set the model input parameters with the different n_z values, saving them into separate files, and set them up to be run consecutively. This allows the user to batch up multiple runs and have them run automatically without any interaction or need to be present.

The resulting models were then examined for each of the refraction lines and the best model was chosen based on the previously mentioned criteria. For 11 of the 12 refraction lines the medium resolution tomogram was chosen as the final velocity model. However, a low resolution model was run and chosen for the A line station 0-36.6 m due to the number of artifacts present in even the best medium resolution model. Figures 3.5(c) and 3.6(c) show the final P-wave velocity tomograms for the A line, and the remaining lines are presented in Appendix A.

3.4 Comparison of the (SRT) Programs

With the final P-wave velocity tomograms chosen from each of the three programs for each of the twelve refraction lines it was now necessary to compare them against one another. Comparing velocity models from different SRT programs against one another can be done by either comparing the calculated final error of the travel times or by visual inspection. An error calculation provides a more effective, less subjective means of evaluating code performance. However, visual inspection best approximates how the results from a real field study will be interpreted. In a field study visual interpretation is necessary because there is no “truth” with which to compare mathematically (Sheehan et al. [2003]).

In real world geotechnical applications models will be evaluated on how consistent they appear to be with the expected geology of the area and with data obtained from more traditional geotechnical techniques, such as SPT, CPT and rock coring. A model chosen solely based on having low error may still show features not consistent with the expected and contain artifacts. It is for this reason that model comparisons between programs will be made based primarily upon visual inspection with error calculations performed to provide an objective comparison.

3.4.1 Creation of Tomograms using Surfer (version 8.04)

Each of the three SRT programs displays its final velocity model in a different format and scale. In order to visually inspect each of the final models from each of the three programs without becoming biased by the visual quality of one SRT’s program model versus another, each was imported into a single mapping program, Surfer. SeisImager and SeisOpt create output files of the velocity model in a format in which the user can directly import them into Surfer to create a contour map, and since Rayfract automatically outputs its velocity model into Surfer, only minimal changes to map properties needed to be made. Once imported, contour maps were created for each of the three models from each of the SRT programs for each of the twelve lines,

as presented in Figures 3.5 and 3.6 as well as in Appendix A. Map properties such as scale, minimum and maximum velocity, and contour interval (set as 100m/s) were made to be identical for each of the three models across a line in order to remove any unintentional visual bias.

3.4.2 General Visual Observations of Tomograms

Even though the models have been imported into Surfer to remove any visual bias some important differences do exist. Most notably the SeisImager models are rectangular in shape, while Rayfract models are bowl like and SeisOpt Pro are pyramidal. The reason for this difference in model geometry is that Rayfract and SeisOpt Pro do not model portions outside the area of ray path coverage, while SeisImager extrapolates the velocity model outward and downward from areas of nearby ray coverage. Any regions of the velocity model, whether in the inner or outer portion of the model, outside the area of ray path coverage should be interpreted carefully as not enough information is available in these regions for the SRT programs to determine features of the subsurface.

Some other general trends were also observed between the three programs. The minimum velocities modeled in the final velocity tomograms tended to be similar in all three programs for a given refraction line, while the maximum velocity tended to be the highest in SeisImager and Rayfract and was usually the lowest in SeisOpt Pro. However, the differences in the maximum velocity seemed to occur only near the bottom of the model and in areas of low ray coverage, while the majority of the velocities in other areas of the models across the programs remained similar. With respect to the depth of the final model for the twelve refraction lines, SeisImager and sometimes Rayfract tended to be the deepest, while SeisOpt always resulted in the shallowest model. It is important to note that SeisImager often had only one or a few ray paths traveling at the bottom of model, with several meters above in which no ray paths traveled through. These areas should be interpreted with caution.

SeisOpt often produced oval shaped artifacts in the lower half of the model that could usually be attributed to areas of low ray path coverage, but not always. Sheehan et al. (2003) also reported model instability in SeisOpt Pro when too many layers (too large a nz value) or too many velocity elements are used (usually at the highest resolution setting). The instability manifests itself in the appearance of high or low velocity artifact “pinnacles,” “cutters” or oval areas, usually within the lower third of the section. The amount of artifacts seemed to decrease in SeisOpt Pro as the resolution was decreased, so some additional runs were made to see if these artifacts could be removed by setting the resolution to the “low” setting. This did seem to help, however the detail of the subsurface features was also greatly reduced.

3.4.4 Specific Visual Observations of Tomograms

Figure 3.5 shows the final velocity models from all three programs for the A line station 0–36.6 m. While some differences do exist between the models the same general subsurface features exist, particularly in the upper portion. All three models show a valley or bowl-like feature in the middle stations with pinnacles on the right and left sides of the lines occurring at approximately the same station numbers and depth. The velocities associated with these features and the remaining portions also compare similarly to each other with depth. Likewise, Figure 3.6 shows the velocity models from the A-line station numbers 36.6–73.2 m with pinnacle like features toward the right and left side of the model, with a valley or bowl-like feature towards the center of the model in each of the three SRT programs.

The resulting final tomograms for each of the three SRT programs for the remaining refraction lines, F, K, P, U, and Z, were examined and compared against each other, see Appendix A. After careful examination of the final tomograms it was noted that, like the A line, each program imaged the same general subsurface features at similar locations and depths. For the most part the P-wave velocities were also observed to be similar with depth at the same

location across the models produced by all three SRT programs. The few minor differences observed usually occurred in areas of low ray path coverage, usually the lower portion of the models, where the programs had to interpret the velocity model with little or no measured ray paths traveling through. This was the case particularly for the SeisOpt Pro models, which resulted in artifacts and other features being modeled that are not consistent with the geological history. Based on visual inspection of the tomograms across the three SRT programs generated for this site, it can be stated that each of the three SRT programs are able to produce final velocity models with the same general subsurface features being imaged.

3.4.5 Quantitative Comparison of Calculated Travel Times

Although visual inspection of the final P-wave tomograms produced by the models is important in the evaluation of the programs, the results are subjective and may vary depending on the viewer. In order to help provide a more objective comparison of the programs, the differences between the measured and the calculated travel times of each program were evaluated for the two A line final tomograms, stations 0-36.6 m and 36.6-73.2 m, see Tables 3-1 and 3-2. Figures 3.7 and 3.8 are provided to show visually the closeness of the measured versus predicted travel time curves for each of the three SRT programs.

The RMS error and the mean and maximum differences were calculated for each of the three programs for the A line. The results show the RMS, mean difference, and maximum difference to be comparatively close between Rayfract and SeisImager calculated travel times, with Rayfract having a lower RMS for the A line 0-36.6 m, and SeisImager having a lower RMS for the A line 36.6-73.2 m. SeisOpt Pro had RMS, mean difference, and maximum difference values slightly higher than the other two programs for the A-line. This closeness between the programs quantitatively as well as through visual inspection should give the user further confidence in the ability of each of the programs to model the general features of the subsurface

similarly. Perhaps the differences that do exist between SeisOpt Pro and the other two programs may help explain the reason why Rayfract and SeisImager were able to produce tomograms with some more detail and less artifacts.

3.4.5 Processing Time

Along with comparisons between the velocity tomograms, the amount of processing time each program requires is also important to take into consideration. The amount of processing time to run an inversion will vary depending upon the data set, the speed of the computer used, and the size of the data in the refraction line, so times recorded can only be used when comparing the three programs for these data sets. Times were recorded for runs made by each of the programs for the A line station numbers 0-36.6 m, however similar times were observed in the remaining runs.

The resulting times showed SeisImager taking approximately 8 minutes and Rayfract taking approximately 10 minutes to run inversion routines for ten iterations. However, Rayfract was run for 20 iterations, approximately 20 minutes, in order to bring out some finer subsurface details. The SeisOpt Pro run made using the medium resolution setting took approximately 1 hour, as it is the most complex inversion routine. Similar processing times were observed for the other refraction lines. The length of the processing times reflect the complexity of the inversion routines behind the programs, with SeisImager being the simplest and SeisOpt Pro being the most complex. However, simply using the most complex and time intensive inversion does not guarantee the best final model. SeisImager and Rayfract were able to produce a final model that seemed to be consistent with the known geology as well as containing fewer artifacts than SeisOpt Pro in a significantly less amount of time.

3.5 General Assessment of Performance of the SRT Programs Evaluated

Although each of the three programs rely upon completely different inversion methods, each was capable of producing final tomograms showing similar subsurface features. With the three SRT programs evaluated based on visual inspection as well as quantitatively the following statements may be made:

- 4 All three SRT programs when visually compared to one another for a given refraction line were able to generate tomograms showing similar subsurface features and P-wave velocities.
- 5 Quantitatively, the error between the measured and calculated travel times for each of the three SRT programs were comparatively close to one another. However, the slightly larger error calculated for the calculated SeisOpt Pro travel times may account for the differences and artifacts modeled.
- 6 An increase in processing time does not necessarily lead to a better model being produced as SeisOpt Pro took significantly longer to run and generally produced models with more artifacts.

Table 3-1 Comparison of Calculated Travel Time Differences Between Programs for A Line Station 0-36.6 m

	Rayfract	SeisImager	SeisOpt
RMS (ms)	24.4	29.6	34.5
Mean Difference (ms)	0.68	0.84	0.99
Maximum Difference (ms)	3.29	3.77	4.14

Table 3-2 Comparison of Calculated Travel Time Differences Between Programs for A Line Station 36.6-73.2 m

	Rayfract	SeisImager	SeisOpt
RMS (ms)	28.1	25.0	31.6
Mean Difference (ms)	0.66	0.74	0.87
Maximum Difference (ms)	5.61	5.24	6.21

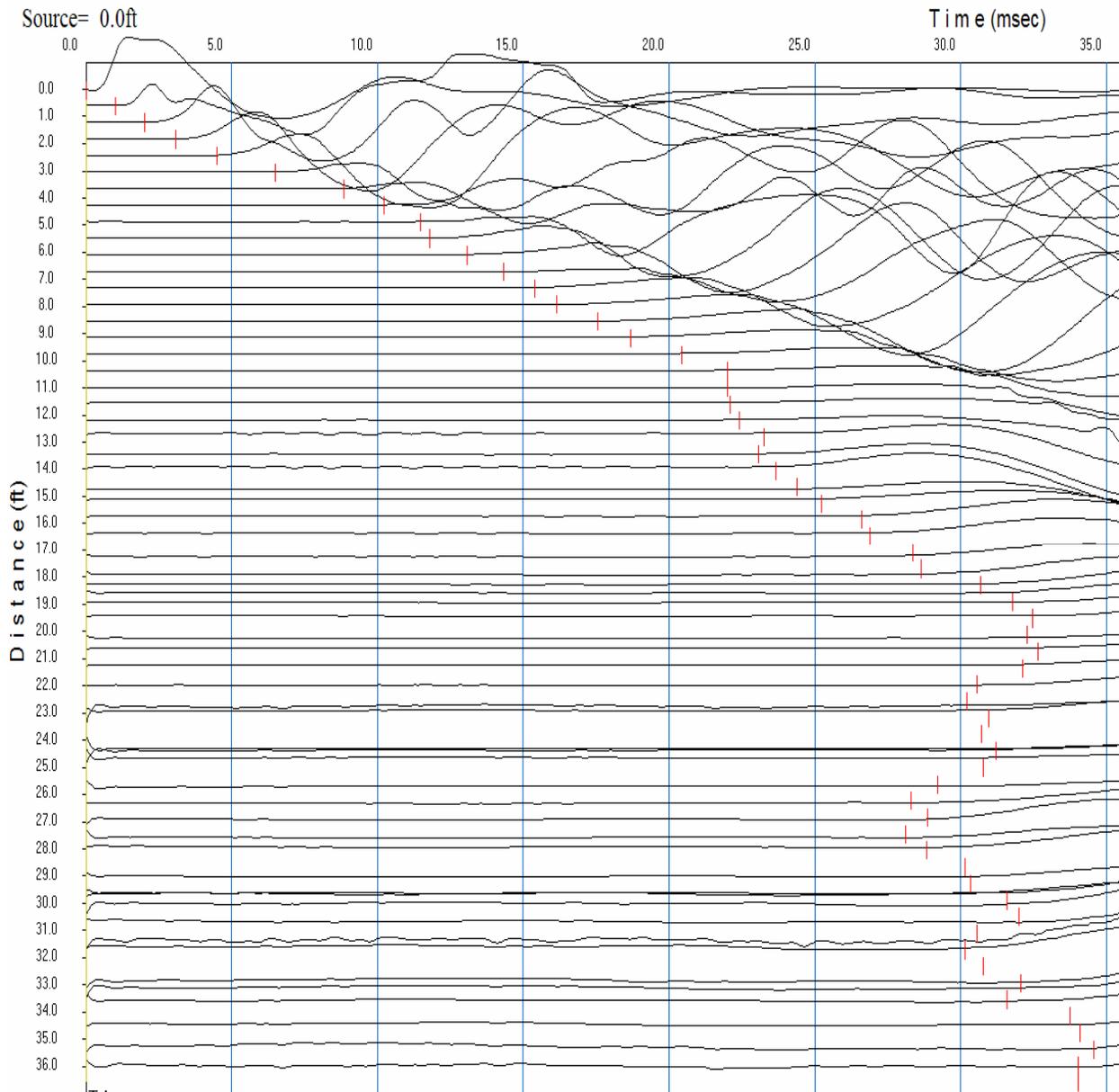


Figure 3-1 Example of PickWin95 time record along survey line A from stations 0-36.6 m for source location 0 m. Chosen first arrival times are denoted for each trace by the horizontal red line.

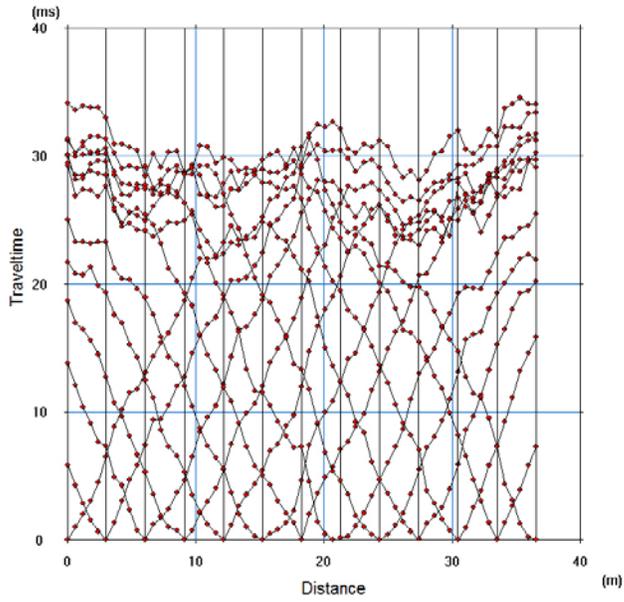


Figure 3-2 PlotRefa travel time curves, A line, station 0-36.6 m

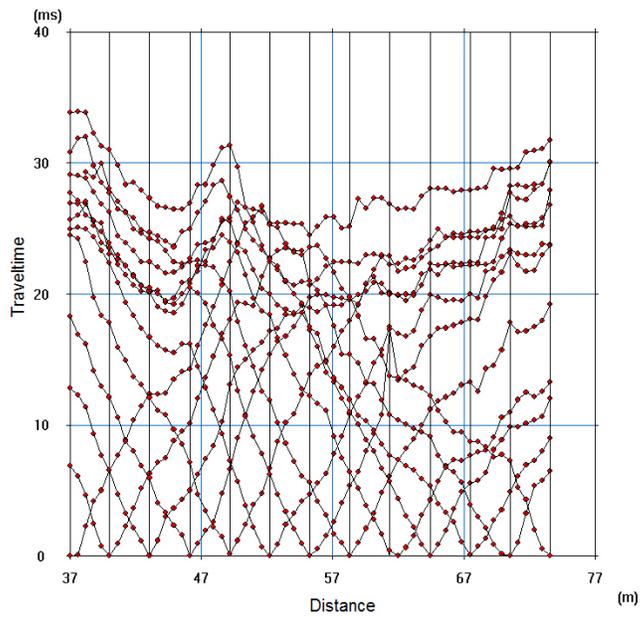


Figure 3-3 PlotRefa travel time curves, A line, station 36.6-73.2 m

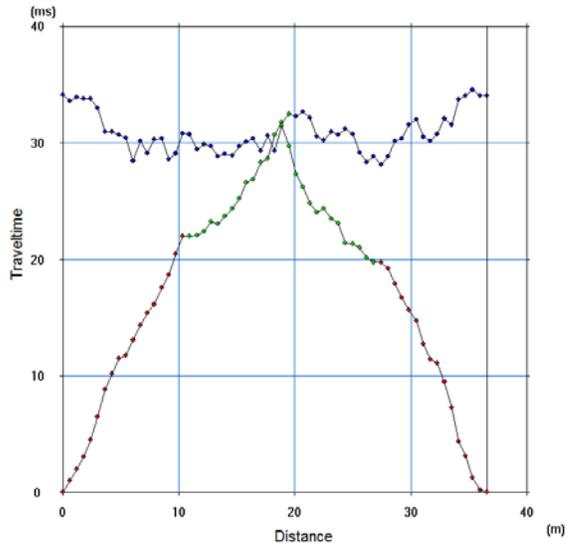
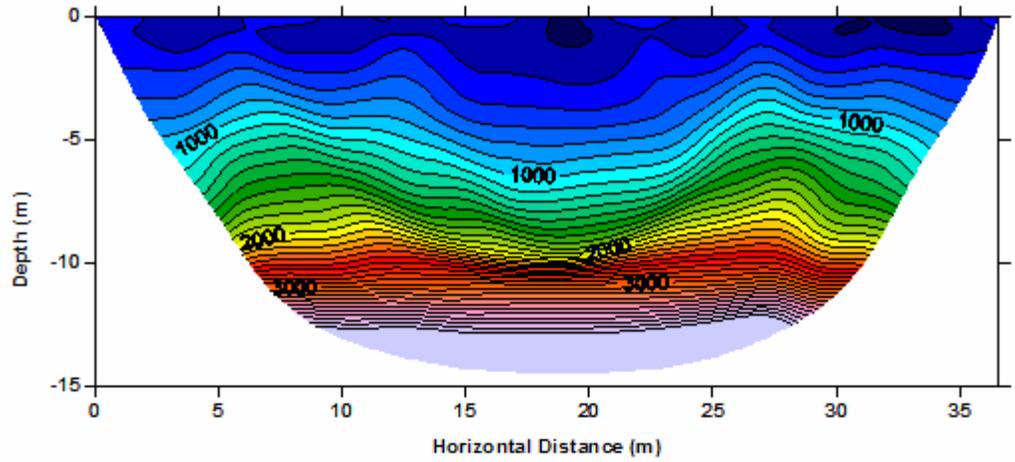
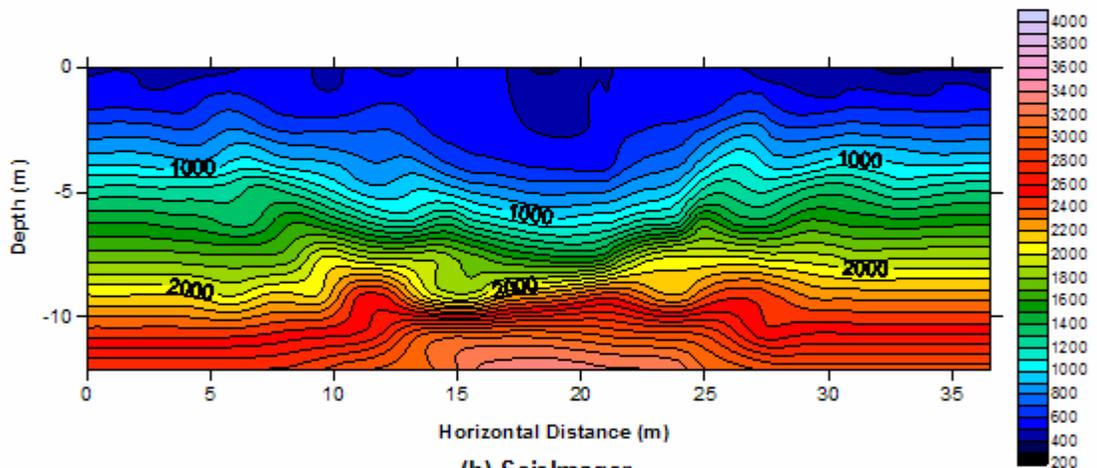


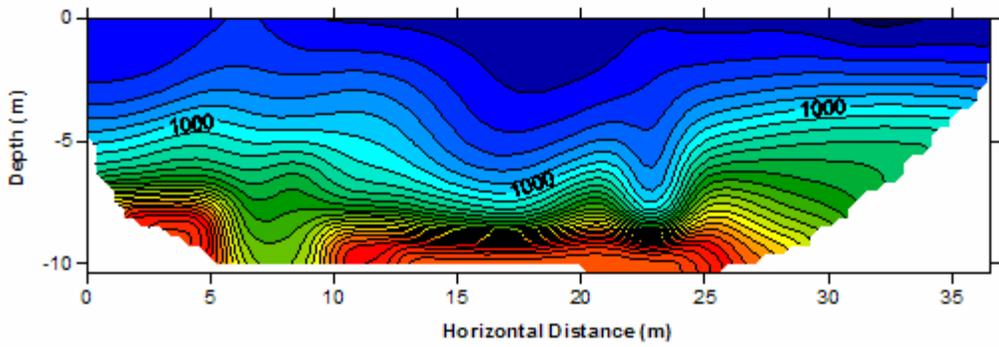
Figure 3-4 PlotRefa outside source location travel time curves, A line, station 0-36.6 m



(a) Rayfract

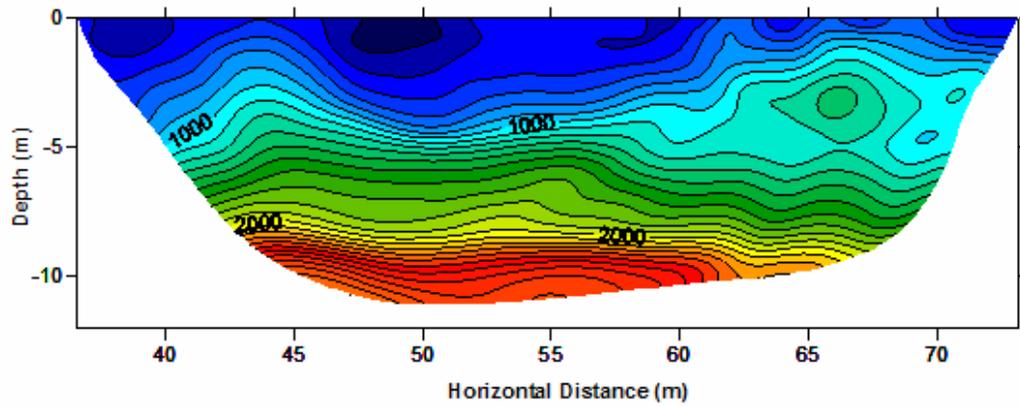


(b) SeisImager

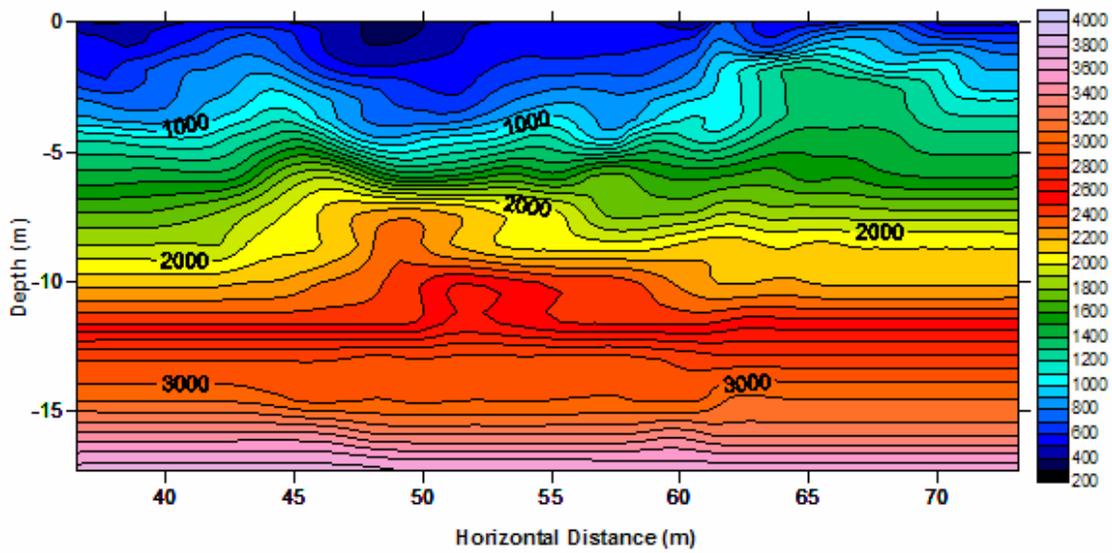


(c) SeisOpt Pro

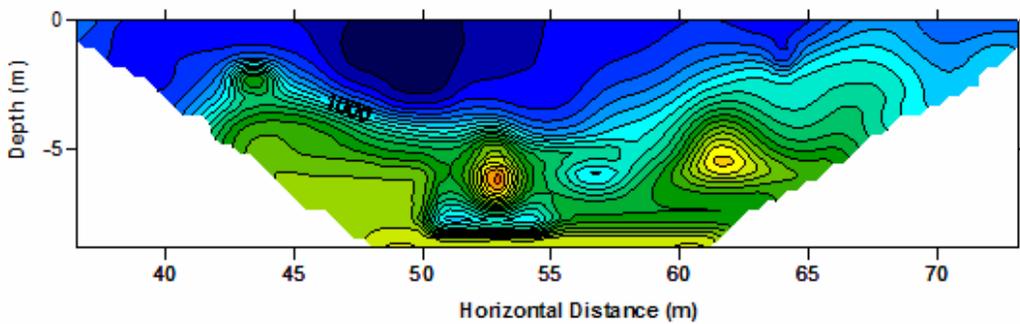
Figure 3-5 P-wave Tomograms, A line, Station 0 – 36.6 m. (a) Rayfract tomogram, (b) SeisImager tomogram, and (c) SeisOpt Pro tomogram.



(a) Rayfract

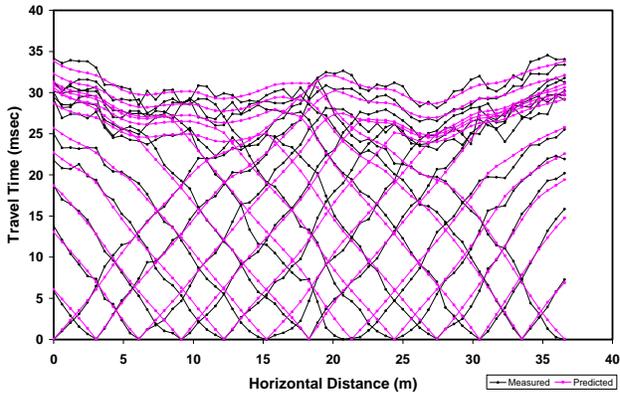


(b) SeisImager

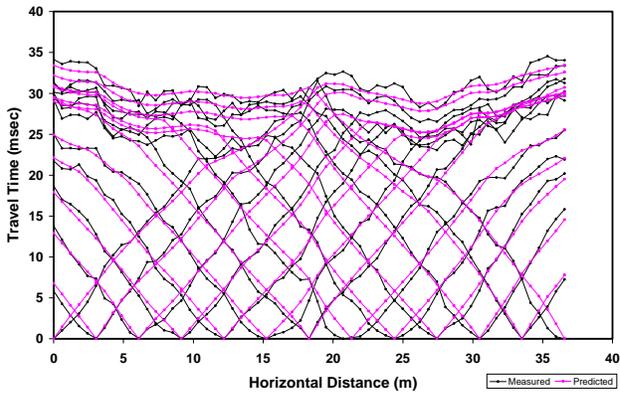


(c) SeisOpt Pro

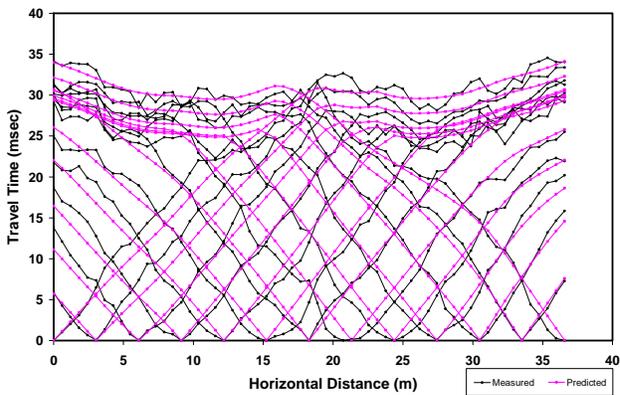
Figure 3-6 P-wave Tomograms, A line, Station 36.6-73.2 m. (a) Rayfract tomogram, (b) SeisImager tomogram, and (c) SeisOpt Pro tomogram.



(a)

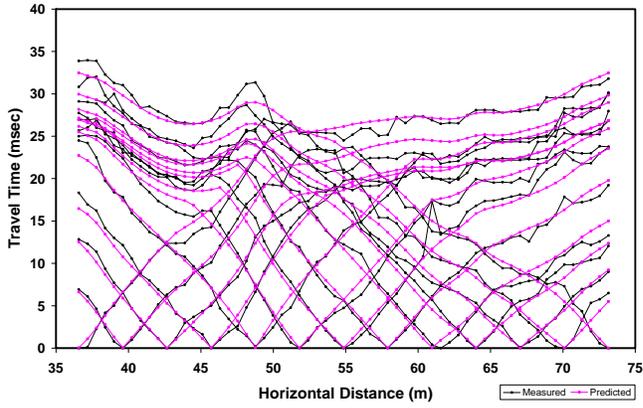


(b)

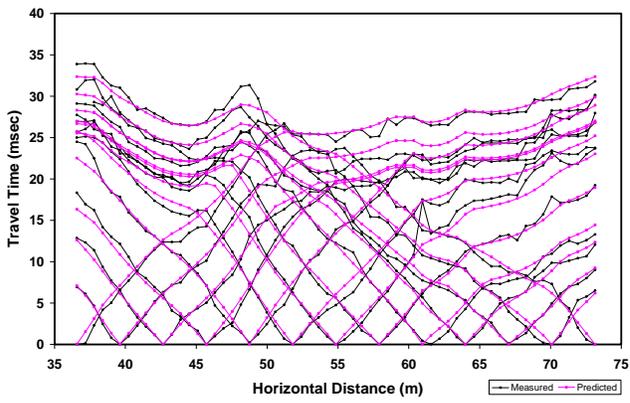


(c)

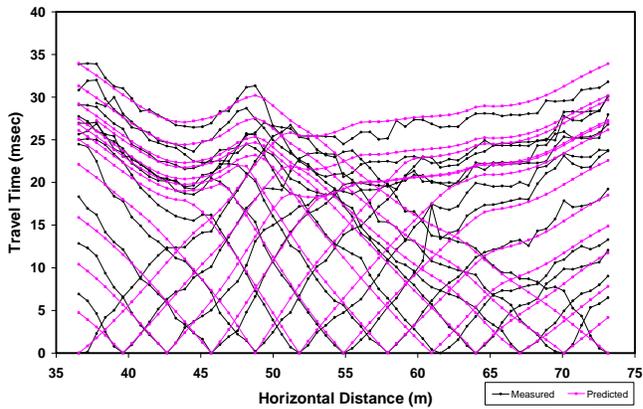
Figure 3-7 Measured vs. predicted travel time curves, A Line, station 0 – 36.6 m. (a) Rayfract travel times, (b) SeisImager travel times, and (c) SeisOpt Pro travel times.



(a)



(b)



(c)

Figure 3-8 Measured vs. predicted travel time curves, A Line, station 36.6-73.2 m. (a) Rayfract travel times, (b) SeisImager travel times, and (c) SeisOpt Pro travel times.

CHAPTER 4 COMPARISON OF SRT PROGRAM RESULTS AND INTRUSIVE TESTING DATA

4.1 Selection of Intrusive Test Locations

The selection of the seismic refraction testing locations were made blindly, with no information known regarding the subsurface from traditional geotechnical exploration methods, such as SPT and CPT borings. The seismic refraction field testing was performed and the data was then collected, processed, and imported into SeisImager to generate initial P-wave velocity tomograms. These preliminary velocity models were then reviewed and locations for the CPT soundings were selected based on features of interest such as valleys, or bowl-like features, and pinnacles.

Once the CPT soundings were completed the P-wave velocities from the SeisImager tomograms were noted at the top of bedrock depths. The P-wave velocities for these locations at the top of bedrock were found not to be consistent, but rather ranged from 600 m/s to 2200 m/s. In an effort to explain this, subsequent SPT and rock coring locations were then chosen in some of these locations, as well as others, to recover physical samples to try to find out why the P-wave velocity in the tomograms for the top of bedrock varied so greatly. Since the project did have financial constraints an intrusive test would not be able to be performed at every feature of interest, consequently intrusive tests were only performed along the A, F, U, and Z lines. However, the selections made were broad enough to ensure the major features of the subsurface imaged in the preliminary SeisImager tomograms would be able to be explored.

4.2 Types of Intrusive Testing Performed

The field exploration at this site consisted of three types of physically intrusive tests: CPT, SPT, and rock coring. These tests were chosen because they represent the most commonly used intrusive tests in practice, and in order for seismic refraction testing to be considered for

widespread use it will be necessary to show how well it compares against traditional methods. The following three sections provide technical detail and discuss the test procedures used for each of the three test types of intrusive tests used.

4.2.1 Cone Penetration Test (CPT) Procedure

CPT soundings were performed first at ten selected locations within the site during November of 2005. These locations, as previously discussed, were chosen as areas of interest based on the SeisImager tomograms. A Florida Department of Transportation (FDOT) field crew, using a Hogentogler Electric Cone Penetration Rig, performed the soundings at the locations selected. The soundings were performed in general accordance with the testing procedures outlined in the FDOT 2004 Soils and Foundations Manual. The CPT soundings were terminated at depths in which the tip met refusal due to the top of bedrock, approximately 30 MPa. This refusal was inferred to mean that the top of the bedrock had been encountered, SPT borings would later be performed at some of these locations to confirm this.

4.2.2 Standard Penetration Test (SPT) Procedure

SPT boring locations were chosen after the CPT soundings had been performed and were also compared to the tomograms. They were utilized in order to confirm the top of bedrock depth determined by the CPT soundings, as well as to recover a physical sample to learn more about the properties of the subsurface material. It was hoped that this would help explain the wide range of P-wave velocities encountered in the top of bedrock material. The SPT borehole locations were performed at eight selected locations during December of 2005 by Universal Engineering Sciences, Inc., and were performed in general accordance with the FDOT Soils and Foundations Handbook 2004.

A standard split spoon sampler was advanced 450 mm by dropping a 63.5 kg hammer on the drill rod from a height of 760 mm. The SPT boring was advanced continuously from 0.3 m

below the ground surface until the top of the bedrock was encountered and the Standard Penetration “N” values were recorded. To prevent the borehole from collapsing, and to wash away the soil cuttings, drilling mud was circulated as a 0.1 m diameter auger was used to widen the borehole after each sampling interval. The depth of the groundwater table was recorded and soil samples were classified.

Once the SPT borehole encountered the top of bedrock, 0.1 m diameter casing was set inside the borehole. The casing had “teeth” on the bottom of the initial length of casing to enlarge the hole and embed it several centimeters into the top of bedrock. With the casing now firmly set inside the borehole the rock coring was ready to proceed.

4.2.3 Rock Coring Procedure

Once the top of bedrock was encountered in each of the eight SPT boring locations, rock coring was initiated. The rock coring was performed using a diamond impregnated double barrel core bit with an inner barrel diameter of 85 mm. Water was circulated through to the bottom to cool the bit and wash away any cuttings. Rock coring was performed through the limestone in 1.5 m runs by the same drill rig used to perform the SPT borings. Coring was continued to a depth at which “good quality rock” was encountered. The rock core samples were recovered and later examined to provide more detailed information such as: Recovery (%), Rock Quality Designation (RQD) (%), and a physical description of the rock itself. The samples were saved so that future laboratory tests may be performed to further characterize them.

4.3 General Results of Intrusive Testing

The subsurface information obtained through the various intrusive testing methods revealed how variable the site is, see Appendix B for complete results of the intrusive testing. The top of bedrock varied from being visible at the ground surface to 9 m below the surface, depending on the location. Along with the changes in the depth to top of bedrock, the quality of

the rock, (RQD), varied greatly from each borehole and even within a single borehole. The overburden soil layers varied not only in depth due to the changing top of bedrock elevation, but also in type of soil at a particular depth from borehole to borehole, with no discernable pattern. One of the only constants in this extremely variable subsurface was the depth of the groundwater table, which was measured at approximately 4.6 m in each of the boreholes. The following sections provide a brief summary of the material encountered during the intrusive testing.

4.3.1 A Line Intrusive Testing Results

CPT soundings were performed at stations 19.8, 39.6, 44.2, and 65.5 m along the A line, with SPT borings and rock coring performed at stations 19.8, 36.6, and 65.5 m, see Appendix B for detailed information from these intrusive tests. The results showed the top of bedrock depth to vary greatly along the line ranging from 0.2 to 9.0 m, see Table 4-1 for specific top of bedrock depths at each intrusive test location. Likewise the overburden soil above the limestone also varied considerably, consisting of very loose to loose sand and clayey sands at varying depth and thickness, with station 19.8 m containing a layer of clay from 8.5 to 13 m deep. The limestone encountered not only varied in depth in which it was encountered, but also varied greatly with respect to RQD (%) as the rock coring was advanced. The logs frequently describe the limestone as being weak and containing fracture zones, with a cavity encountered at station 36.6 m from 5 to 5.3 m.

4.3.2 F Line Intrusive Testing Results

Along the F line from station 0-36.6 m two SPT borings with rock coring were performed at stations 3.0 and 13.7 m, see Appendix B for detailed information from these intrusive tests. A summary of the top of bedrock depths may also be seen in Table 4-2. The logs show at station 3.0 m highly weathered limestone was encountered at a depth of approximately 4.5 m. This limestone was overlain by alternating layers of soft to very soft clay and loose to medium dense

clayey sand, each of about 1 m in thickness. The RQD of the underlying limestone also alternated between the lengths of core run from 0% and approximately 40 to 60%.

The boring logs at station 13.7 m showed that heavily weathered limestone was encountered at 1.7 m with more competent limestone, RQD 70%, being encountered at 3.4 m. The overburden material consisted of a 1 m layer of soft clay underlain by a 0.7 m layer of loose sand with clay and gravel. Numerous fractures and fossils were noted within limestone in the rock coring logs.

4.3.3 U Line Intrusive Testing Results

CPT soundings were performed along the U line at stations 8.5, 24.4, 36.6 and 73.2 m along with a single SPT boring and rock coring performed at station 24.4 m, detailed logs for each of the intrusive tests performed on this line may be found in Appendix B. The depth to top of limestone varied at the intrusive test locations along the line from 1.2 to 8.2 m, see Table 4-3 for specific top of limestone depths at each intrusive test location. Because soil sampling was only performed at the single SPT location along the line, the only description of subsurface is available at station 24.4 m, which showed the top of limestone to be at a depth of 8.2 m, overlain by layers of loose sand and very soft to soft clay. The rock coring logs show the RQD to gradually decrease from 60% at 9.5 m to 20% at 14 m where a sandy clay filled cavity was encountered from 14 m to the end of hole depth at 15.5 m.

4.3.4 Z Line Intrusive Testing Results

Along the Z line two CPT soundings were performed at stations 35 and 64 m along with two SPT borings and rock corings at stations 21.9 and 35 m, the complete logs of the intrusive testing performed along the Z line may be seen in Appendix B. Based on the intrusive tests the depth to the top of competent limestone ranged from 6.1 to 7.8 m along the line, see Tables 4-4 and 4-5 for a summary of the top of limestone depths encountered along the Z line. Compared to

the results from the other lines tested this was the least amount of variation with respect to top of bedrock depth along a single survey line, using the limited amount of intrusive data available.

At station 21.9 limestone was encountered 7.3 m deep, with a RQD of 50%, and was overlain by an approximately 1.0 m thick layer of heavily weathered limestone, overlain by 1.2 m of stiff clay, overlain by 5.3 m of sand. Likewise the boring logs from station 35 m show limestone to be at a depth of 6.4 m, RQD of 50%, overlain by 1.2 m of heavily weathered limestone with clay overlain by 3.7 m of soft to stiff clay overlain by 1.5 m of loose clayey sand and sand. Both of the rock coring logs note core runs containing fractures within the limestone, with station 21.9 m noted as containing a sand and clay filled cavity between 13.6 and 15.1 m deep.

4.4 Comparison of Intrusive Testing to the SRT Tomograms

Upon completion of the intrusive field testing program, final tomograms were produced using each of the three SRT programs, as described in Chapter 3. The next step was to see how these tomograms compared to the information obtained from the intrusive testing. In comparing, the principal objective was the ability of the SRT programs to delineate the laterally variable soil/bedrock interface. The ability to delineate this interface accurately for the locations in which this information is known would give the user confidence about the programs abilities to delineate this interface in regions for which no information is available. At sites with uniform bedrock properties this may be accomplished by simply identifying the P-wave velocity of the material, which should remain relatively constant along the survey line, and tracing it across the tomogram to delineate the soil/bedrock interface. For this site a simple constant P-wave velocity delineation of the soil/bedrock interface will probably not be possible due to variation in the bedrock material due to its geologic history.

4.4.1 Comparison of A Line Tomograms to Intrusive Test Results

The intrusive testing results were first compared along refraction survey line A from stations 0-36.6 m, see Figure 4.1. The first step in the comparison was to make note of the P-wave velocity in the tomograms at the depth in which the intrusive tests encountered the top of bedrock to see if a specific velocity or a small range of velocities could be identified as the top of bedrock velocity. The top of bedrock at station 19.8 m was encountered by the intrusive testing at a depth of approximately 9.0 m below the ground surface. When the tomograms for each of the three programs were examined at this location the P-wave velocity was approximately 2000 m/s, depending on which of the three tomograms was used.

Three CPT soundings and one SPT boring were performed along the second A line of refraction, stations 36.6-73.2 m, see Figure 4.2. The CPT sounding at station 39.6 m was terminated before a large tip resistance was encountered at depth of about 2.2 m because the CPT rod was bending seriously to the south as penetration was attempted. After a close review of the tomograms, Figure 4.2, it can be seen that station 39.6 m appears to be just to the left, or south, of the top of a block/pinnacle feature, and that the bending of the CPT rod to the south of the site is consistent with the subsurface featured in the tomograms (Hiltunen et al. 2007). The P-wave velocity of the material at the depth the CPT met refusal was approximately 700 m/s, based on the tomograms.

CPT soundings were also performed at stations 44.2 m and 65.5 m, with the tip resistance approaching 30 MPa at approximately 0.2 and 0.4 m, respectively. A SPT boring was also performed at station 65.5 m, which confirmed the top of limestone depth to be at 0.3 m, with the RQD being approximately 75 %. The P-wave velocities determined from the tomograms for this shallow top of limestone region ranged between 600 and 800 m/s, depending on the tomogram. Small limestone outcrops were visible at the ground surface, and noted for the A line for station

62.5 to 64 m and 66.1 through 67.1 m. This shallow depth to top of bedrock appears to be consistent with the pinnacle/block type feature imaged by each of the tomograms at these locations.

After review of the P-wave velocities at the top of bedrock depth it became obvious that not only did the depth of limestone vary greatly across the line, ranging from the ground surface to 9.0 m deep, but so did the P-wave velocity, ranging from 600 m/s to 2000 m/s, see Table 4-1 for a summary of the top of bedrock P-wave velocities determined from the tomograms. As a result it would not be possible to determine the top of bedrock depth by simply tracing a single velocity contour line across the tomogram, as the top of bedrock velocity changed greatly along the survey line. With the contour interval for the tomograms set at 100 m/s, general subsurface features were evident such as valley and block/pinnacle type features. However, the depth to the soil/bedrock interface is not immediately obvious to the user.

In an attempt to try and make the soil/bedrock interface within the tomograms more visually apparent, the contour intervals within Surfer were reduced for each of the three SRT programs. It was found that by reducing the contour interval to 10 m/s for the Rayfract tomograms along the A line stations 0-36.6 m that the contour intervals would concentrate to the point of being so close that they appeared solid or near solid at depths corresponding with the top of bedrock measured from the intrusive tests, see Figure 4.4. The contour fill coloring and labeling was also removed to make this concentration of contour lines more apparent. This concentration at the location of the soil/rock interface makes physical sense because there should be a large gradient (change) in P-wave velocity due to the abrupt material change, and this large change should be observed in the tomogram via a dense concentration of contour lines.

In order to confirm this, the next step was to compare the location of the increased contour line concentration in the Rayfract tomograms against the results of the intrusive testing program. The top of limestone depth seemed to corresponded well with the depth of contour line concentration, see Table 4-2 for a comparison of intrusive top of limestone depth versus the depth of the contour line concentration at that depth. For example, along the A line at station 19.8 m the SPT and CPT testing determined the top of limestone to be at approximately 9.0 m, see Figure 4.3 (a). Looking at the Rayfract model, a large concentration of contour lines occurs at depth of approximately 8.8 m in the Rayfract tomogram. Although no further intrusive test data exists for this line, if one were to trace the front of contour line concentration from station 19.8 m, presuming this did delineate the top of bedrock, one would expect to find pinnacle/block like features at depth of approximately 1.0 m at stations 13.0 and 27.0 m with the top of bedrock undulating from left to right. It would be interesting to see if future intrusive testing confirmed this hypothesis. A similar trend was noted for the A line station 36.6-73.2 m Rayfract tomogram, see Figure 4.5.

In their analysis of synthetic models, Sheehan et al. (2005b) found SRT programs to be incapable of accurately imaging abrupt velocity changes. Instead they smear the boundary into a gradient. Therefore, boundaries must be interpreted from areas of maximum gradient. Reducing the contour interval to 10 m/s visually shows this increase in gradient as closely spaced P-wave velocity contour lines. The largest increase in gradient, or concentration of contour lines, should occur where the greatest increase in P-wave velocity occurs, typically at the soil/rock interface.

It should also be noted that a similar procedure was tried for the SeisImager and SeisOpt tomograms, however they were unable to show any concentration of contour lines at locations corresponding to the top of bedrock depth, see Figures 4.3 (b) and (c) and Figures 4.5 (b) and (c).

However, when the contour interval was set at 50 m/s for SeisImager and SeisOpt Pro for the A line 0-36.6 m tomograms, some concentrations were able to be seen near depths corresponding to the top of bedrock depth at some of the intrusive test locations. However, this close contour depth was not as obvious, and did not correspond as closely to the intrusive test results as the Rayfract tomogram did, see Figure 4.4.

The reason believed as to why Rayfract was able to show this concentration of contour lines clearer and more accurate than the other two SRT programs probably is due to the fact that during the inversion process it creates a dense grid file of the velocity model that is updated after each iteration and is exported to Surfer. A grid is a rectangular region composed of evenly spaced rows (the y coordinate), and columns (the x coordinate), with the intersection of a row and a column called a grid node. By generating a grid file Surfer will interpolate or extrapolate a Z value (velocity) at each unknown grid node based on known data values. For the models produced in Rayfract the grid size was typically 300 rows by 600 columns. SeisImager and SeisOpt Pro simply provide the x and y coordinates with the respective velocity (z) at a data point, and do not interpolate for values in between. Rayfract models typically contained approximately 2000 data points in the initial model, compared to approximately 1200 in SeisImager and 3000 in SeisOpt Pro.

However, because Rayfract updated the entire velocity grid file after each iteration, interpolating to determine unknown values at the grid nodes, it typically contained between 70,000-100,000 node values. By having so many more nodes to create contour lines with, Rayfract was able to show this concentration clearer, smoother, and more accurately than SeisImager or SeisOpt Pro, despite having less actual data points in the initial model than SeisOpt Pro. Grid sizes were also increased to the same Rayfract values from the Surfer default

values for the SeisImager and SeisOpt Pro models, with little, if any, improvement in accuracy noted visually. The possibility also exists that Rayfract may be more accurate due to a setting in the code that automatically creates a Surfer file of the final velocity model, although no differences could be found through a basic inspection of the code.

4.4.1.1 Sinkhole Observations Along the A Line

As noted above, the seismic refraction field testing was conducted during the summer of 2005, with the intrusive testing performed during November and December of 2005. Following a period of heavy rain and storm water runoff in February 2006, two sinkholes formed along the A line at approximately stations 19.5 m and 52.1 m. These two locations appear as valley/bowl features in the P-wave velocity tomograms, Figures 4.1 and 4.2. The valley/bowl feature was especially well documented for station 19.5 m, as a CPT and SPT boring had been performed at station 19.8 m. Sinkhole formation in these valley/bowl type features seems much more likely than at the top of the block/pinnacle features, and the ability to image these valley/bowl type features could potentially make seismic refraction tomography useful in identifying high-risk areas for sinkhole development (Hiltunen et al. [2007]).

4.4.2 Comparison of F Line Tomograms to Intrusive Test Results

Two SPT borings along with rock coring were performed along the F line. The first boring at station 3.0 m showed highly weathered limestone encountered at approximately 4.5 m, with limestone of higher quality, RQD 50%, encountered at 6.4 m. Due to the proximity of the boring at station 3.0 m to the end of the refraction array, and resulting shallow tomogram modeling in these areas, P-wave velocities can only be compared in the very top of the limestone material using the SeisImager tomogram because the other two programs did not produce a tomogram to

that depth. This P-wave velocity was found to be approximately 700 m/s, see Table 4-3 for a summary of the top of bedrock P-wave velocities and Appendix A for the tomograms.

The second SPT boring performed along the survey line was at station 13.7 m. Highly weathered limestone with numerous large voids and a RQD of 0% was encountered at 1.7 m extending to 3.4 m where the quality of the rock increased to 70%. The P-wave velocity of this more competent limestone at 3.4 m was 800 m/s. The tomograms appear to show more of a valley/bowl like feature at station 3.0 m when compared to station 13.7 m, and results from the intrusive testing seem to confirm that the top of bedrock is at a greater depth.

A close examination of the tomograms, Figure C-1 in Appendix C, reveals that the downward slope of the velocity contour lines toward station 13.7 m from the pinnacle/block feature at station 8.0 m is less than the slope from station 8.0 m to station 3.0 m. Station 3.0 m also appears to be more at the bottom of a valley, while station 13.7 m appears to be slightly before the bottom of the valley. The shapes within the tomograms seem to indicate that the top of rock elevation should be deeper at station 3.0 m than 13.7 m. The SPT tests confirm this hypothesis as the top of bedrock was encountered at 4.5 m for station 3.0 m, and at 1.7 m at station 13.7 m.

An examination of the Rayfract and SeisOpt Pro tomograms with a contour interval of 10 m/s at station 13.7 m, using the same procedure used in the A-line comparison, showed a concentration of contour lines at depth of approximately 3.5 m, see Figure D-1 in Appendix D. This compares well with the SPT result at this location, which showed the depth to the top of limestone to be at 3.4 m. The SeisImager tomogram was also examined, however the concentration of contour lines was observed to begin at approximately 2 m.

4.4.3 Comparison of U Line Tomograms to Intrusive Test Results

Along the U line from station 0-36.6 m, three CPT soundings and one SPT boring with rock coring were performed. The first CPT sounding was performed at station 8.5 m, and recorded the top of limestone depth to be 1.8 m, see Table 4-4 for a summary of these depths and Figure D-2 in Appendix D for the tomograms. The approximate P-wave velocity determined from the tomograms at this depth was 700 m/s. The second CPT sounding was performed at approximately station 24.4 m, and was pushed to refusal at a depth of 8.2 m. A SPT boring at this location confirms the top of limestone to be at a depth of 8.2 m. The P-wave velocity from the tomograms at this depth of 8.2 m was approximately 1600 m/s.

During the rock coring at station 24.4 m a cavity containing sandy clay was encountered from 14.0 m and extending past the end of the hole at 15.5 m. The tomograms were examined to see if they were able to image this cavity encountered. The SeisImager tomogram is the only one of the three that shows anything, an oval feature that may be indicative of a cavity. However, this is most likely the result of the lack of ray path coverage passing through this area and not due to SeisImager actually imaging the cavity.

The third CPT test along this line was performed at the very end of the refraction array, station 36.6 m, with the tip meeting refusal at approximately 1.5 m below the ground surface. The approximate P-wave velocity from the tomograms at this depth was 600 m/s. Data evaluated at the end of an refraction array should be viewed with caution as often the ray coverage is insufficient for the user to rely on features of the tomogram produced, however, for this location and depth, 1.5 m, the ray path coverage appears to be adequate for comparison.

When looking at the gross features of the tomograms the two outer locations of intrusive testing, stations 8.5 and 36.6 m, appear to be on more pinnacle/block type features, see Figure D-2. The top of bedrock depths determined from the intrusive testing, 1.8 and 1.5 m, also support

this. On the other hand, station 24.4 m appears to be near the bottom of a valley based on the tomograms, confirmed by the top of rock being encountered at 8.2 m. Simply by looking at the tomograms the user could note the gross features and probably expect the boring at station 24.4 m to encounter top of limestone at a greater depth.

However, it was not visually obvious from the tomograms that the variation in top of bedrock depth would be as great as was encountered. While rock coring was not performed at stations 8.5 and 36.6 m, the reason for this variation is most likely due to the fact the limestone encountered at these locations has been weathered heavily to the point where the P-wave velocity has been reduced to velocities closer to the surrounding particulate overburden material. As a result, the P-wave velocity contrast between the limestone and overburden soil in the tomograms using a 100 m/s contour interval is not as great.

However, once the contour interval was reduced to 10 m/s in the Rayfract model, the top of limestone depth could be observed as a boundary where the contour lines experienced a large concentration, see Appendix D. At station 8.5 m the top of bedrock was encountered at approximately 1.8 m, and at station 24.4 m the top of bedrock was encountered at a depth of 8.2 m. When comparing these locations and associated depths to top of limestone depth to the reduced contour interval tomogram, the concentration of contour lines present appears to be in agreement with the location of the top of bedrock as determined by the intrusive testing. The SeisImager and SeisOpt Pro tomograms were examined as well. However, the correlation between the beginning of the close contour lines and the top of bedrock was not as strong as Rayfract, see Figure D-2.

4.4.4 Comparison of Z Line Tomograms to Intrusive Test Results

Along the Z line from stations 0-38.4 m, two SPT and one CPT test were performed, see Table 4-5 for a summary of the top of bedrock depths along with P-wave velocities and Figure

C-3 in Appendix C for the tomogram. The first SPT test was performed at station 21.9 m, and the top of bedrock was encountered at depth of approximately 7.3 m, with highly weathered limestone encountered at 6.5 m. The P-wave velocity determined from the tomograms at the top of the more competent limestone at 7.3 m was approximately 1300 m/s, depending on the SRT program. A SPT and CPT test was also performed at station 35.0 m, with the heavily weathered limestone encountered at a depth of 5.2 m, and the more competent limestone found at 6.4 m. This test was performed near the end of the refraction line, and only SeisImager generated a tomogram to that depth, showing a P-wave velocity of 1100 m/s.

A CPT was also performed at station 64 m with refusal at 7.8 m, see Figure C-4. The Rayfract and SeisImager tomograms show the P-wave velocity as 1400 m/s, while the SeisOpt model shows it as 1900 m/s. This was the largest disparity noted when comparing the P-wave velocity at the depth of the top of bedrock between the three SRT programs across all lines, and can probably be attributed to the fact that this depth was near the bottom of the SeisOpt model, and appeared to be located at or near an artifact in the model.

The Z line exhibited the least amount of variability in the depth to top of bedrock, ranging from 6.4 to 7.8 m. While this may be the line that exhibits the least depth to top of bedrock variability, it provides an important test for the close contour interval tomograms to see if it will hold up the along a more horizontal surface, see Figures D-3 and D-4 in Appendix D. Perhaps the imaging of the valleys in the previous tomograms was the result of something within the Rayfract inversion routine and merely coincidental. The close contour tomograms for the two lines do appear to show the largest contour line concentrations pretty consistently at about the 6 to 7m depth across the Z line, which is consistent with what was found using the limited amount of intrusive testing. However, upward curvatures of lesser contour line concentrations do exist in

the tomograms, as there is only limited intrusive test data available, it remains to be seen if they are indicative of actual subsurface features or just an artifact of the modeling.

4.5 Geological Explanations for Variability in P-wave Velocity

The limestone bedrock (Ocala Limestone) was formed in the Upper Eocene (Scott[1991]). The limestone itself was formed in a variety of environments, notably open marine, shallow water, and middle shelf deposition, with a wide variety of organisms that contributed to the formation of the limestone. The upper surface of the Ocala limestone has undergone dissolution during a major sea level drop that occurred during the late Oligocene and early Miocene. This event is the precursor to the karst terrain that later developed (Randazzo [1997]).

As discussed in the previous sections the P-wave velocity of the limestone measured at the top of a block/pinnacle structure is significantly less than the P-wave velocity measured at the bottom of a valley. During the weathering/dissolution/ karstification that occurred, the limestone was most susceptible to weathering was weathered from the top down, leaving behind slots and valleys. The more competent limestone was able to withstand this weathering and is marked today by the block and pinnacle structures, which are highly weathered but are the most competent of the highest weathered rock. So the low P-wave velocities measured at these block pinnacle structures, and the comparatively higher P-wave velocities measured within the valley regions may be explained by the geologic history of the limestone.

4.6 CPT Tip Penetration and P-Wave Velocity

As previously discussed, the P-wave velocity at the depth to the top of bedrock, where CPT refusal was met, ranged from 600 to 2000 m/s. In looking at the tomograms produced it is also interesting to note that the CPT tip will penetrate through a high velocity particulate material such as sand, like along the A line at station 19.8 m, but met refusal in lower velocity rock, like at station 65.5 m. This is because P-wave velocity is related to the small-strain modulus of the

material, while CPT tip resistance is related to the strength of the material. So even though the rock at station 65.5 m is broken and has a velocity much lower than the particulate material at station 19.8 m, it will have a higher local tip resistance because the broken pieces are still an intact, cemented material, and highly resistant to local CPT penetration (Hiltunen et al. [2007]).

4.7 Comparison of the SRT Raytracing Models to Intrusive Test Results

A further step that was taken in comparing the raytracing diagrams produced by the SRT programs to the intrusive test results. Areas of relatively large contrast in P-wave velocity, like the boundary between soil and bedrock, should show up on the raytracing diagram as a location in which the P-waves concentrate and travel laterally along the higher velocity material. This shows itself on the raytracing diagram as areas in which there is a concentration of propagated rays traveling through. These areas should be indicative of changes in the P-wave velocity, type of material, and consequently should correspond with changes noted on the intrusive testing data logs.

4.7.1 A line 0-36.6 m SRT Raytracing Models to Intrusive Test Results

Rayfract was the first SRT program raytracing diagram to be examined. Rayfract outputs its raytracing diagram, which shows the wavepaths used to generate the velocity model, as a contour map into Surfer in which areas with greater contour values correspond to areas in which a greater number of wavepaths travel through. The Rayfract wavepath model for refraction survey line stations 0-36.6 m diagram was examined first at station 19.8 m, where SPT and CPT data were available, see Figure 4.6(a). A sudden increase in number of wavepaths traveling through was measured starting at a depth of approximately 9.0 m, the same depth at which the top of bedrock was noted for the SPT and CPT tests. A distinctive bowl shaped feature, characteristic of severely weathered karstic limestone with known previous sinkhole formation,

was also observed at this location. This indicates that the program has modeled a relatively higher velocity layer at 9.0 m along which the rays travel laterally along.

The SeisImager raytracing model was examined next. SeisImager uses a simpler raytracing method that shows the calculated straight line path from the source and the layer along which the refracted arrivals travel laterally to the receiver for the first arrival P-waves propagated. The SeisImager raytracing model was viewed within the program, as it did not provide an option to save in a format in which it could be imported into Surfer. At station 19.8 m at a depth of approximately 9.1 m several rays travel laterally, which indicates that the program has modeled a relatively higher velocity layer along which the rays travel along, see Figure 4.6(b). This depth corresponds with the depth to the top of limestone determined via the intrusive testing. SeisImager also showed several other areas of laterally traveling rays, making it less visually obvious as to where the soil/bedrock interface was.

SeisOpt computes the ray paths for each source/receiver pair, and then determines the number of times each cell in the model is crossed (“hit”) by a ray path and then creates an output file known as a “hitfile” (Optim LLC, [2004]). This hitfile was imported into Surfer and a contour map was created to provide a visual representation of this for the A line from 0-36.6 m, see Figure 4.6(c). A significant increase in the number of “hits” is can be observed at a depth of approximately 9.1 m at station 19.8 m, corresponding with the depth of to the top of bedrock determined by the intrusive testing.

4.7.2 Comparison of A Line 36.6-73.2 m Raytracing Models to Intrusive Test Results

The same procedure described in the previous section was used to compare the ray path models to the intrusive testing data, see Figure 4.7. Three CPT penetrations were performed at stations 39.6, 44.2, and 65.5 m, as well as one SPT boring at station 65.5 m. In the SeisImager model at test station 39.6 m, the nearest area of laterally traveling rays to the top of bedrock

determined to be at approximately 2.2 m is at approximately 1.6 m below the surface, see Figure 4.7(b). The difference between the two may be a result of the limited ray path coverage on the end of a refraction array. At station 44.2 m a strong refractor appears to be present at 0.2 m based on the ray paths, corresponding with the depth to the top of limestone determined by the CPT test. Next the ray paths were examined at station 65.5 m and a concentration of ray paths existed at 0.3 m, the depth at which the CPT and SPT borings determined the top of limestone to be at.

The Rayfract wavepath model was also examined to see if the depth to the top of limestone at the three intrusive test locations corresponded with significant increases in wavepaths. This seemed to be visually obvious at only one of the three test locations, station 65.5 m, see Figure 4.7(a). Likewise the SeisOpt Pro model was examined and nothing was visually apparent to indicate where the depth to the top of limestone may exist, see Figure 4.7(c). The reason for this is most likely due to the fact that the P-wave velocity of the shallow top of bedrock material encountered is relatively low, 600-800 m/s, and does not provide enough contrast against the velocity of the overburden soil to show any features indicative of the soil/bedrock interface.

4.7.3 General Observations for each of the Three SRT Programs Ray Path Diagram Comparisons to the Intrusive Test Data

The ray path diagrams were also examined for each of the three SRT programs for the four remaining lines that intrusive test data was available for, F line station 0-36.6 m, U line station 0-36.6 m, Z line station 0-38.4 m, and Z line station 36.6 -73.2 m, shown in Appendix E. For each of these remaining lines, the Rayfract wavepath diagrams were able to show a significant increase in the number of wave paths traveling through depths that corresponded with the depth to the top of competent limestone. The SeisOpt Pro ray path diagrams showed an increase in the number of ray paths going through cells at depths corresponding to the top of competent

limestone for all of the remaining ray path models, with the exception of F line stations 0-36.6 m. The SeisImager ray path diagrams showed the ray paths traveling laterally for each of the 4 remaining lines at depths corresponding to the top of limestone.

Interestingly, the SeisImager ray path diagrams also showed several laterally traveling ray paths that corresponded with changes in the overburden material in all of the models, such as changes from sandy to clayey material. Although an area of lateral ray path travel can be found at the depth of the top of limestone for SeisImager, many other areas of lateral ray path travel exist at various depths of the model. The SeisImager model shows where changes in material occur, however, the user would probably not be able to tell what that change was, i.e. the soil/rock interface or a sand to clay layer change. Despite SeisImager not being able to show visually easily where the soil/rock interface was, it is still able to pick up actual changes in material type at the proper depth, giving the user more confidence in the tomograms generated of the subsurface.

The ability of SeisImager to identify the depths of soil changes via refraction boundaries may be a function of the simple, thin line ray tracing model it produces as opposed to Rayfract and SeisOpt which show the number of times a ray has traveled through a cell. SeisImager does not show the number of rays which travel through a cell in the model making it difficult to determine where the soil/rock interface begins because this interface typically has a large P-wave velocity contrast and consequently is an area through which a large number of rays should travel through. So, while SeisImager may be able to show where changes in materials take place visually, it does not clearly show where the top of limestone begins as well as Rayfract and SeisOpt. Obviously, being able to delineate the top of bedrock is an important ability that SRT programs must have.

Table 4-1 P-wave velocities from tomograms at top of bedrock depths determined by intrusive test data for the A line

Location	Intrusive Test Method	Depth to Bedrock (m)	P-wave Velocity from Tomograms (m/s)
A-19.8	CPT and SPT	9.0	2000
A-39.6	CPT	2.1	700
A-44.2	CPT	0.2	600
A-65.5	CPT and SPT	0.3	800

Table 4-2 Comparison of depth to bedrock determined from intrusive testing and visually inferred from close contour interval, 10 m/s, tomograms for the A line. Note: (1) Unable to differentiate an exact depth of concentration from Rayfract tomogram

Location	Intrusive Test Method	Intrusive Testing Depth to Bedrock (m)	Approximate Depth to Concentration of Contour Lines in Rayfract Tomogram (m)
A-19.8	CPT and SPT	9.0	8.8
A-39.6	CPT	2.1	N/A ⁽¹⁾
A-44.2	CPT	0.2	0.3
A-65.5	CPT and SPT	0.3	0.2

Table 4-3 P-wave velocities from tomograms at top of bedrock depths determined by intrusive test data for the F line. Note: (1) Velocity determined only from the SeisImager tomogram.

Location	Intrusive Test Method	Depth to Bedrock (m)	P-wave Velocity from Tomograms (m/s)
F-3.0	SPT	6.4	700 ⁽¹⁾
F-13.7	SPT	3.4	800

Table 4-4 P-wave velocities from tomograms at top of bedrock depths determined by intrusive test data for the U line.

Location	Intrusive Test Method	Depth to Bedrock (m)	P-wave Velocity from Tomograms (m/s)
U-8.5	CPT	1.8	700
U-24.4	CPT and SPT	8.2	1600
U-36.6	CPT	1.5	600

Table 4-5 P-wave velocities from tomograms at top of bedrock depths determined by intrusive test data for the Z line.

Location	Intrusive Test Method	Depth to Bedrock (m)	P-wave Velocity from Tomograms (m/s)
Z-21.9	SPT	7.3	1300
Z-35	CPT and SPT	6.4	1100
Z-64	CPT	7.8	1400

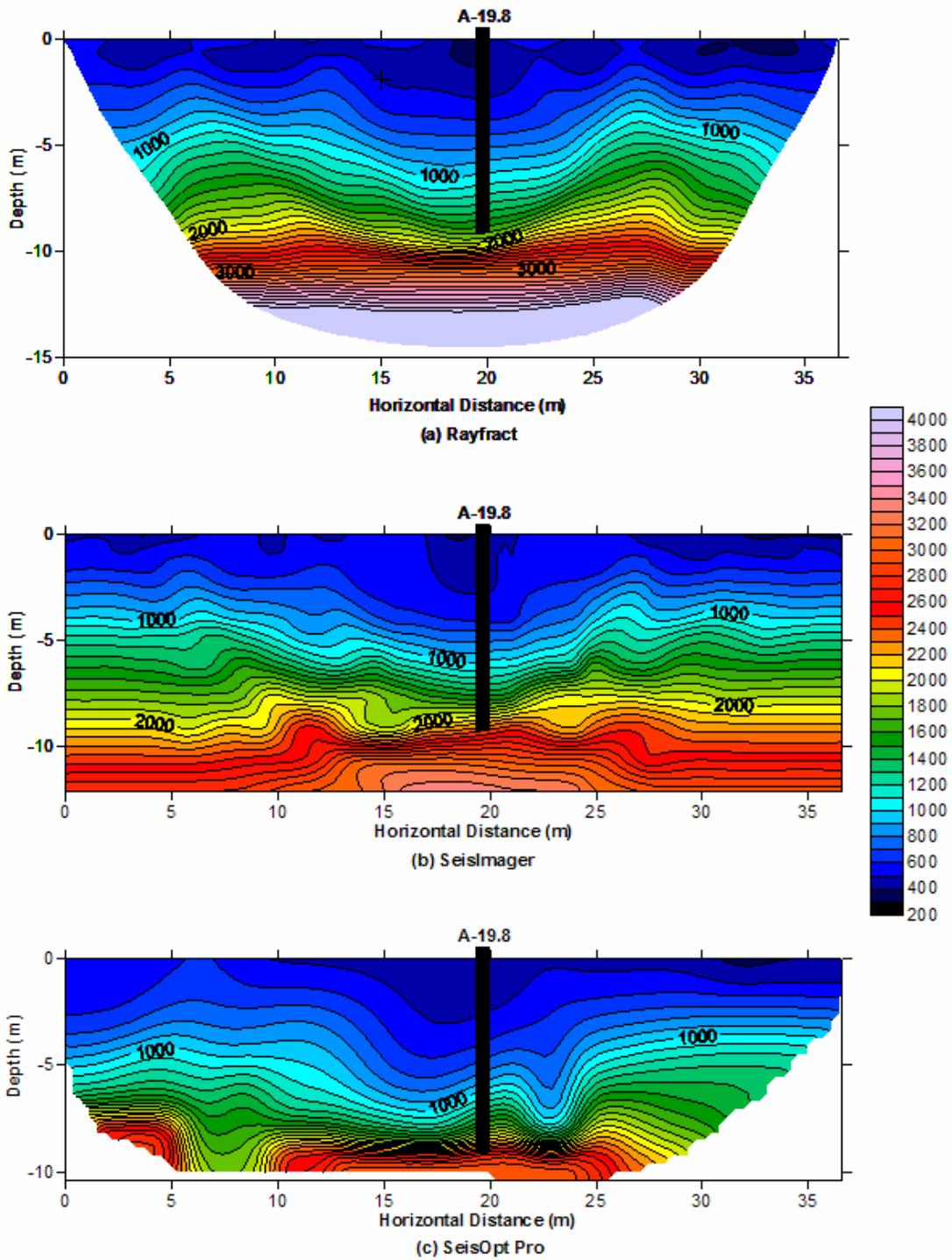


Figure 4-1 Estimated top of bedrock from intrusive testing overlain onto tomograms produced for A line station 0-36.6 m. (a) Rayfract, (b) SeisImager, and (c) SeisOpt Pro.

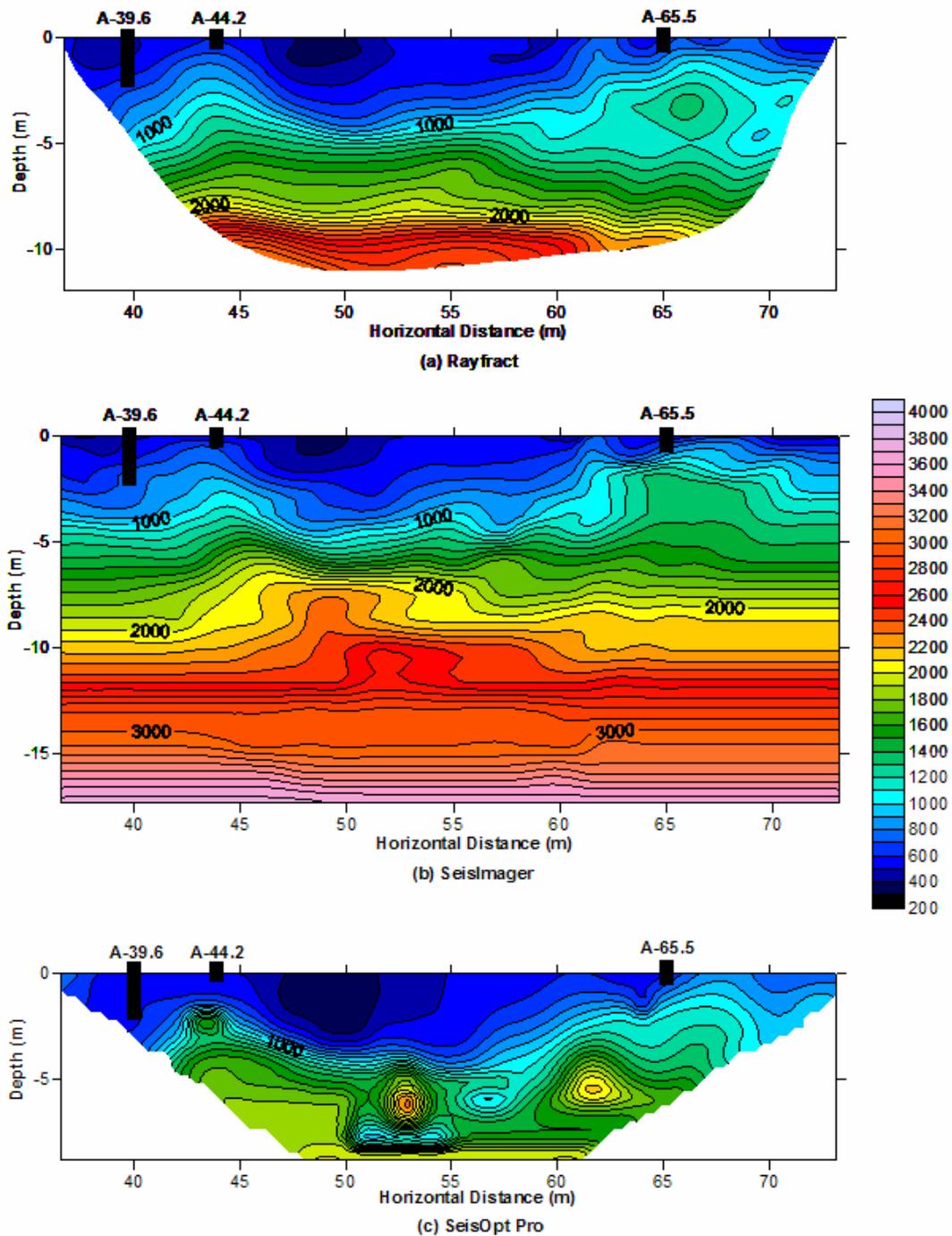
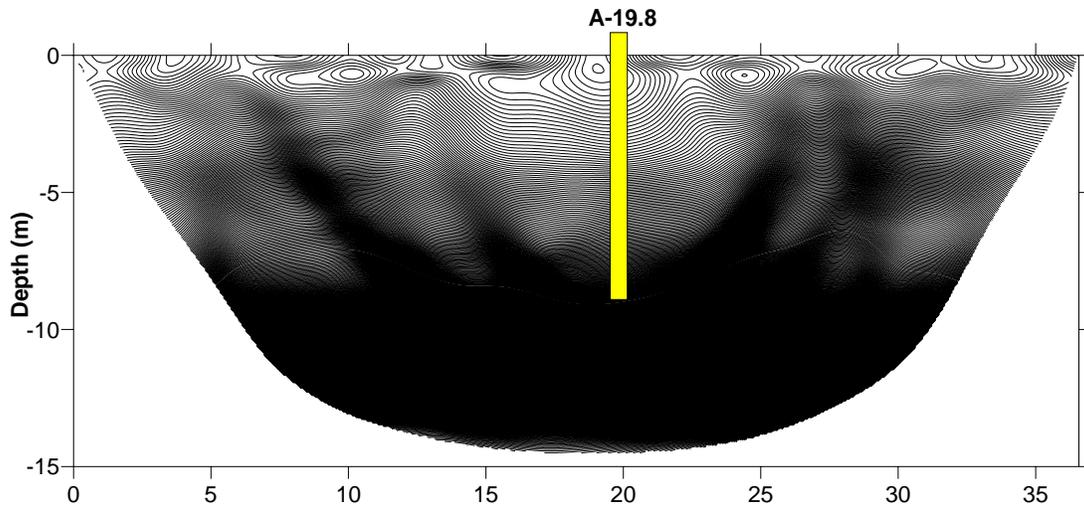
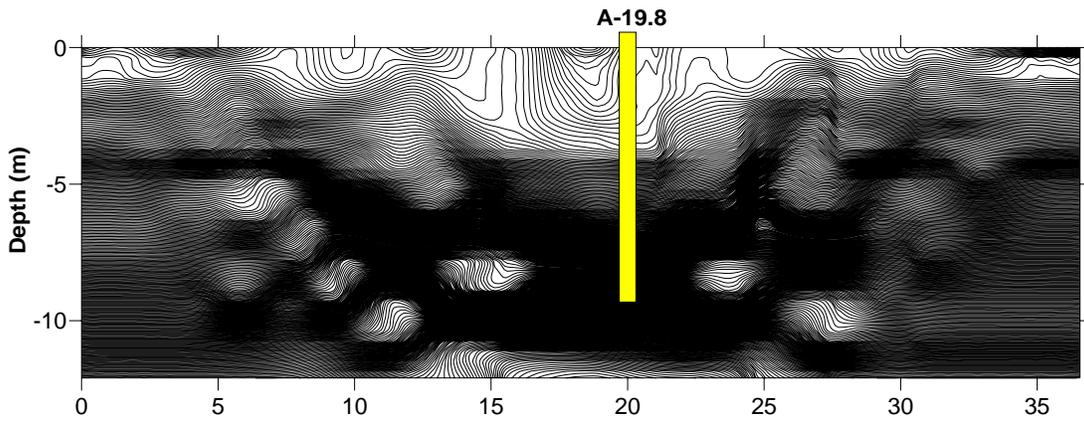


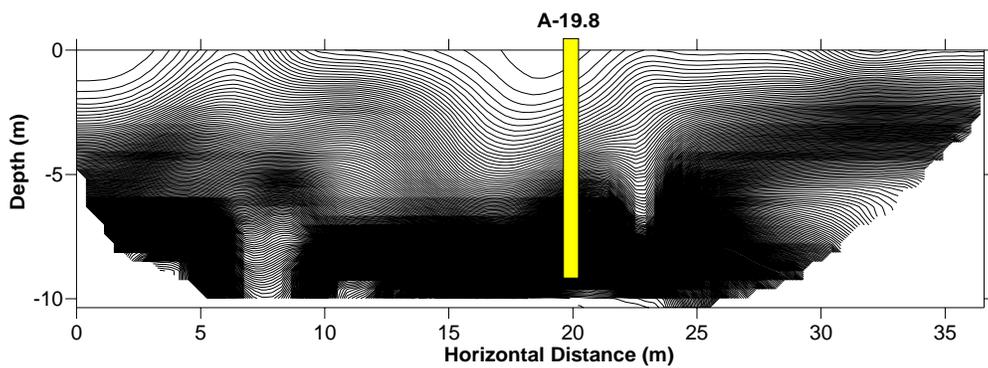
Figure 4-2 Estimated top of bedrock from intrusive testing overlain onto tomograms produced for A line station 36-73.2 m. (a) Rayfract, (b) SeisImager, and (c) SeisOpt Pro.



(a) Rayfract



(b) SeisImager



(c) SeisOpt Pro

Figure 4-3 Estimated top of bedrock from intrusive testing overlain onto 10 m/s contour interval tomograms produced for the A line 0-36.6 m. (a) Rayfract, (b) SeisImager, and (c) SeisOpt Pro.

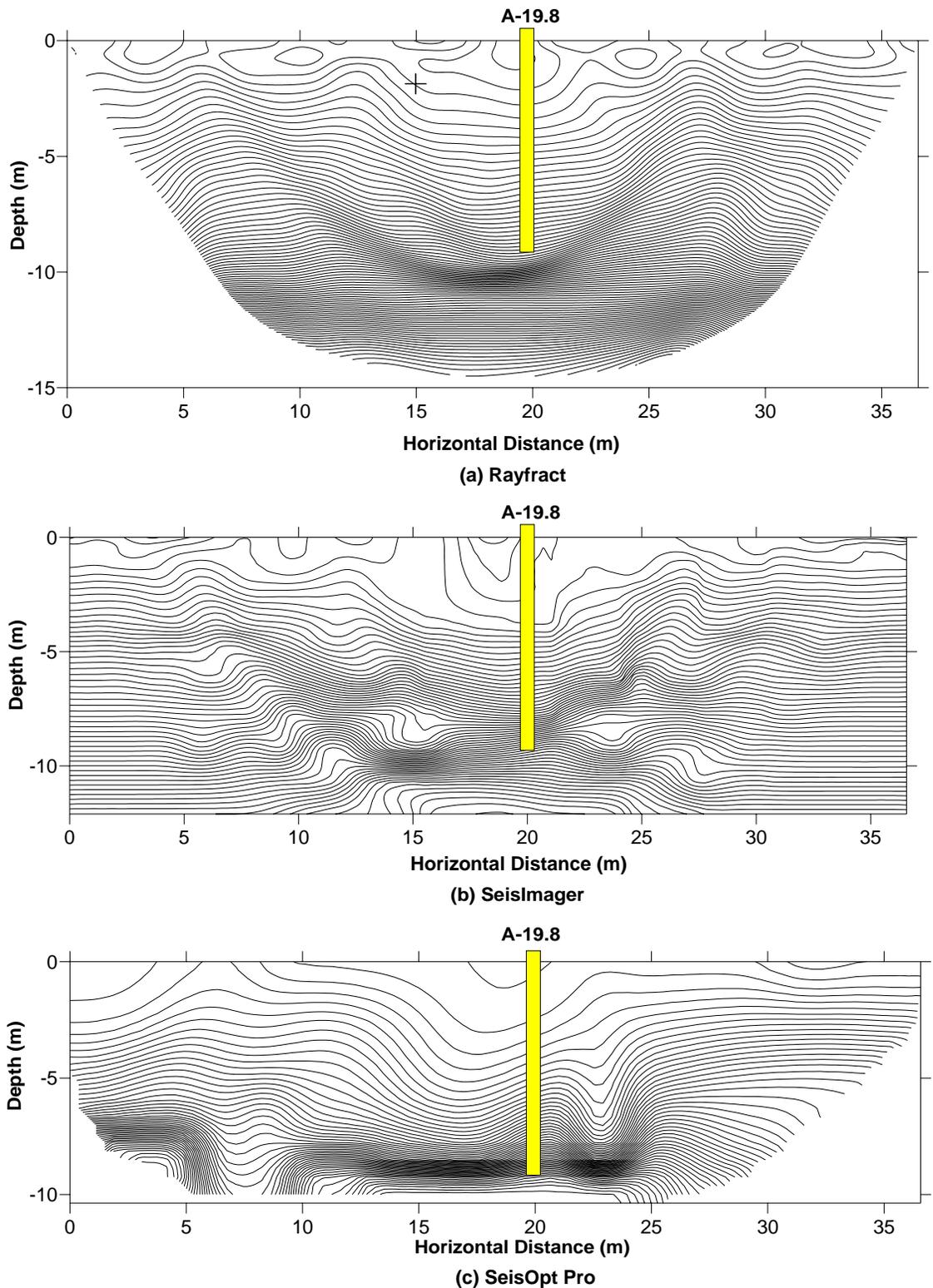
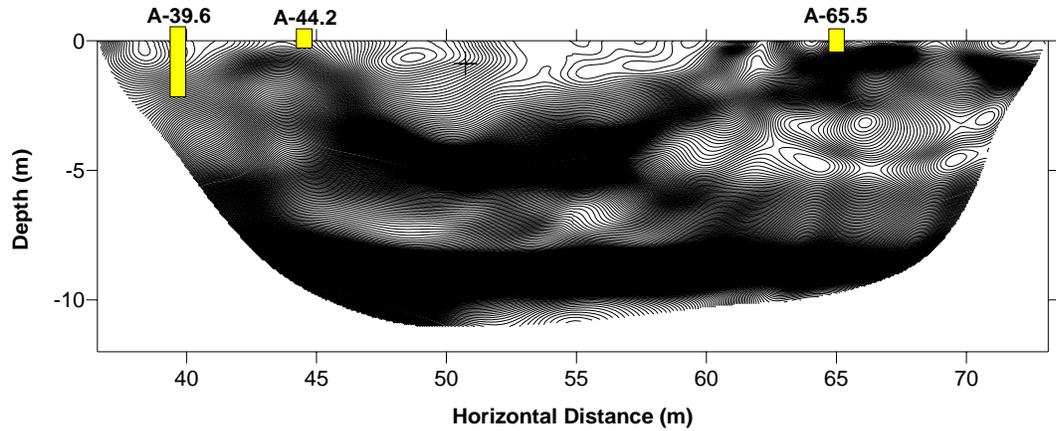
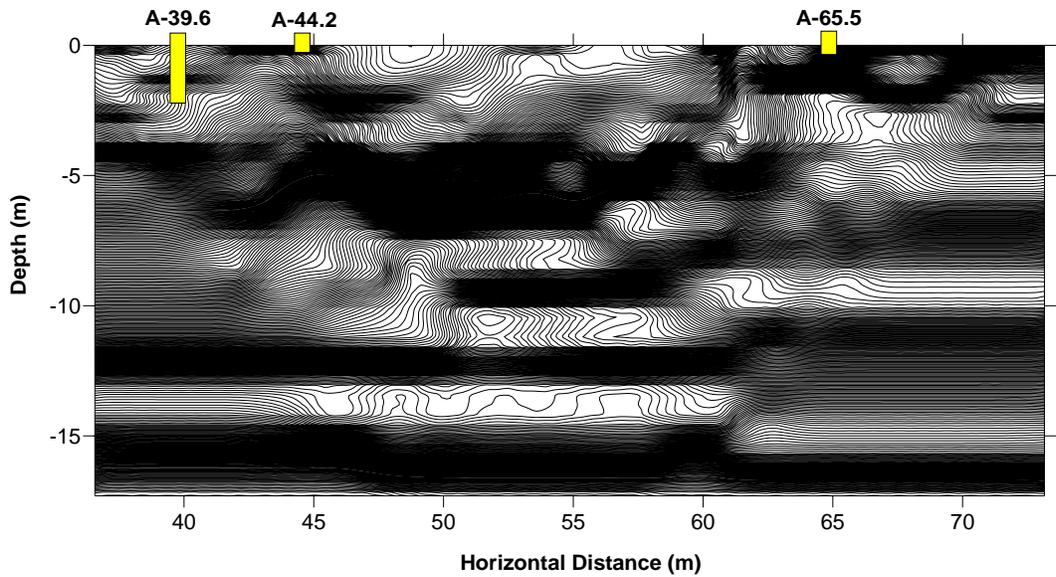


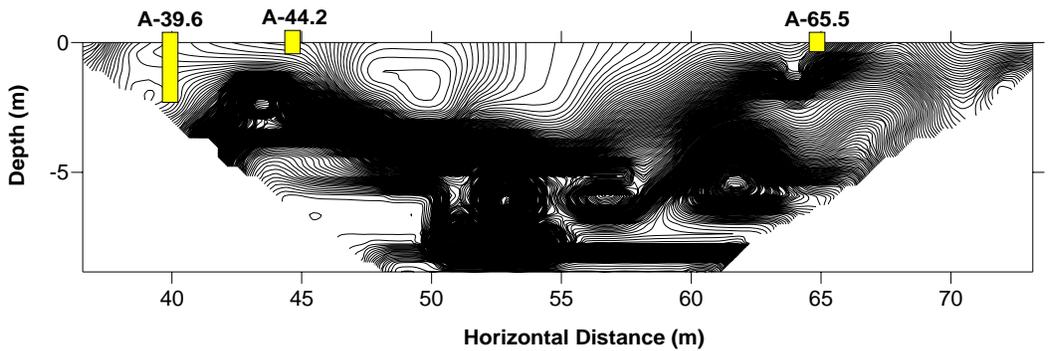
Figure 4-4 Estimated top of bedrock from intrusive testing overlain onto 50 m/s contour interval tomograms produced for the A line 0-36.6 m. (a) Rayfract, (b) SeisImager, and (c) SeisOpt Pro.



(a) Rayfract



(b) SeisImager



(c) SeisOpt Pro

Figure 4-5 Estimated top of bedrock from intrusive testing overlain onto 10 m/s contour interval tomograms produced for the A line 36.6-73.2 m. (a) Rayfract, (b) SeisImager, and (c) SeisOpt Pro.

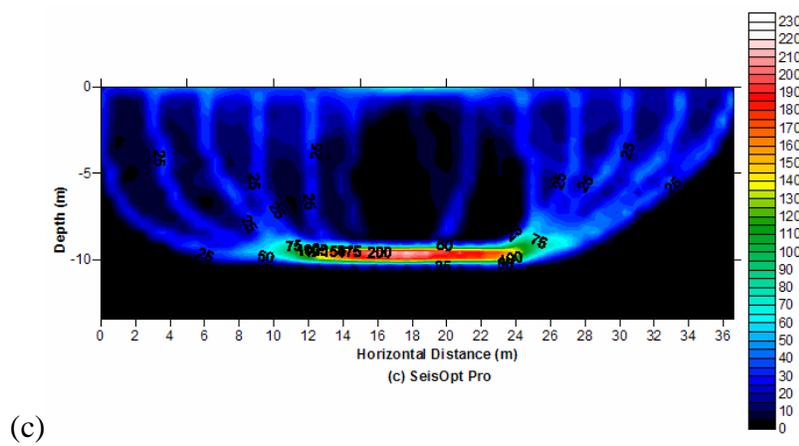
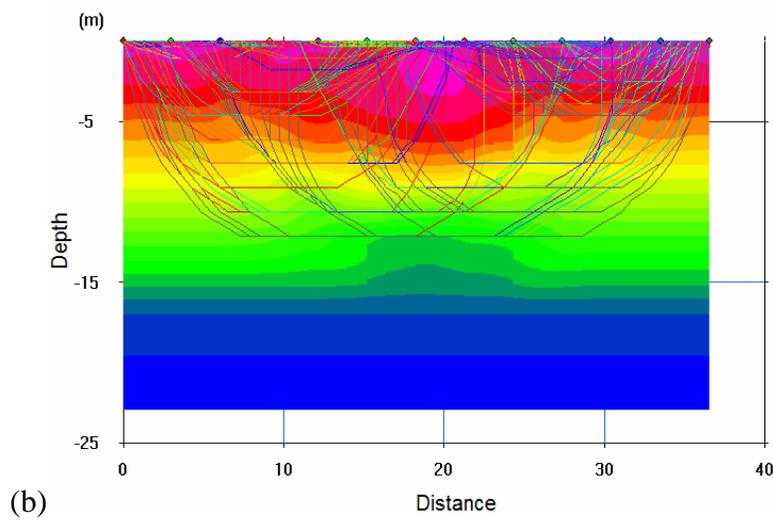
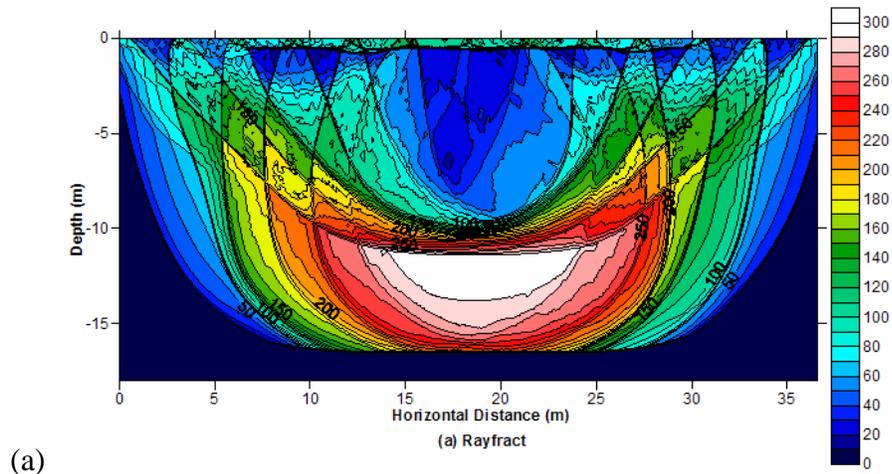


Figure 4-6 Raytracing diagrams from each of the three SRT programs for A line 0-36.6 m. (a) Rayfract, (b) SeisImager, and (c) SeisOpt Pro.

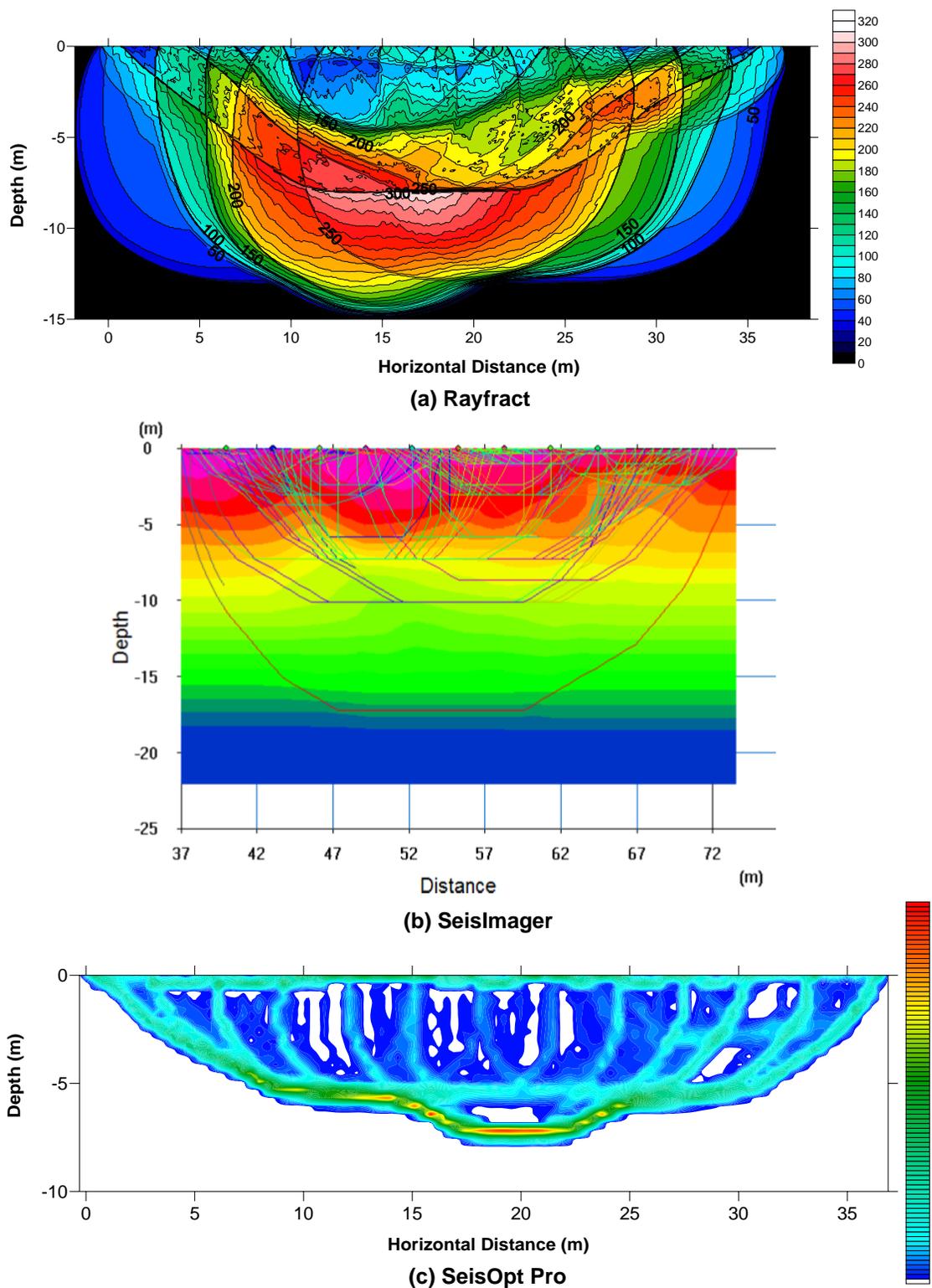


Figure 4-7 Raytracing diagrams from each of the three SRT programs for A line 36.6-73.2 m. (a) Rayfract, (b) SeisImager, and (c) SeisOpt Pro.

CHAPTER 5 CLOSURE

5.1 Summary of Findings

After completing the analysis of the three different Seismic Refraction Tomography SRT programs several findings may be stated that not only to show the capabilities of SRT programs but just as importantly their limitations. It is the hope that they will help to serve as a guide for future seismic refraction testing conducted in similar laterally variable karstic terrain. These findings are listed below and may be broken down into two distinct categories: findings about the SRT programs themselves and findings between the comparisons of SRT programs and the intrusive testing data.

5.1.1 Summary of Findings from the SRT Programs

- Despite each of the programs using completely different methods to develop their final P-wave velocity models, for the most part, they each produced models showing the same gross features of the subsurface, particularly in the upper portion.
- P-wave velocities at the top of bedrock depth at an intrusive test location were close across the tomograms from the three SRT programs, often only varying by only 100 m/s.
- The best tomogram cannot be chosen from each SRT program solely based on lowest error between the measured and calculated travel time curves. The model must be examined carefully to make sure it does not contain any artifacts and that features modeled make sense knowing the geological history of the site.
- Review of the ray path diagrams for each of the SRT programs is essential after a tomogram is produced to ensure that there is adequate ray coverage throughout the model.
- SeisImager tended to produce tomograms of the greatest depth, sometimes with several meters between a single ray traveling at the bottom of the model to the next set of rays traveling above it. These large regions in which no rays travel through should be viewed with extreme caution as the program has simply interpolated the tomogram in that region.
- SeisOpt Pro tended to produce the shallowest tomograms, with oval and pinnacle shaped artifacts often produced in the lower portion of the tomogram. This was often, but not always, the result of that area of the subsurface lacking ray path coverage.

- SeisOpt Pro, although systematic, required the most amount of user interaction and number of runs to ensure that the best final tomogram was produced, making it the most time intensive of the three SRT programs evaluated.
- Generally, Rayfract required the least amount of user interaction and number of runs to produce the best final tomogram. Which, for this particular study, when compared to the performance of the other two programs gave the author slight preference towards its use.

5.1.2 Summary of Findings from the Comparison of the SRT Programs to the Intrusive Testing Data

- Each of the three SRT programs were able to show the gross features of the subsurface, such as valleys or pinnacles in the top of limestone that were found through the intrusive testing.
- Due to the geologic history of the limestone formation and subsequent weathering processes the top of bedrock depth cannot be determined from the tomograms by simply tracing a single P-wave velocity, as top of bedrock P-wave velocities range from 600 to 2000 m/s.
- CPT penetrations would meet refusal in limestone that had a P-wave velocity of only 600 m/s but would push through particulate material, sands, with a P-wave velocity of 1500 m/s. The limestone has been severely weathered and fractured, however enough cementation remains to give the material enough strength to resist local CPT penetration.
- P-wave velocities for the top of bedrock at the pinnacle features were significantly less than at the bottom of a valley. This makes sense, and can be explained for by knowing the geologic history of the site and weathering processes that have and continue to take place at the site.
- The combination of a relatively small increase in P-wave velocity at the soil/bedrock interface and range of top of limestone P-wave velocity from 600 to 2000 m/s makes it nearly impossible for the user to delineate the top of limestone by visual inspection of the tomogram produced using typical contour intervals of 100 m/s.
- Using a close contour interval of 10 m/s for the Rayfract, and to a lesser extent the SeisImager and SeisOpt Pro, the tomograms were found to show that areas of extremely close contour intervals matched up to the variable top of bedrock depth determined by intrusive testing. While the increase in P-wave velocity at the soil/rock interface is not dramatic as it would be if the rock were unweathered, a small enough increase still exists so that the top of limestone surface can be delineated through visual inspection of this close contour interval tomogram.
- Reviewing ray path diagrams is not only essential to ensure that the tomogram produced has adequate coverage but often can be used to determine top of bedrock depths by looking for areas of sudden increases in laterally traveling rays. These areas are indicators that a sudden, relatively large change in P-wave velocity has occurred, like the soil/bedrock interface.

5.2 Conclusions

Based on the findings of this study the tomograms produced by each of the SRT programs tested were able to image the gross features of the subsurface. They were also found to be similar to one another when evaluated visually as well as quantitatively. Most importantly, after comparing the tomograms to the intrusive testing data it was shown that they were able to show the gross subsurface features and provide accurate subsurface imaging of the top of bedrock location on a site containing laterally-variable top of bedrock elevations and sinkhole potential. These findings collectively show the potential of SRT programs to accurately image the subsurface of sites with laterally variable karstic bedrock conditions.

As part of a complete subsurface evaluation traditional intrusive geotechnical exploration techniques may be employed more efficiently at locations of interest, when selected from the tomograms produced by the SRT programs, helping to characterize features that would ordinarily be missed if intrusive testing were performed at locations chosen blindly. However, seismic refraction testing cannot be used in place of traditional intrusive methods, as it does not provide physical recovery of the soil sample that is necessary to describe the subsurface. Therefore, seismic refraction tomography should be used in conjunction with traditional intrusive testing techniques in order to characterize a subsurface more completely and efficiently.

5.3 Research Recommendations

In order to help validate using the close contour interval method to delineate the top of bedrock, additional intrusive testing is necessary to determine if the top of bedrock encountered at other locations corresponds with what would be expected from the tomograms produced. Laboratory testing of the limestone collected during the rock coring to learn more about the material properties would also probably help in explaining the reason for the wide range of P-wave velocities encountered throughout the site. Also these findings only apply to this site,

additional testing needs to be performed on similar types of sites to build a database and to confirm these findings.

APPENDIX A
P-WAVE VELOCITY TOMOGRAMS

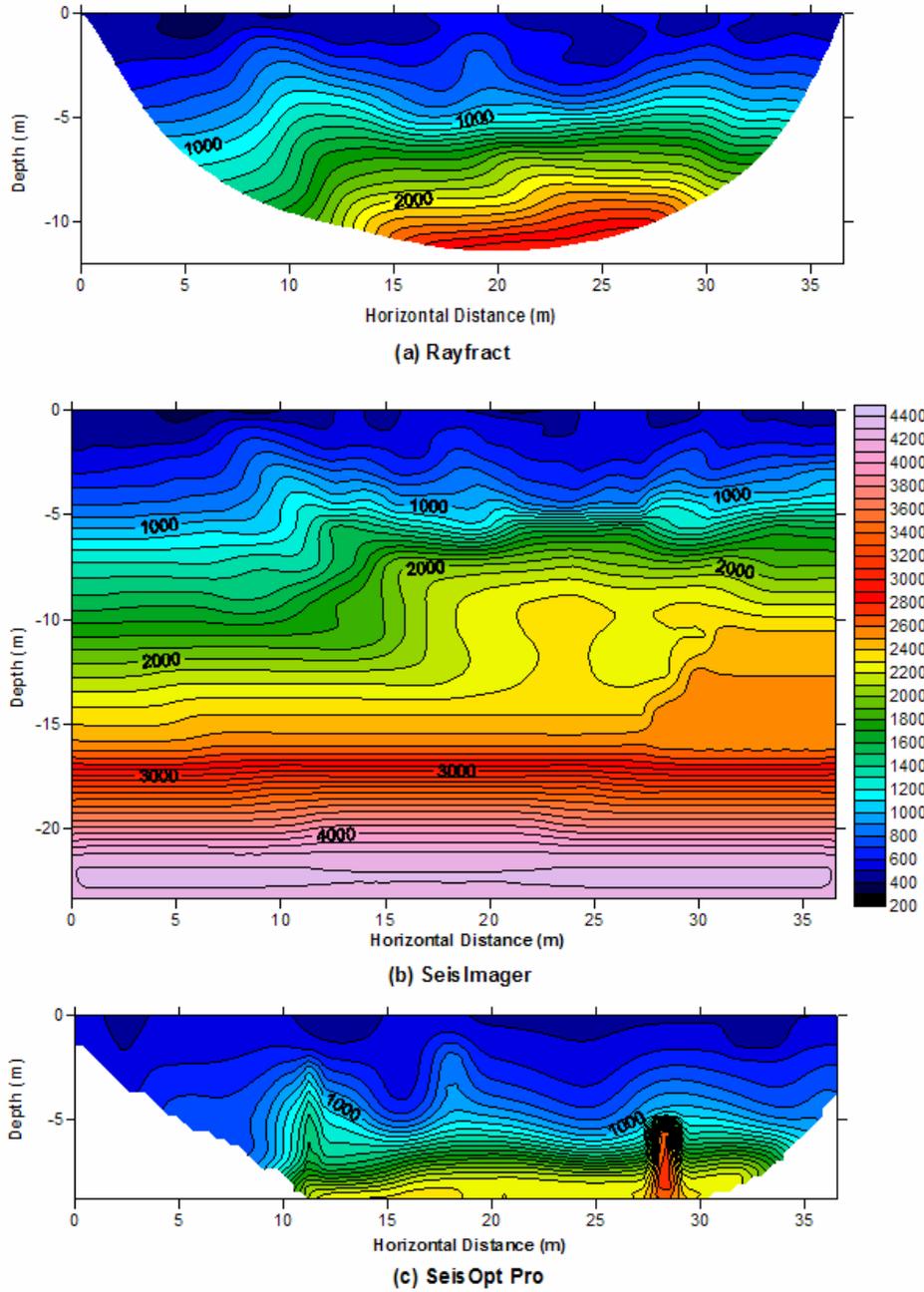
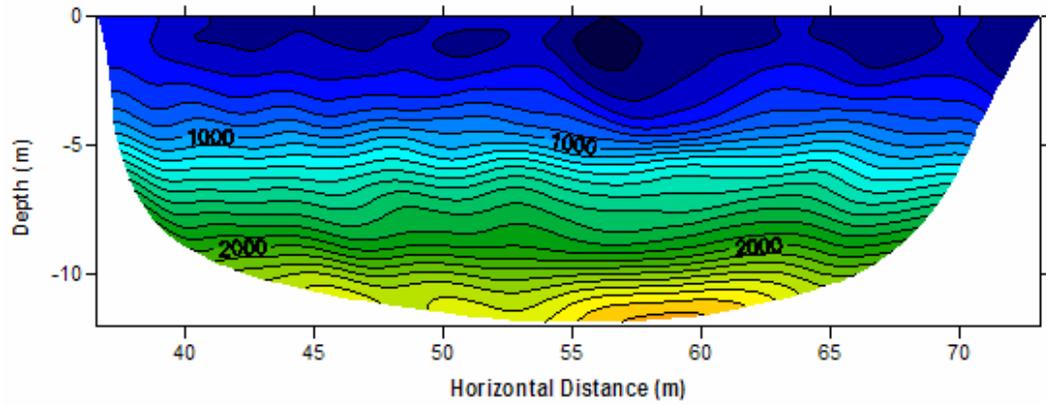
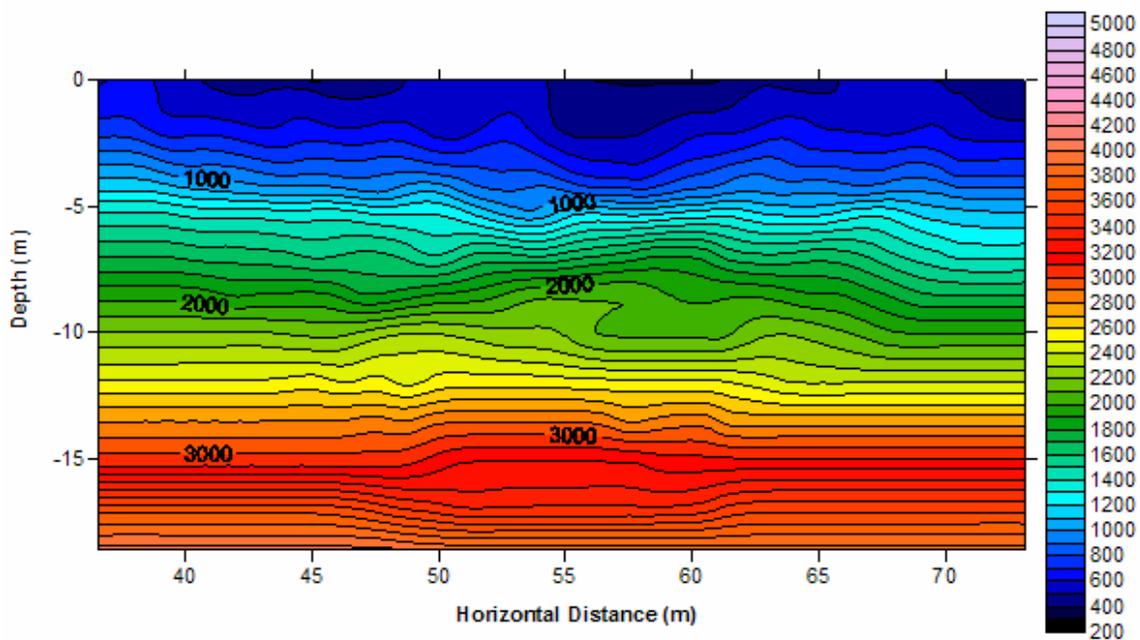


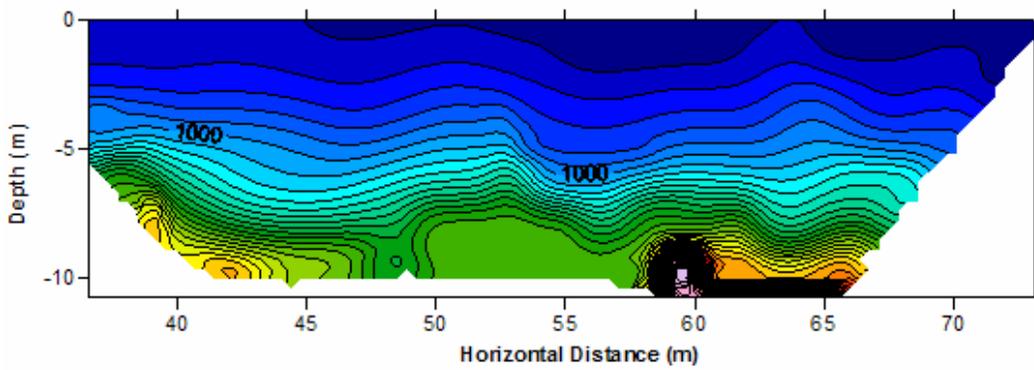
Figure A-1 P-wave tomograms, F line, station 0 – 36.6 m. (a) Rayfract, (b) SeisImager, and (c) SeisOpt Pro.



(a) Rayfract



(b) Seis Imager



(c) SeisOpt Pro

Figure A-2 P-wave tomograms, F line, station 36.6 – 73.2 m. (a) Rayfract, (b) SeisImager, and (c) SeisOpt Pro.

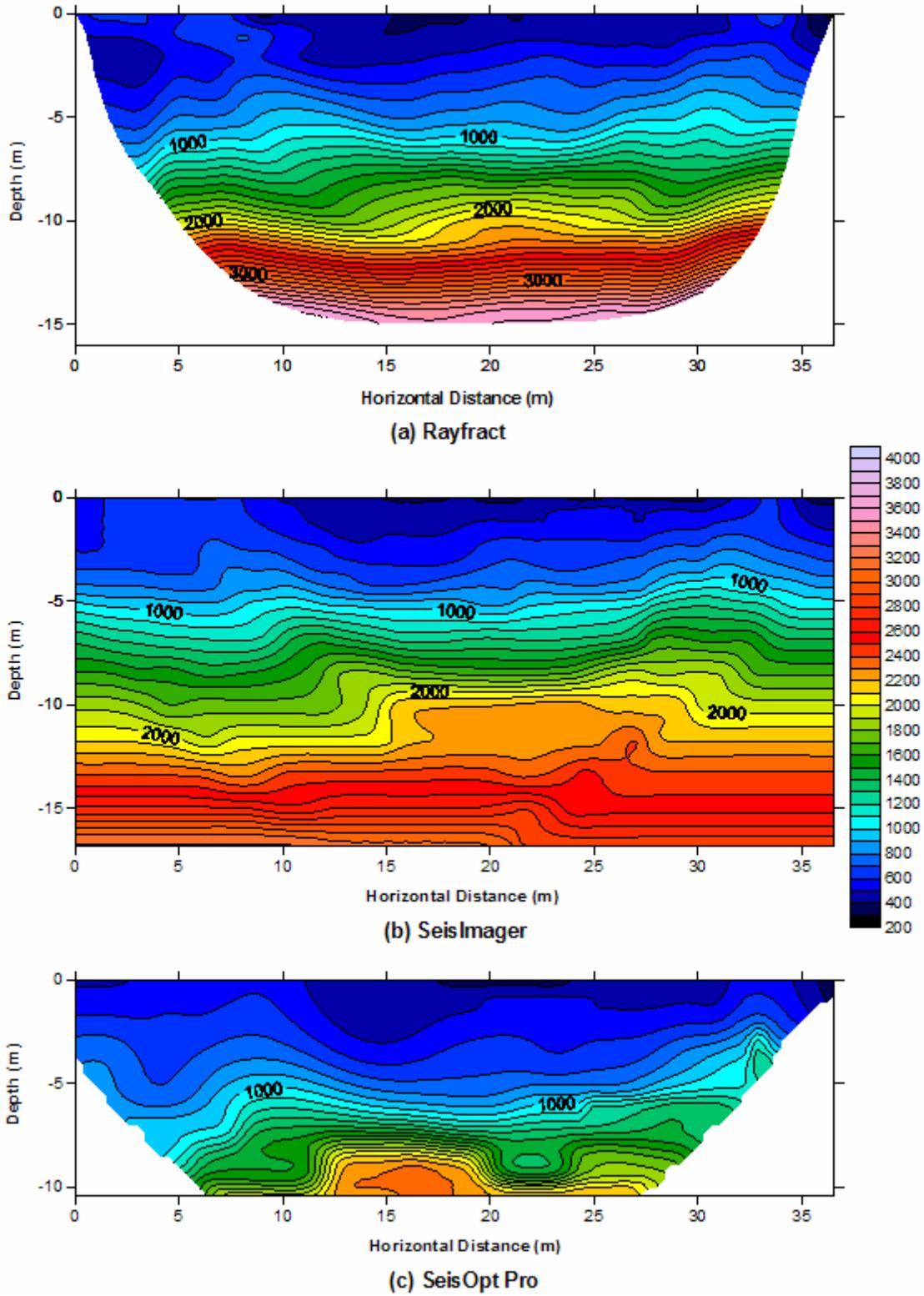


Figure A-3 P-wave tomograms, K line, station 0-36.6 m. (a) Rayfract, (b) SeisImager, and (c) SeisOpt Pro.

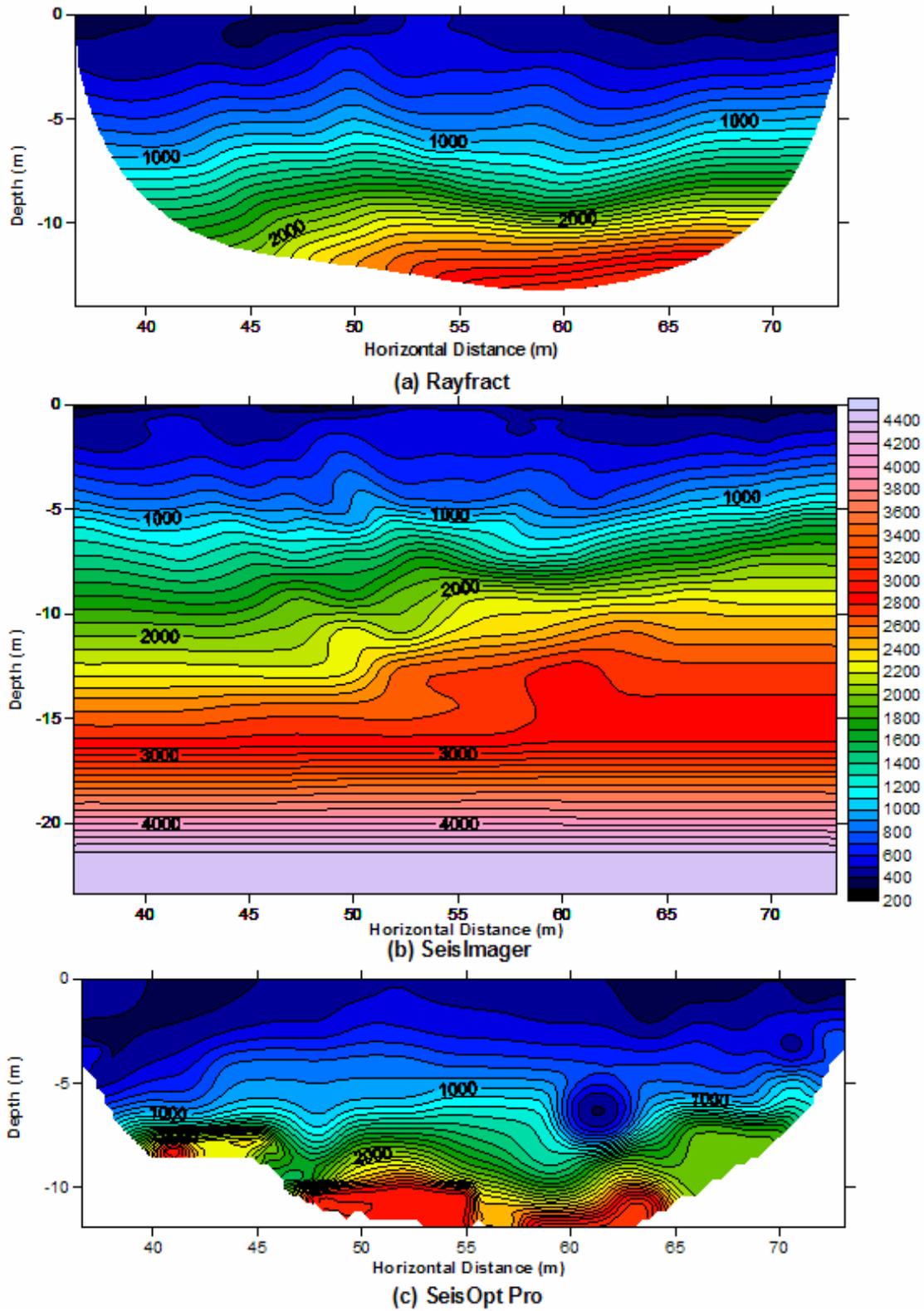


Figure A-4 P-wave tomograms, K line, station 36.6-73.2 m. (a) Rayfract, (b) SeisImager, and (c) SeisOpt Pro.

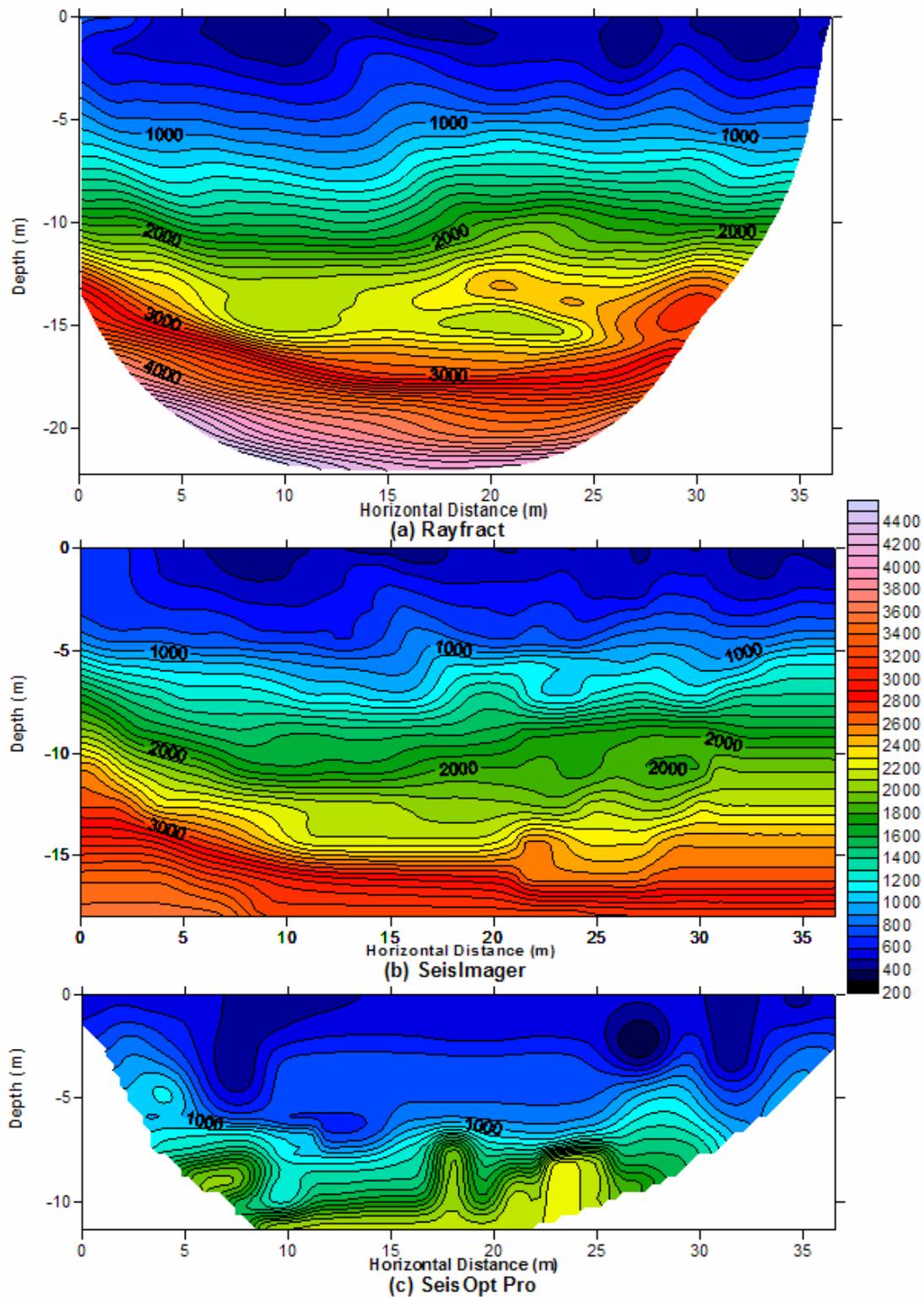
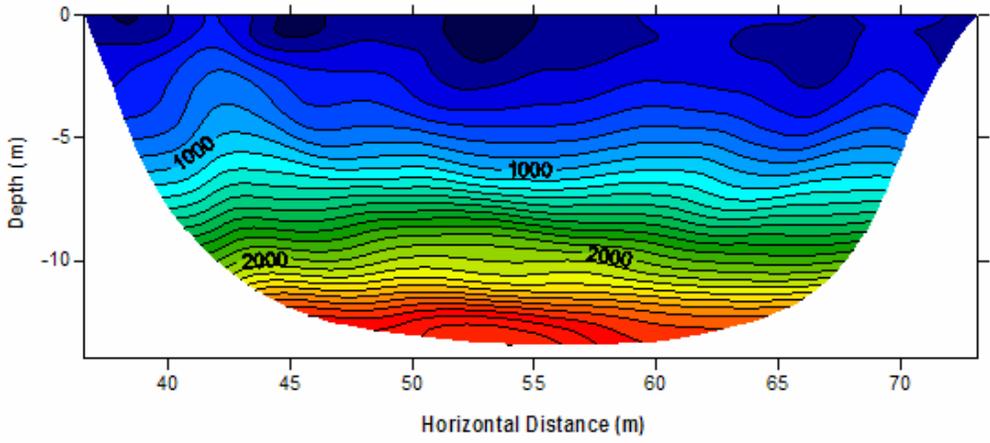
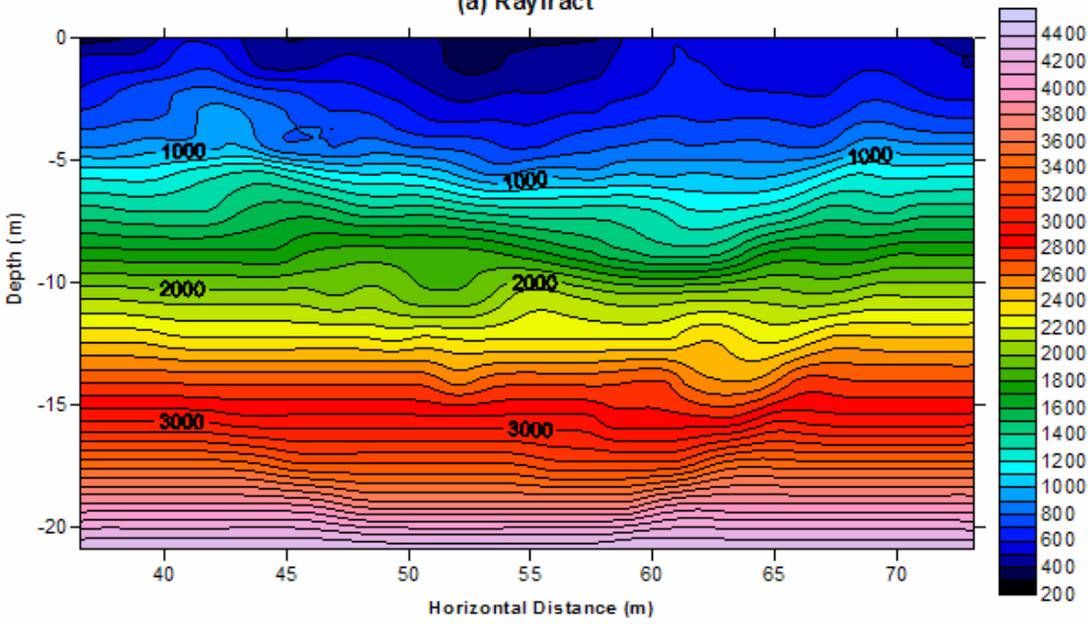


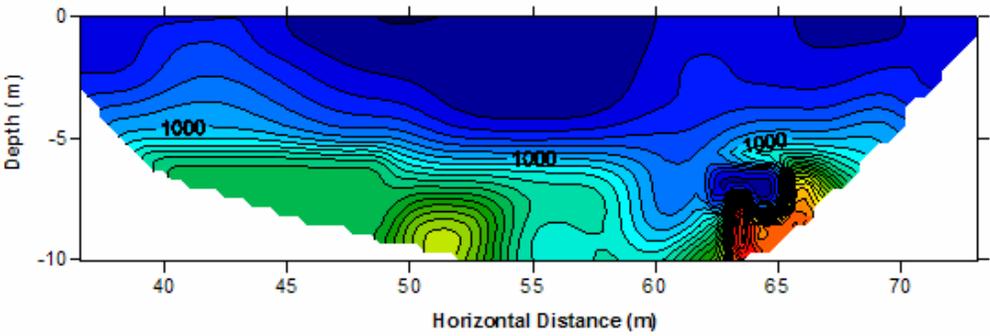
Figure A-5 P-wave tomograms, P line, station 0 – 36.6 m. (a) Rayfract, (b) SeisImager, and (c) SeisOpt Pro.



(a) Rayfract

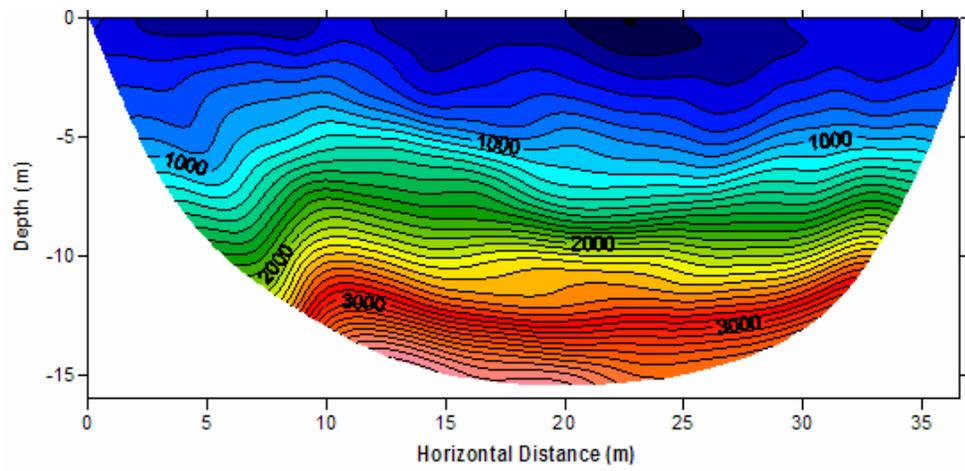


(b) SeisImager

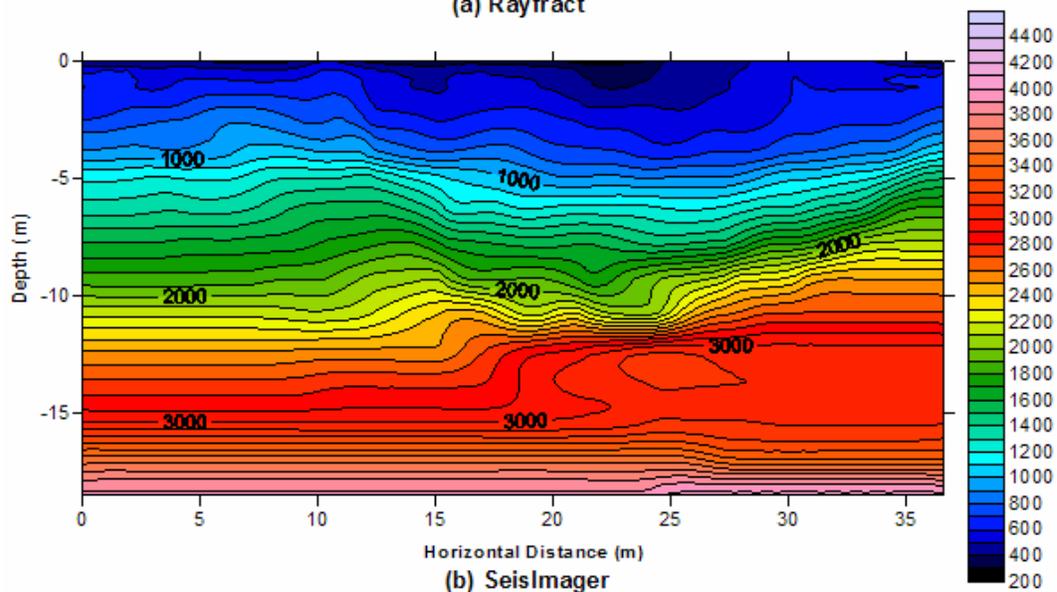


(c) SeisOpt Pro

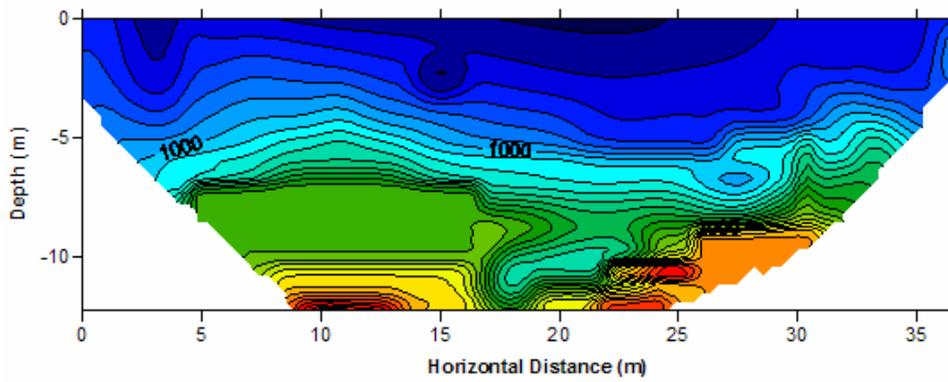
Figure A-6 P-wave tomograms, P line, station 36.6-73.2 m. (a) Rayfract, (b) SeisImager, and (c) SeisOpt Pro.



(a) Rayfract

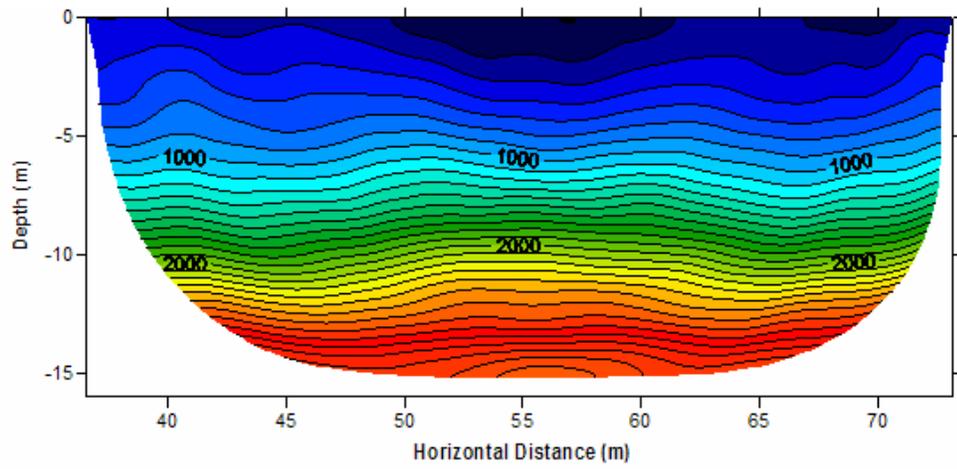


(b) SeisImager

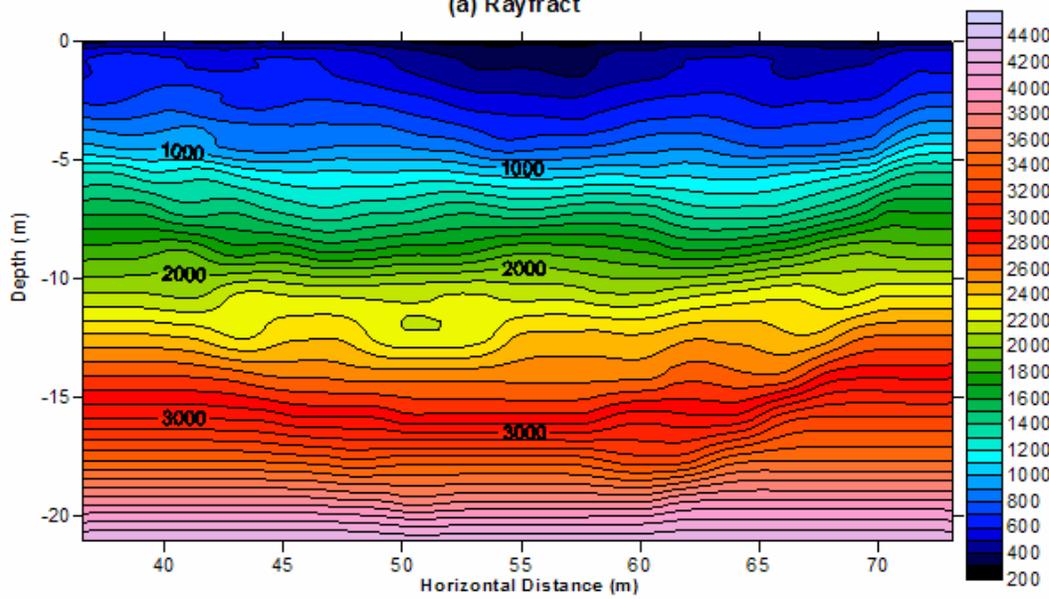


(c) SeisOpt Pro

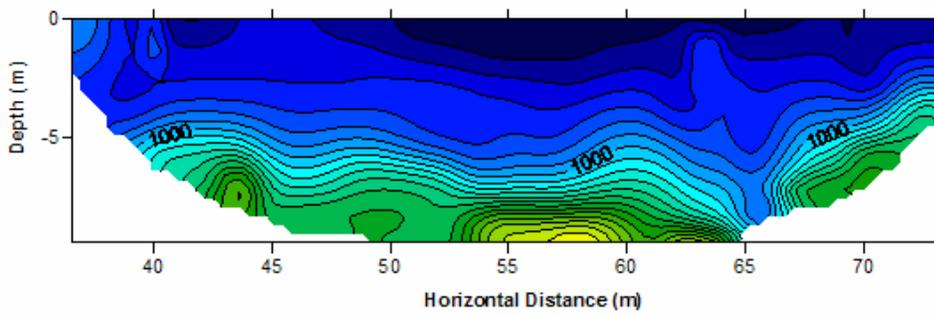
Figure A-7 P-wave tomograms, U line, station 0 – 36.6 m. (a) Rayfract, (b) SeisImager, and (c) SeisOpt Pro.



(a) Rayfract



(b) SeisImager



(c) Seis Opt Pro

Figure A-8 P-wave tomograms, U line, station 36.6-73.2 m. (a) Rayfract, (b) SeisImager, and (c) SeisOpt Pro.

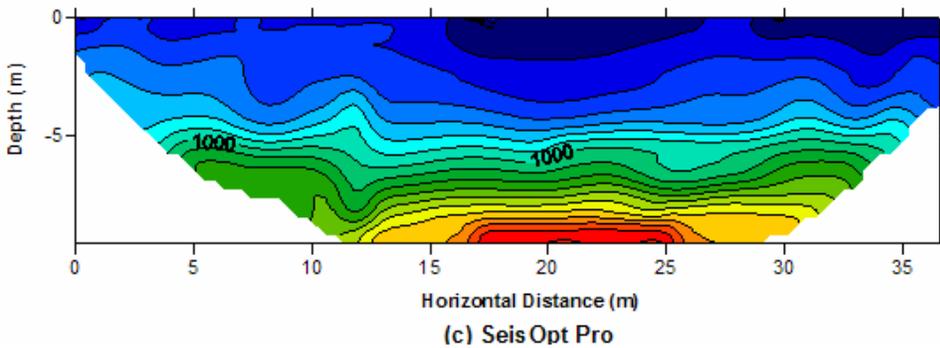
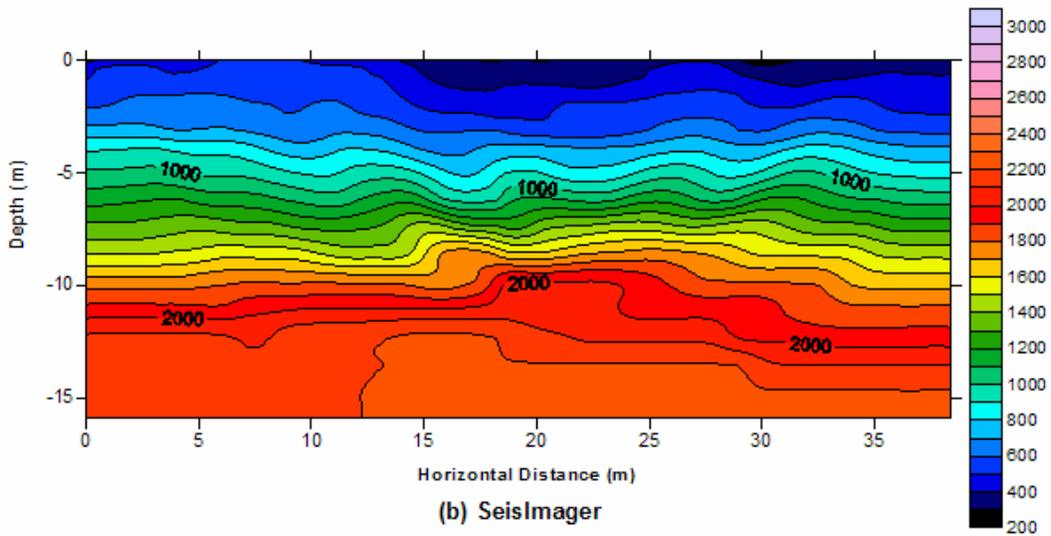
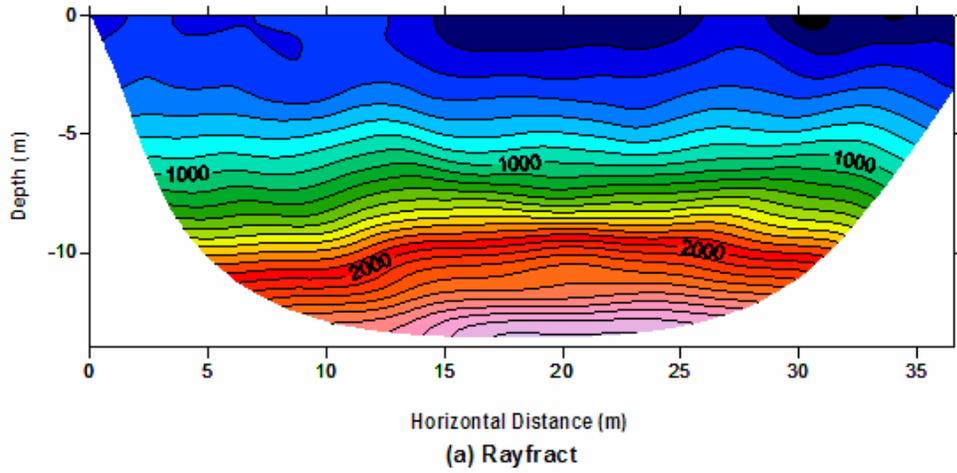
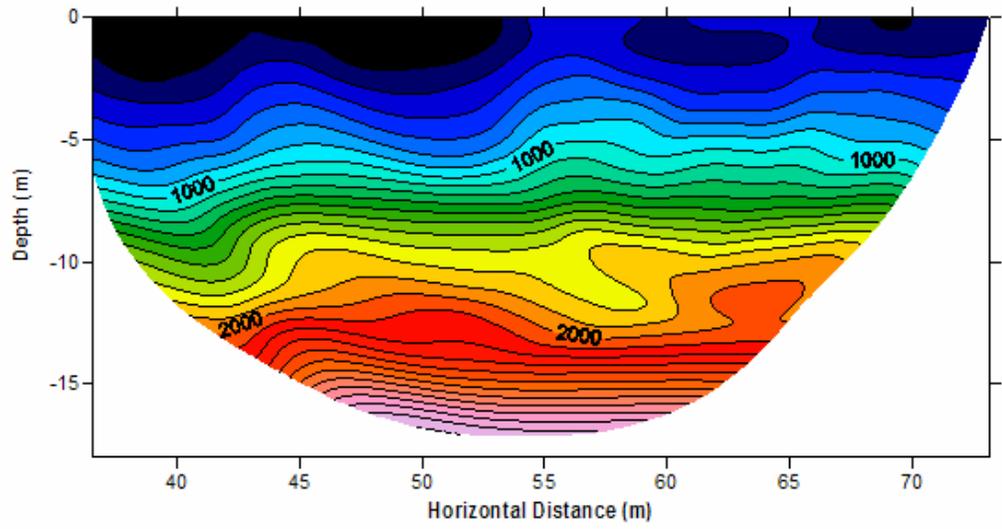
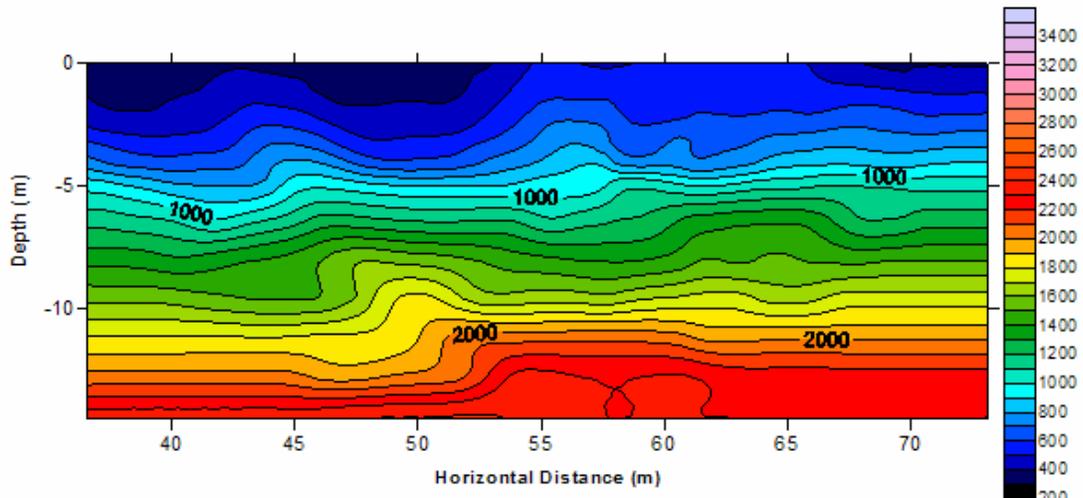


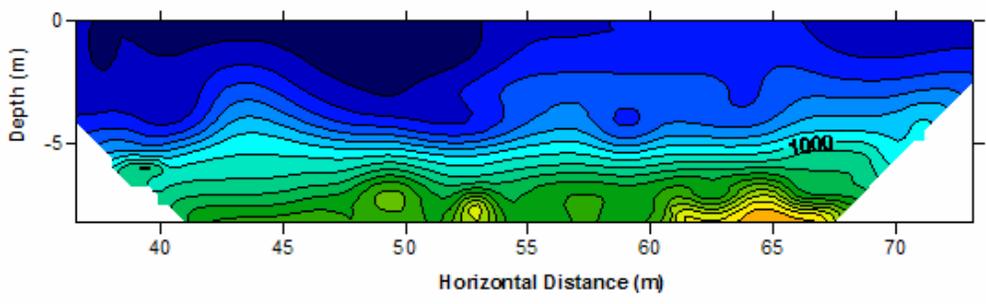
Figure A-9 P-wave tomograms, Z line, station 0 – 38.4 m. (a) Rayfract, (b) SeisImager, and (c) SeisOpt Pro.



(a) Rayfract



(b) SeisImager



(c) SeisOpt Pro

Figure A-10 P-wave tomograms, Z line, station 36.6-73.2 m. (a) Rayfract, (b) SeisImager, and (c) SeisOpt Pro.

APPENDIX B INTRUSIVE TESTING FIELD DATA

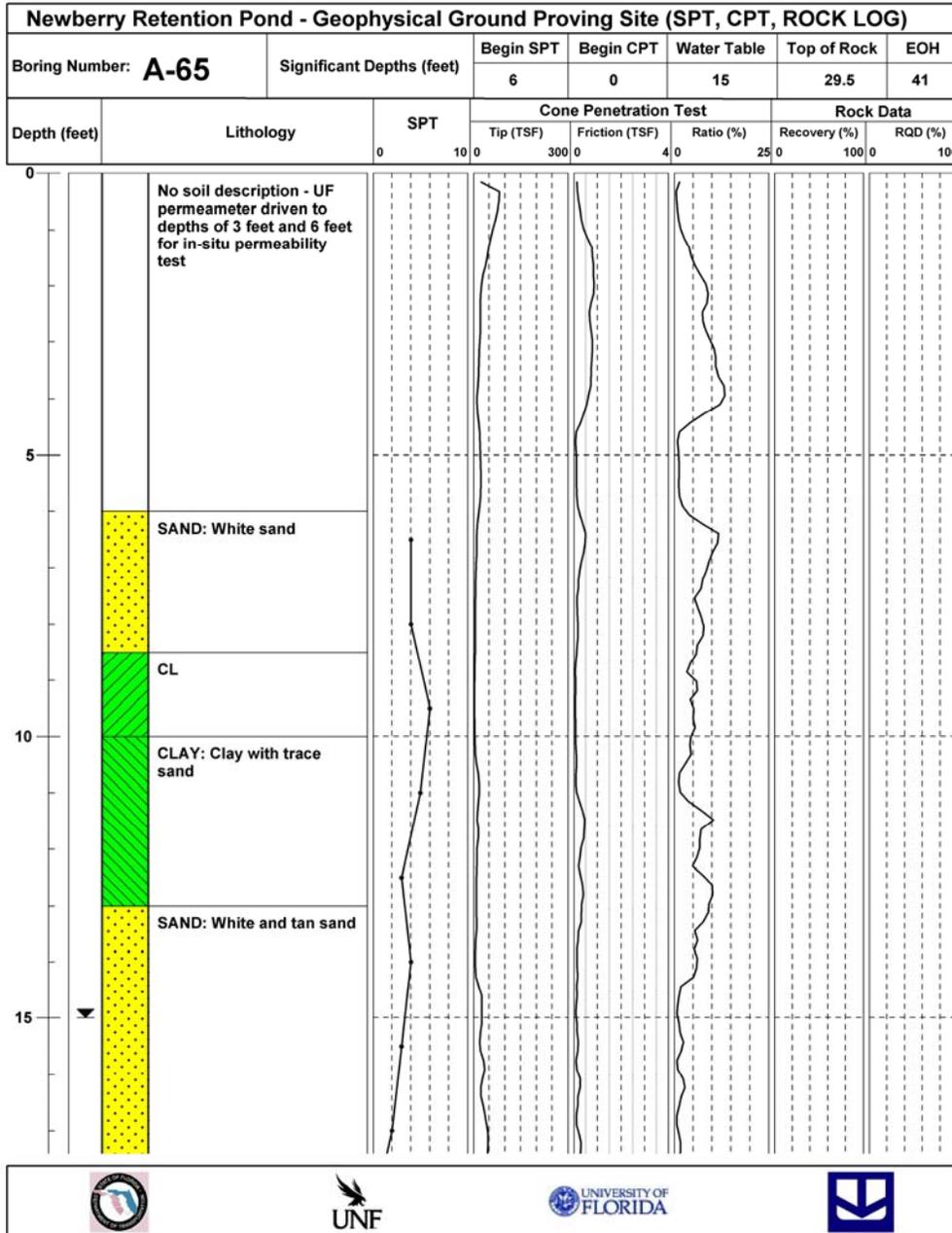


Figure B-1 Intrusive testing data from A Line, station 19.8 m

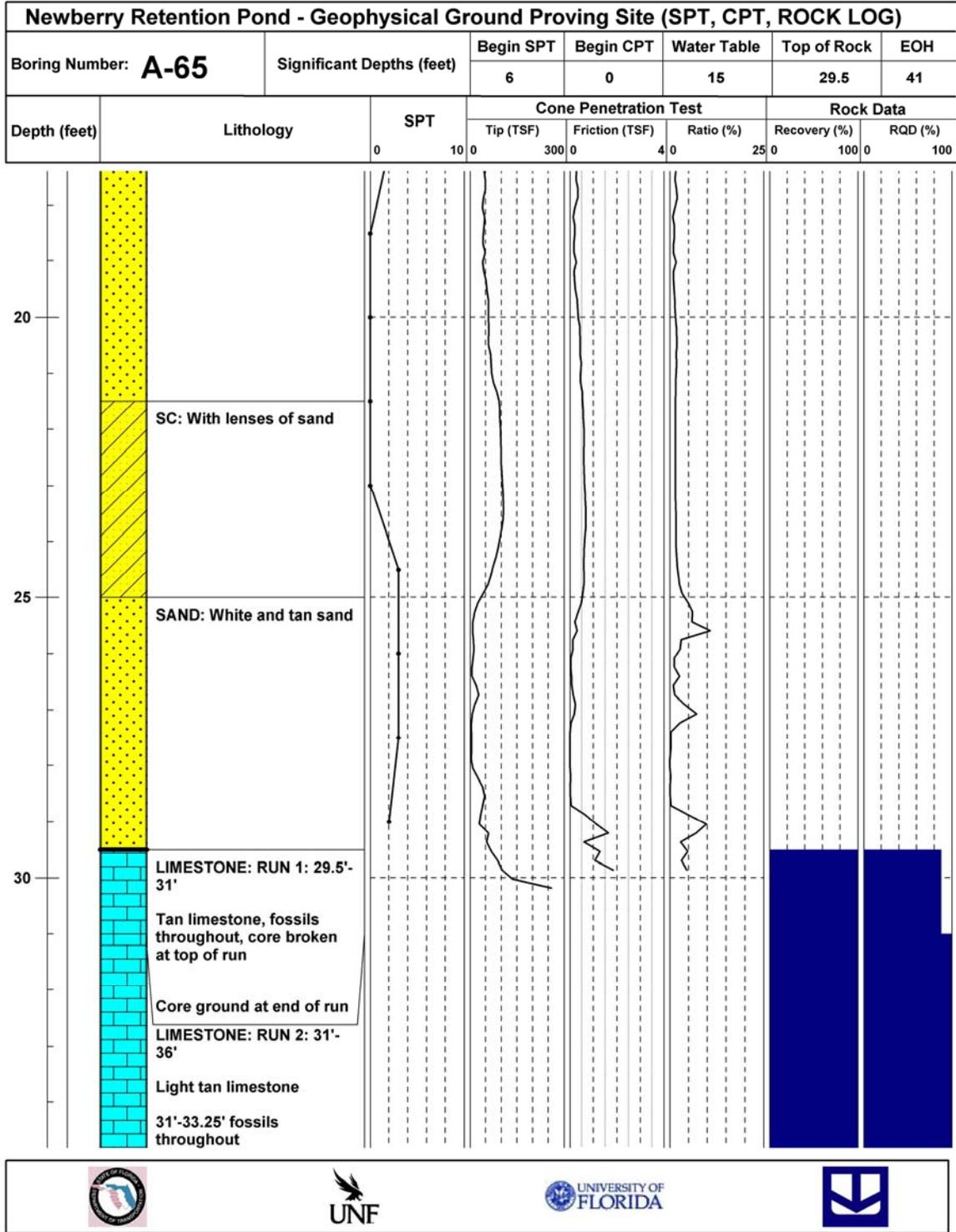


Figure B-1 Continued

Newberry Retention Pond - Geophysical Ground Proving Site (SPT, CPT, ROCK LOG)													
Boring Number: A-65		Significant Depths (feet)		Begin SPT	Begin CPT	Water Table	Top of Rock	EOH					
				6	0	15	29.5	41					
Depth (feet)	Lithology	SPT		Cone Penetration Test			Rock Data						
		0	10	Tip (TSF)	Friction (TSF)	Ratio (%)	Recovery (%)	RQD (%)					
				0	300	0	4	0	25	0	100	0	100
35	33.25'-36' fine grained LIMESTONE: RUN 3: 36'-41' Light tan limestone, fine grained, fossils throughout 38.1'-38.6' weathered zone END OF HOLE 41'												
40													



Figure B-1 Continued

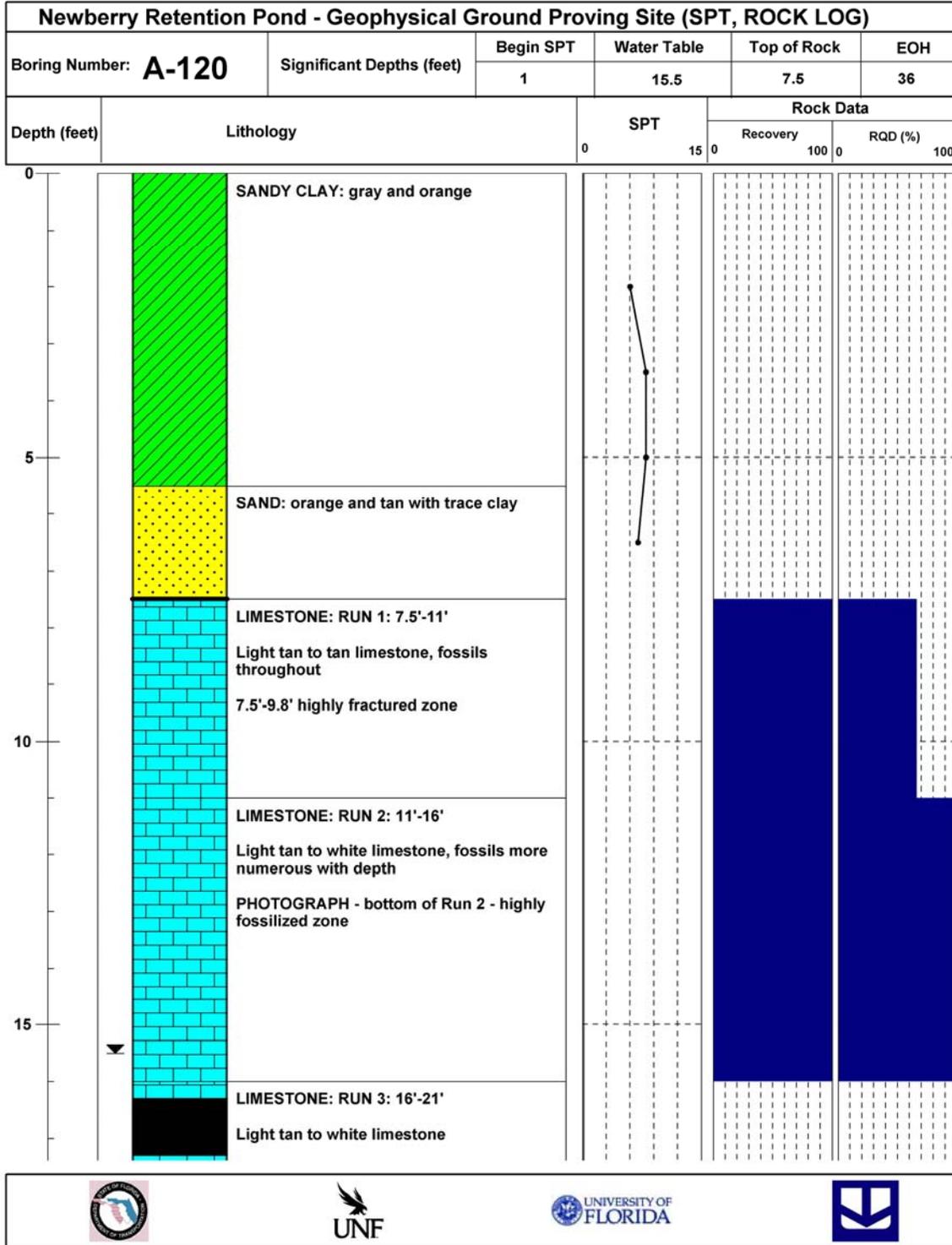


Figure B-2 Intrusive testing data from A Line, station 36.6 m

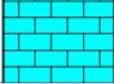
Newberry Retention Pond - Geophysical Ground Proving Site (SPT, ROCK LOG)					
Boring Number: A-120	Significant Depths (feet)	Begin SPT	Water Table	Top of Rock	EOH
		1	15.5	7.5	36
Depth (feet)	Lithology	SPT	Rock Data		
			Recovery	RQD (%)	
		0 15 0	100 0	100	
35					



Figure B-2 Continued

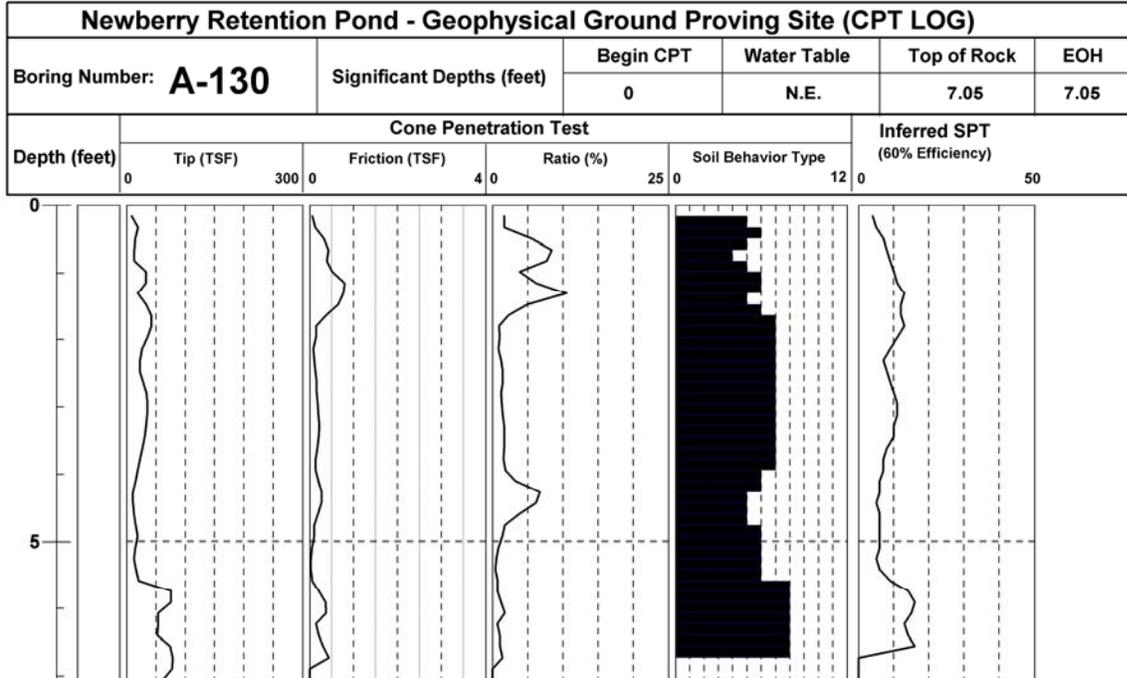


Figure B-3 Intrusive testing data from A Line, station 39.6 m

Newberry Retention Pond - Geophysical Ground Proving Site (CPT LOG)					
Boring Number: A-145	Significant Depths (feet)	Begin CPT	Water Table	Top of Rock	EOH
		0	N. E.	0.66	0.66
Depth (feet)	Cone Penetration Test				Inferred SPT (60% Efficiency)
	Tip (TSF)	Friction (TSF)	Ratio (%)	Soil Behavior Type	
	0 300	0 4	0 25	0 12	0 50
0					



Figure B-4 Intrusive testing data from A Line, station 44.2 m

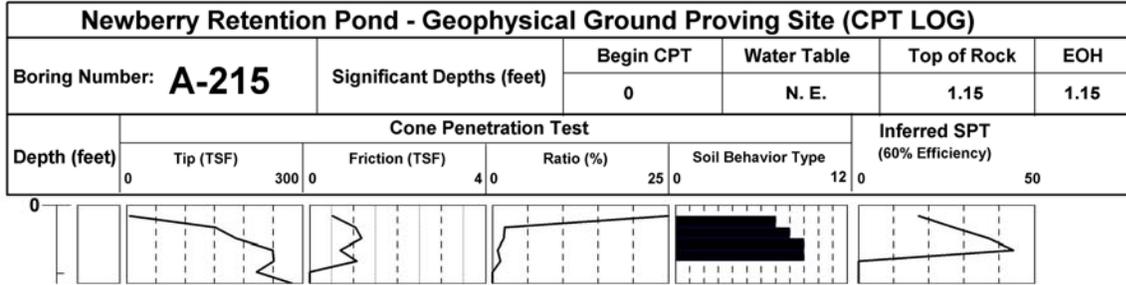


Figure B-5 Intrusive testing data from A Line, station 66.5 m

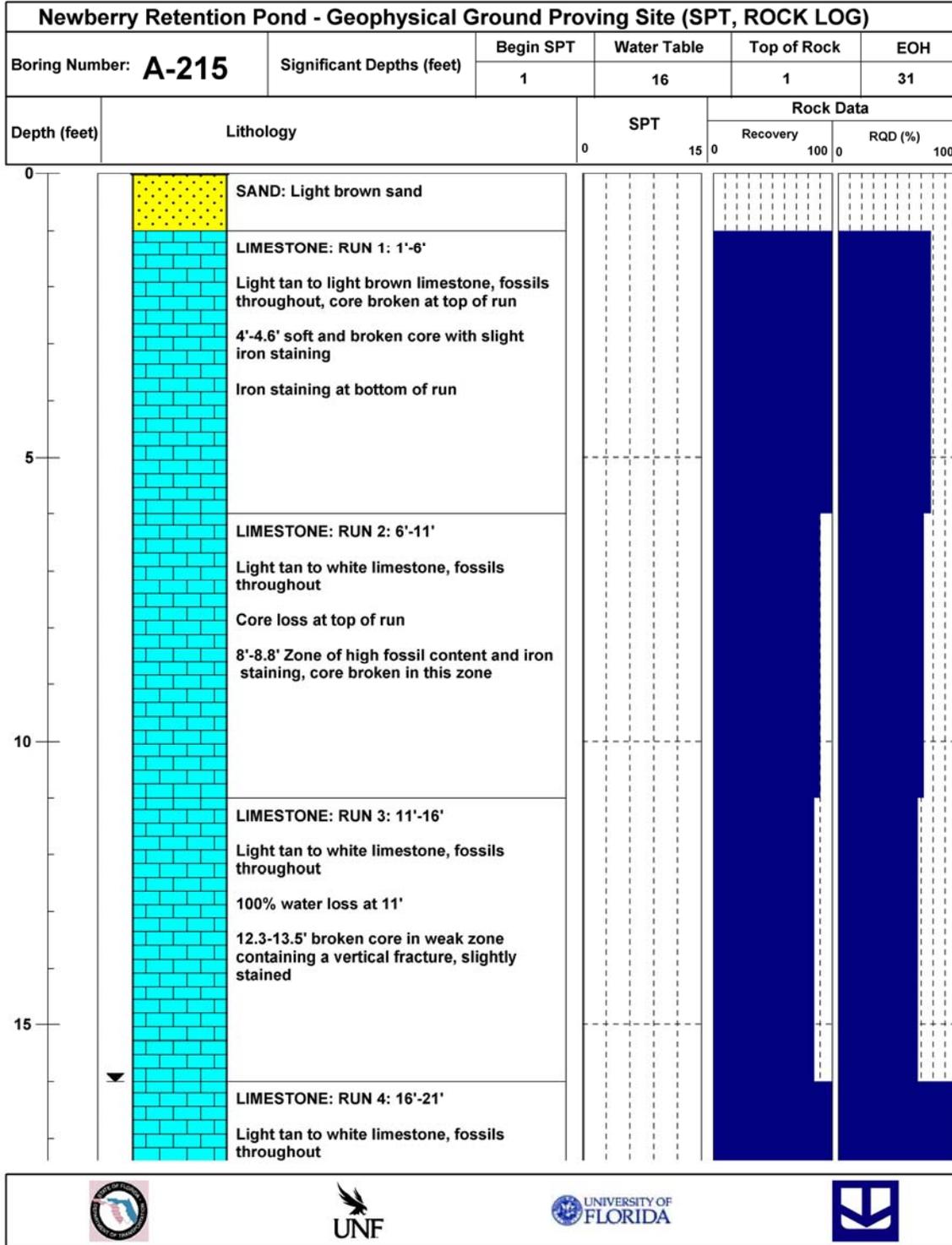


Figure B-6 Intrusive testing data from A Line, station 66.5 m

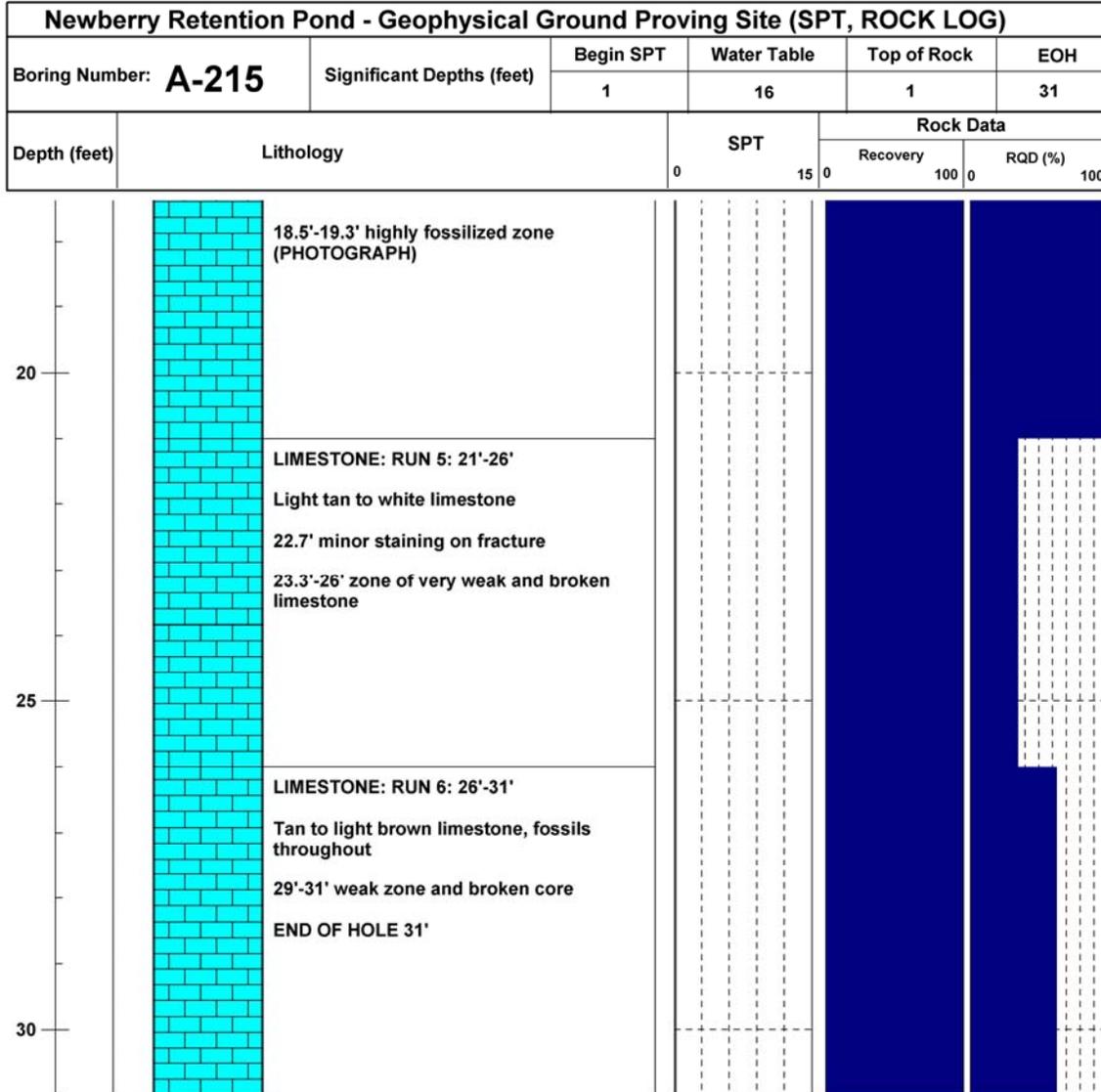


Figure B-6 Continued

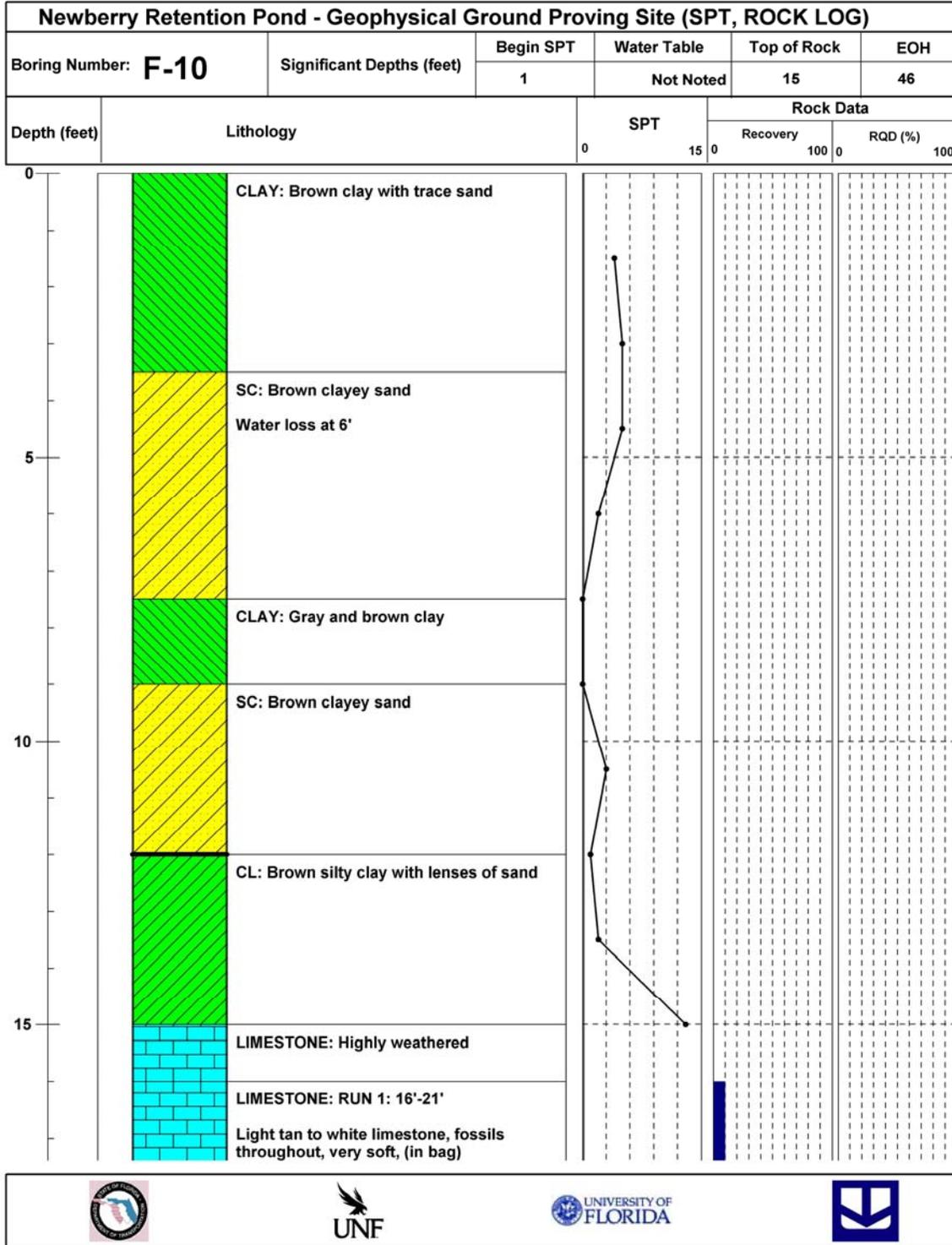


Figure B-7 Intrusive Testing Data from F Line, Station 3.0 m

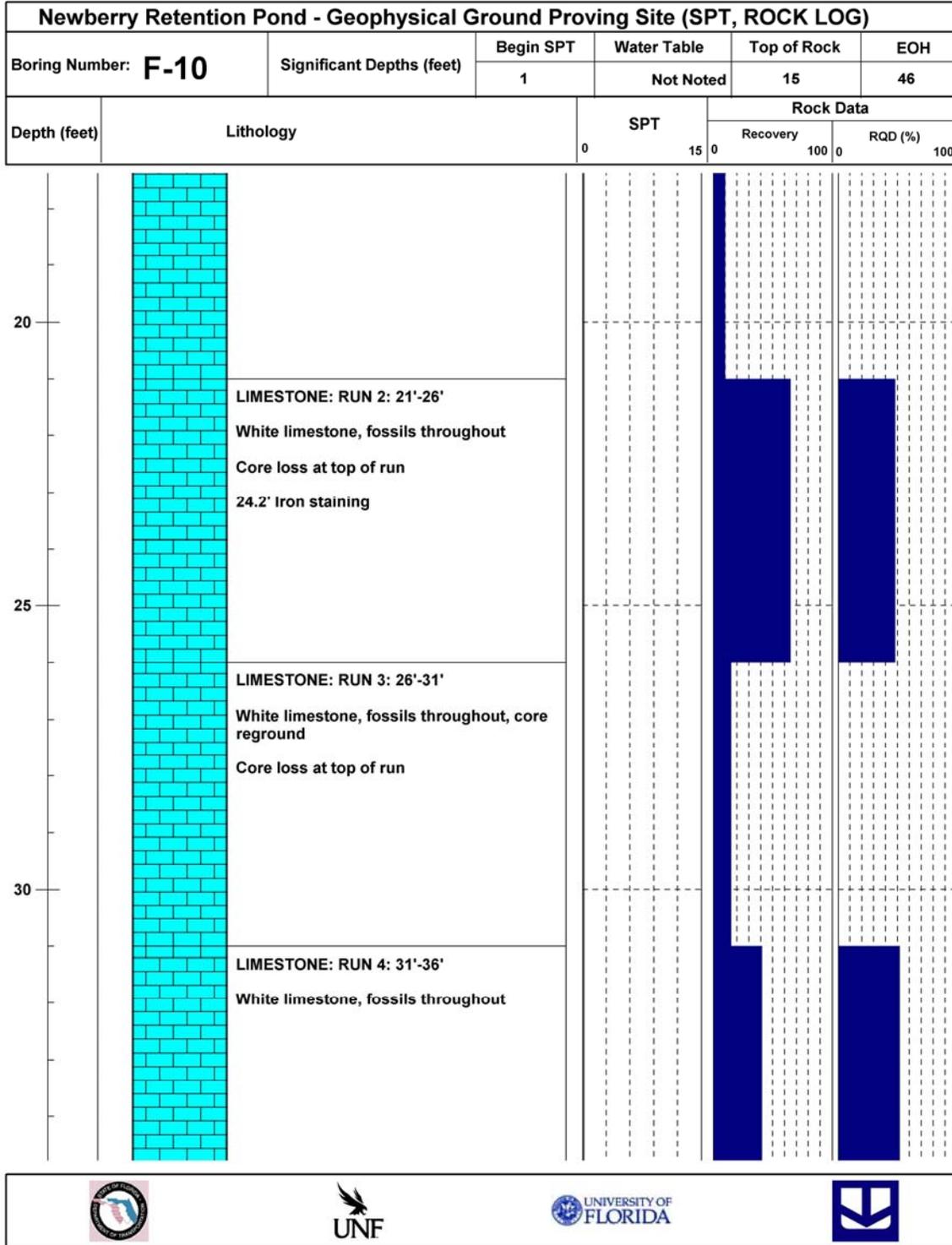


Figure B-7 Continued

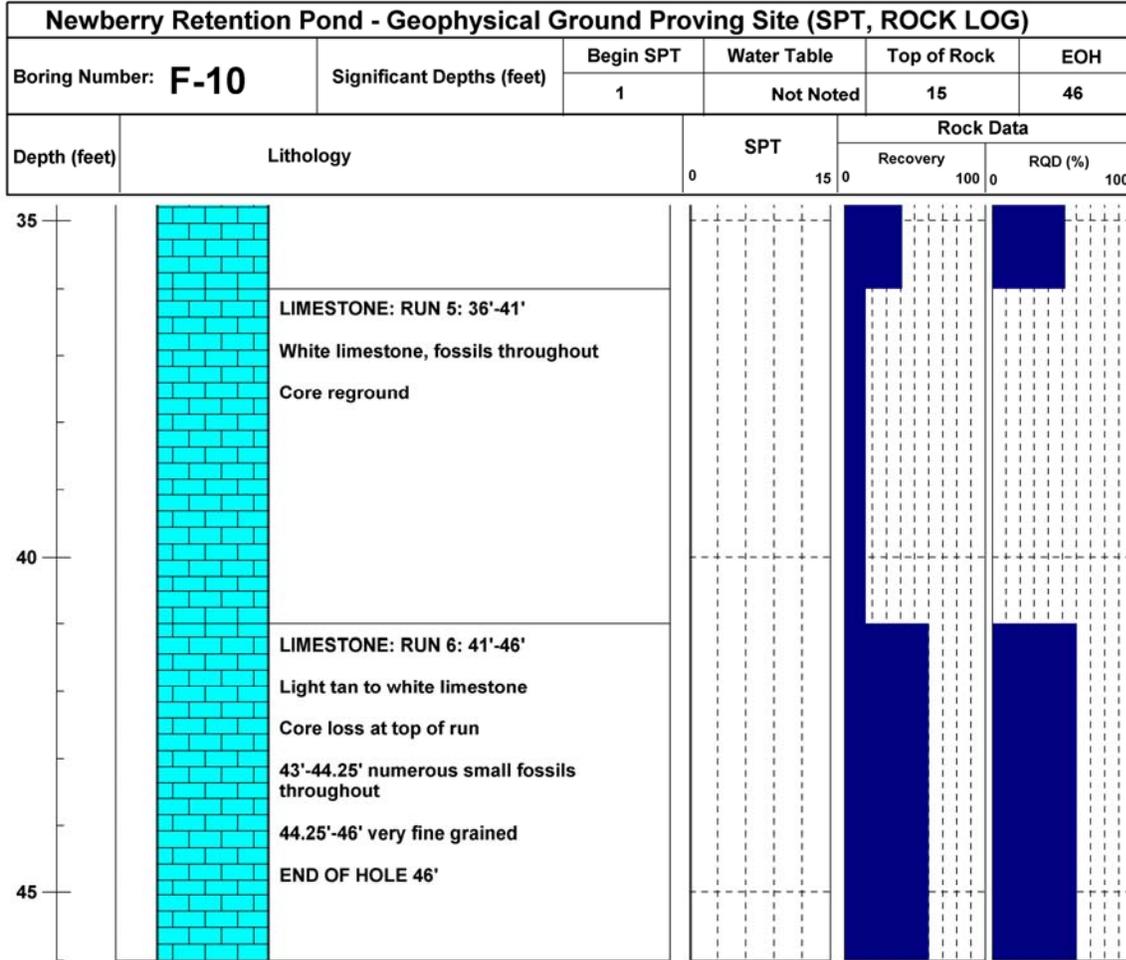


Figure B-7 Continued

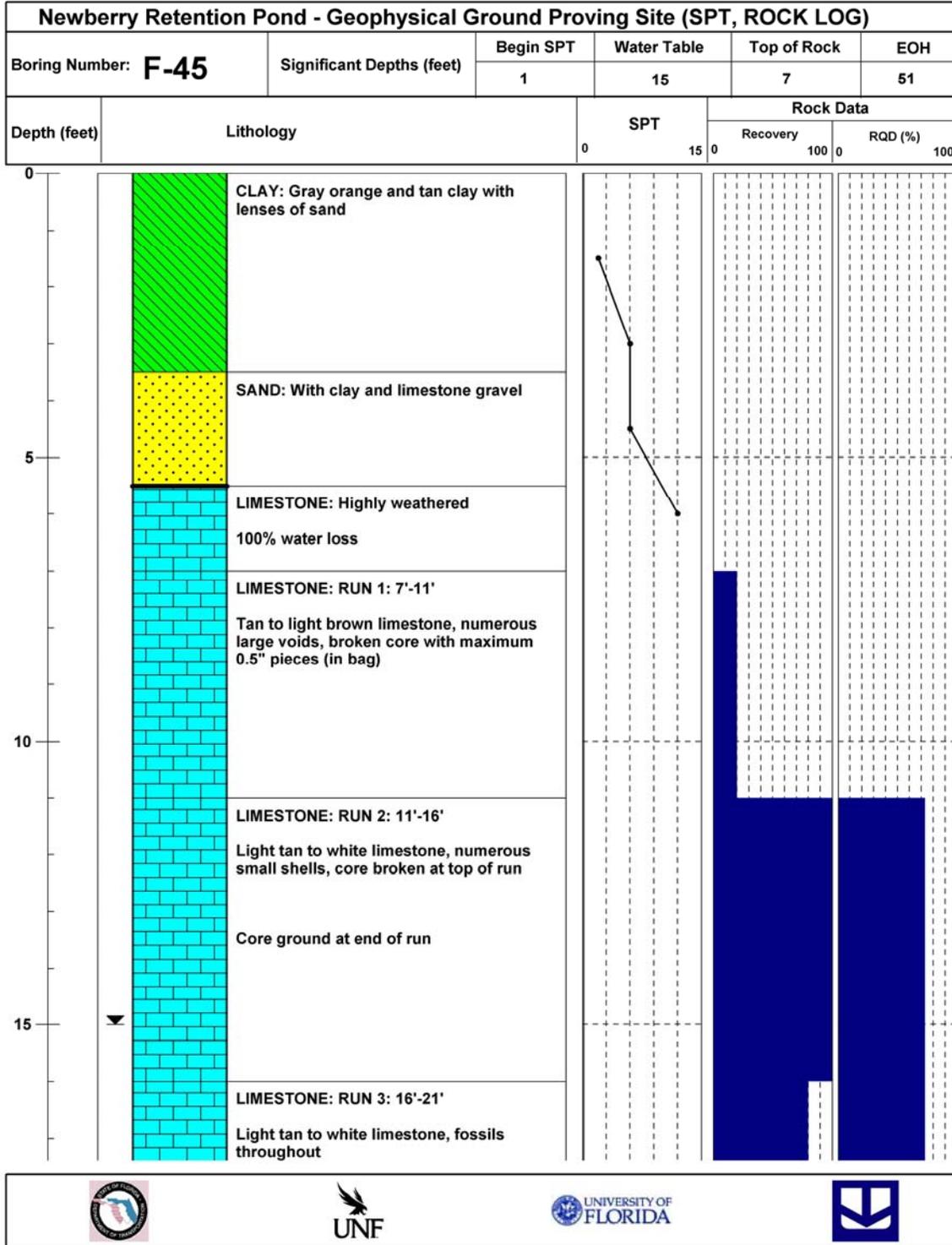


Figure B-8 Intrusive testing data from F Line, station 13.7 m

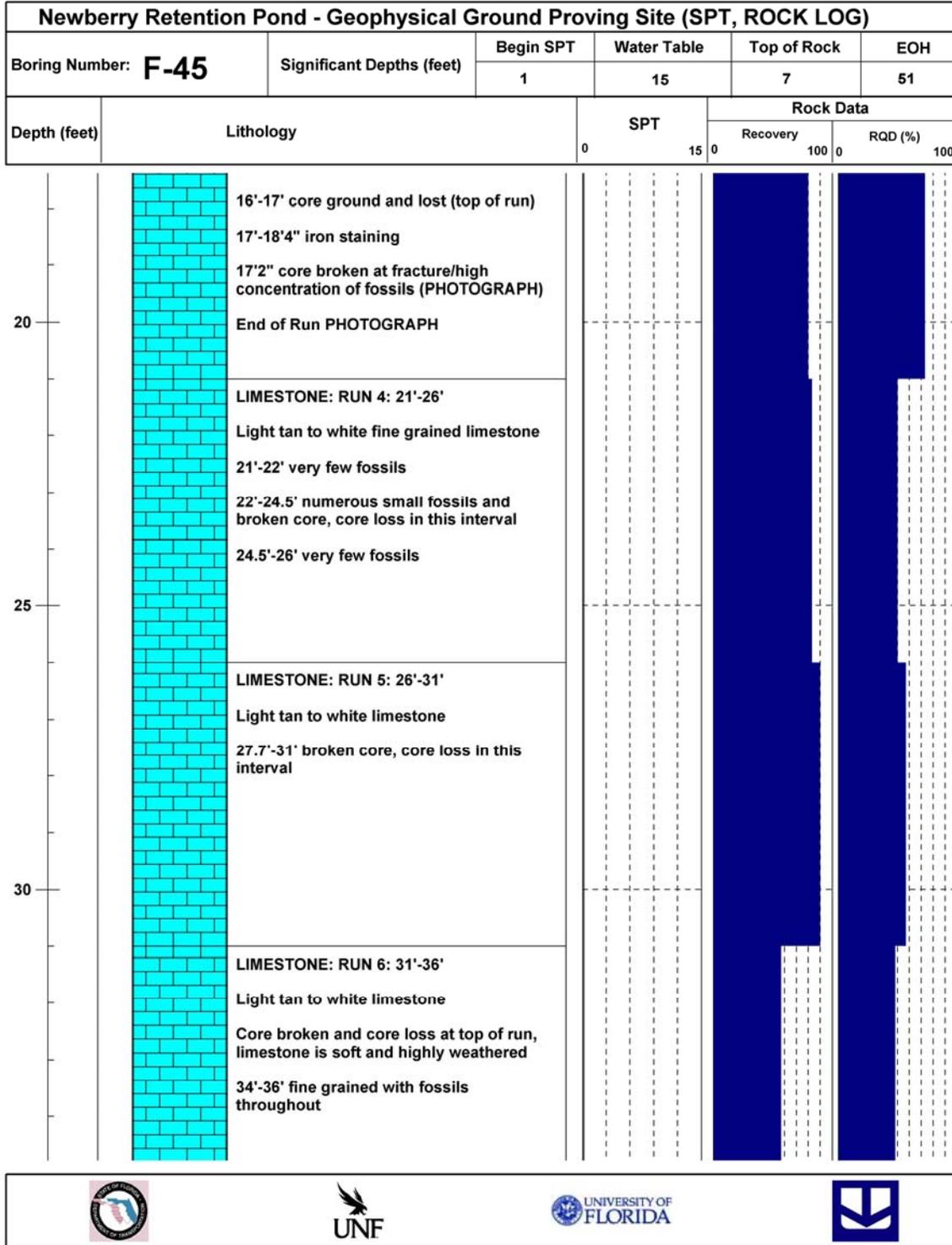


Figure B-8 Continued

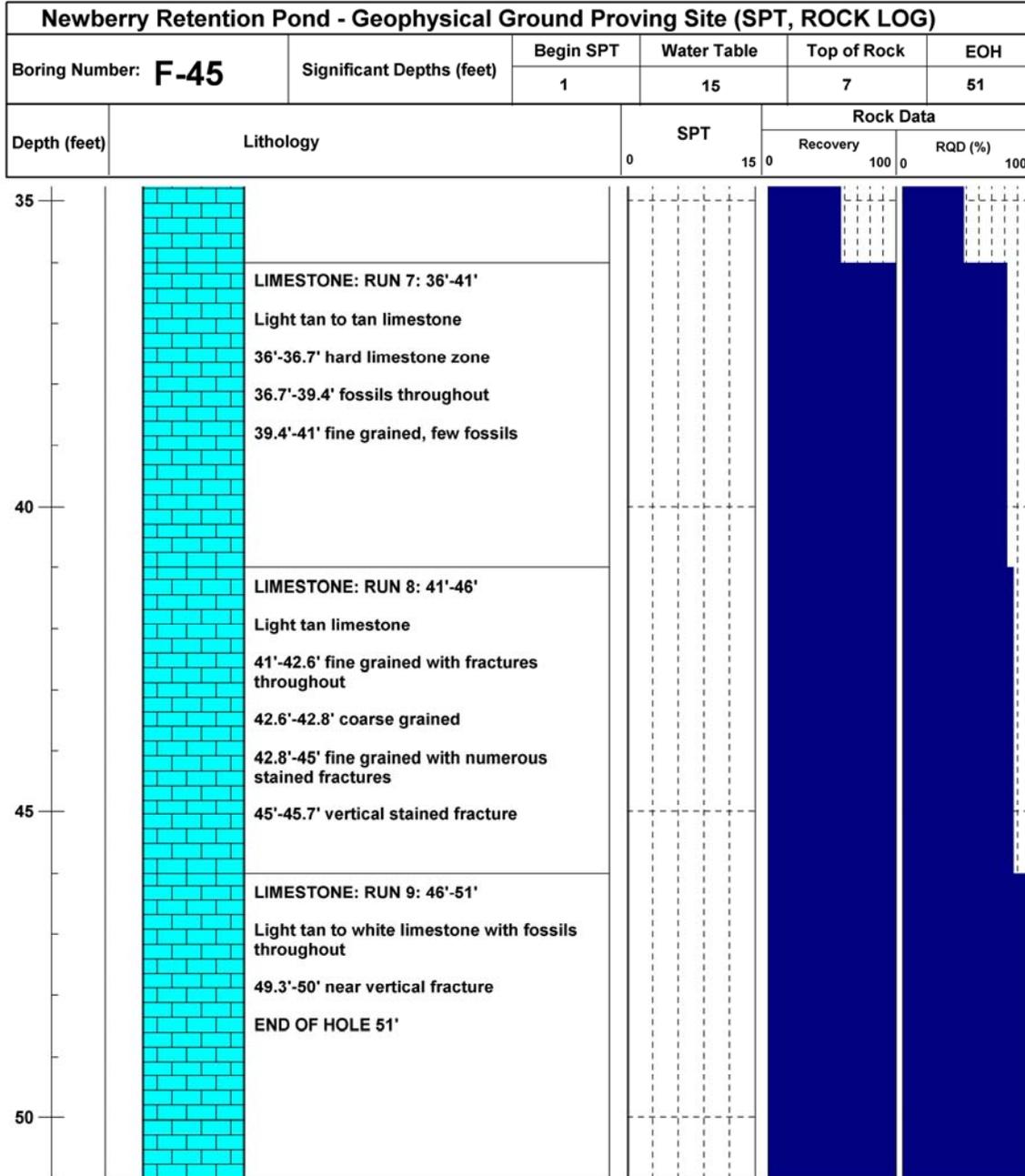


Figure B-8 Continued

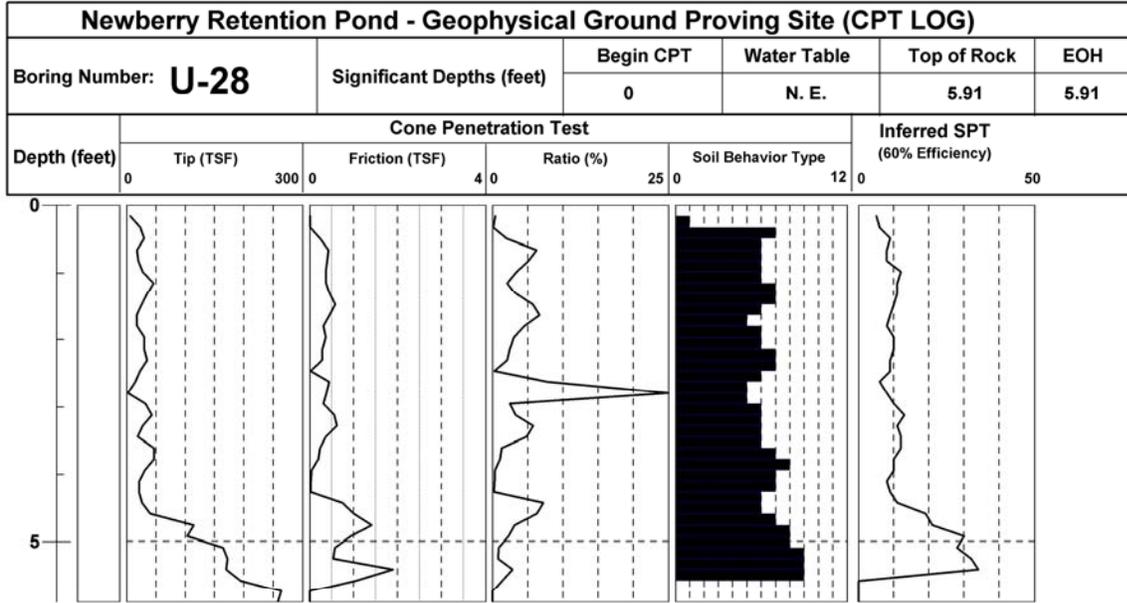


Figure B-9 Intrusive testing data from U Line, station 8.5 m

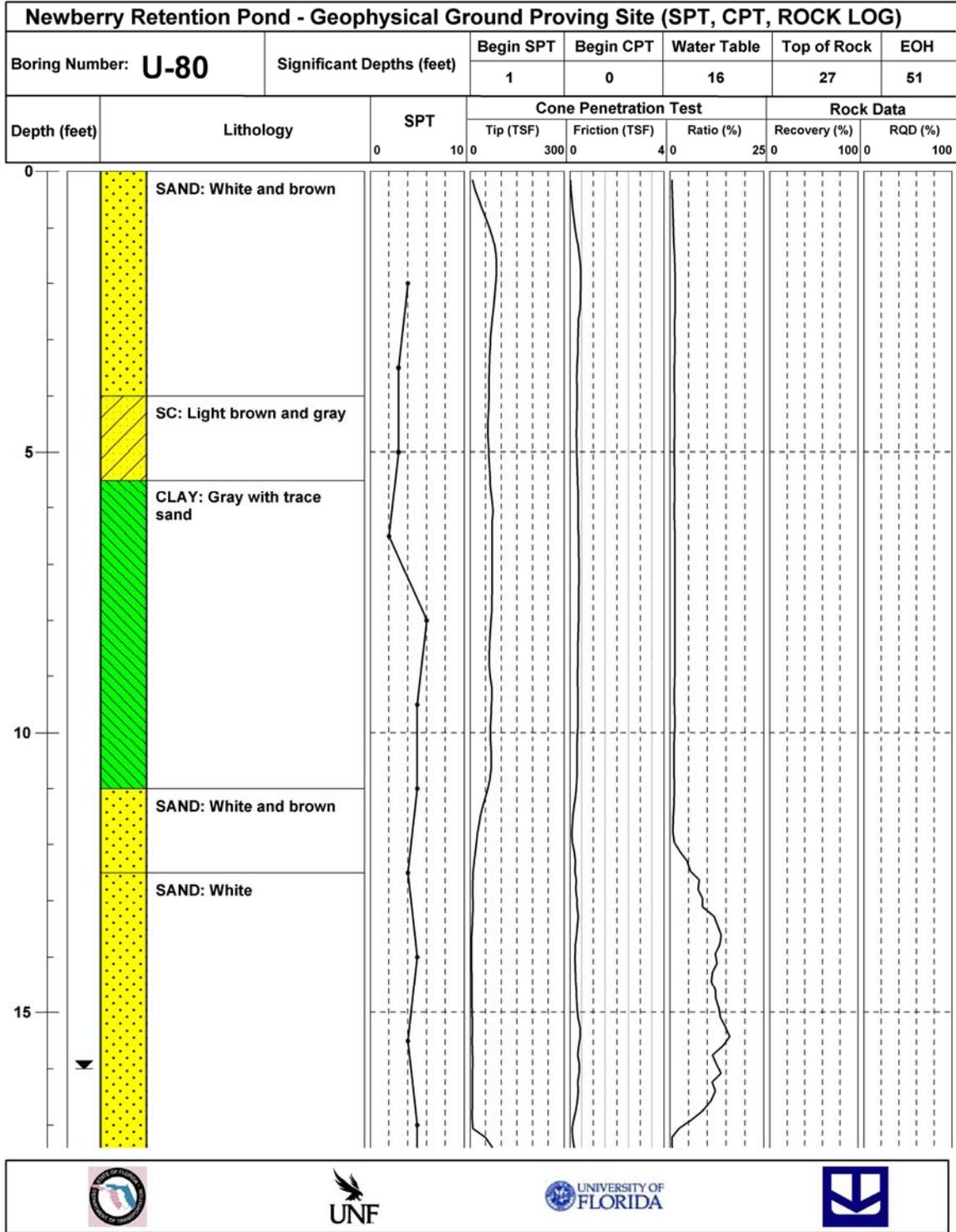


Figure B-10 Intrusive testing data from U Line, station 24.4 m

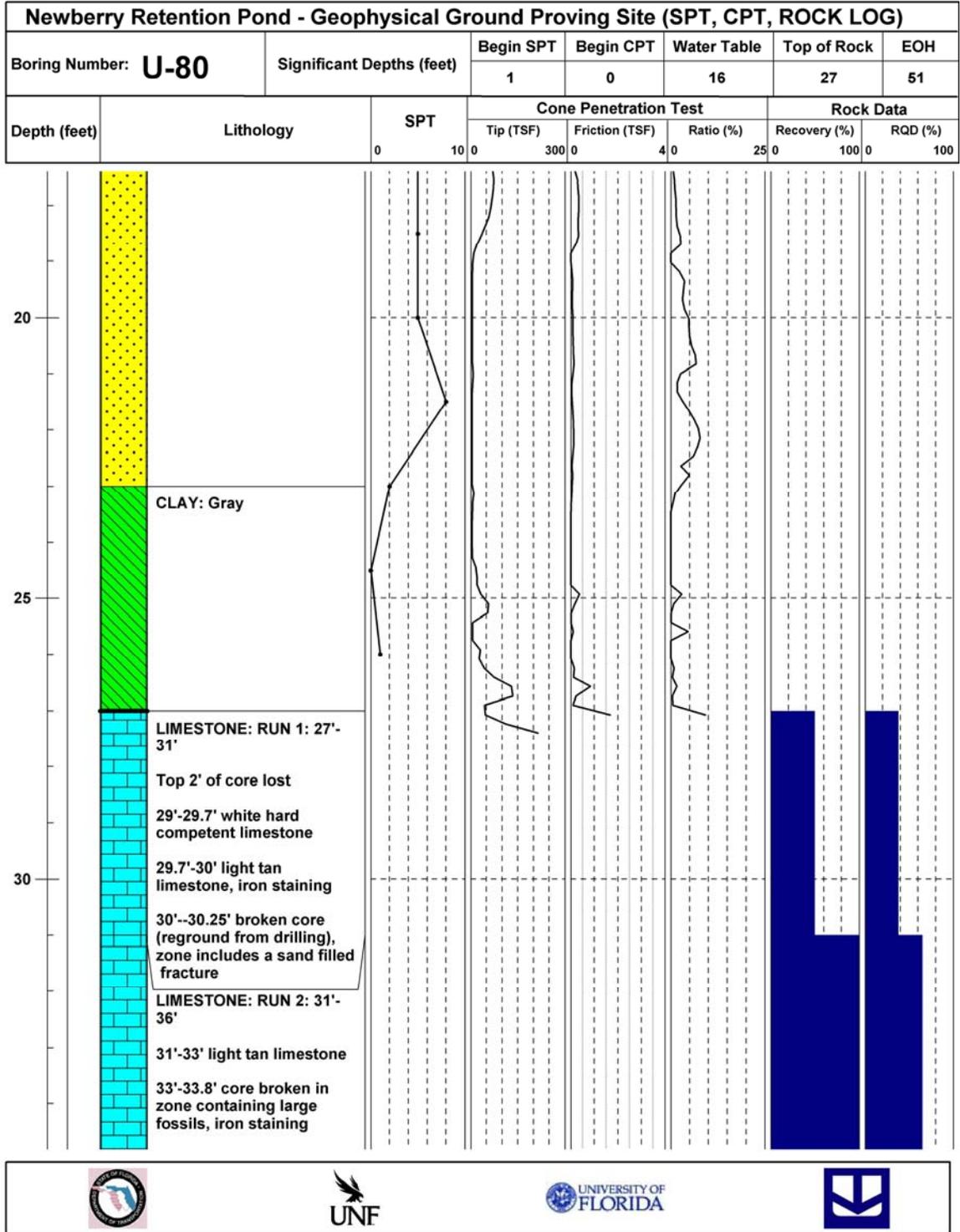


Figure B-10 Continued

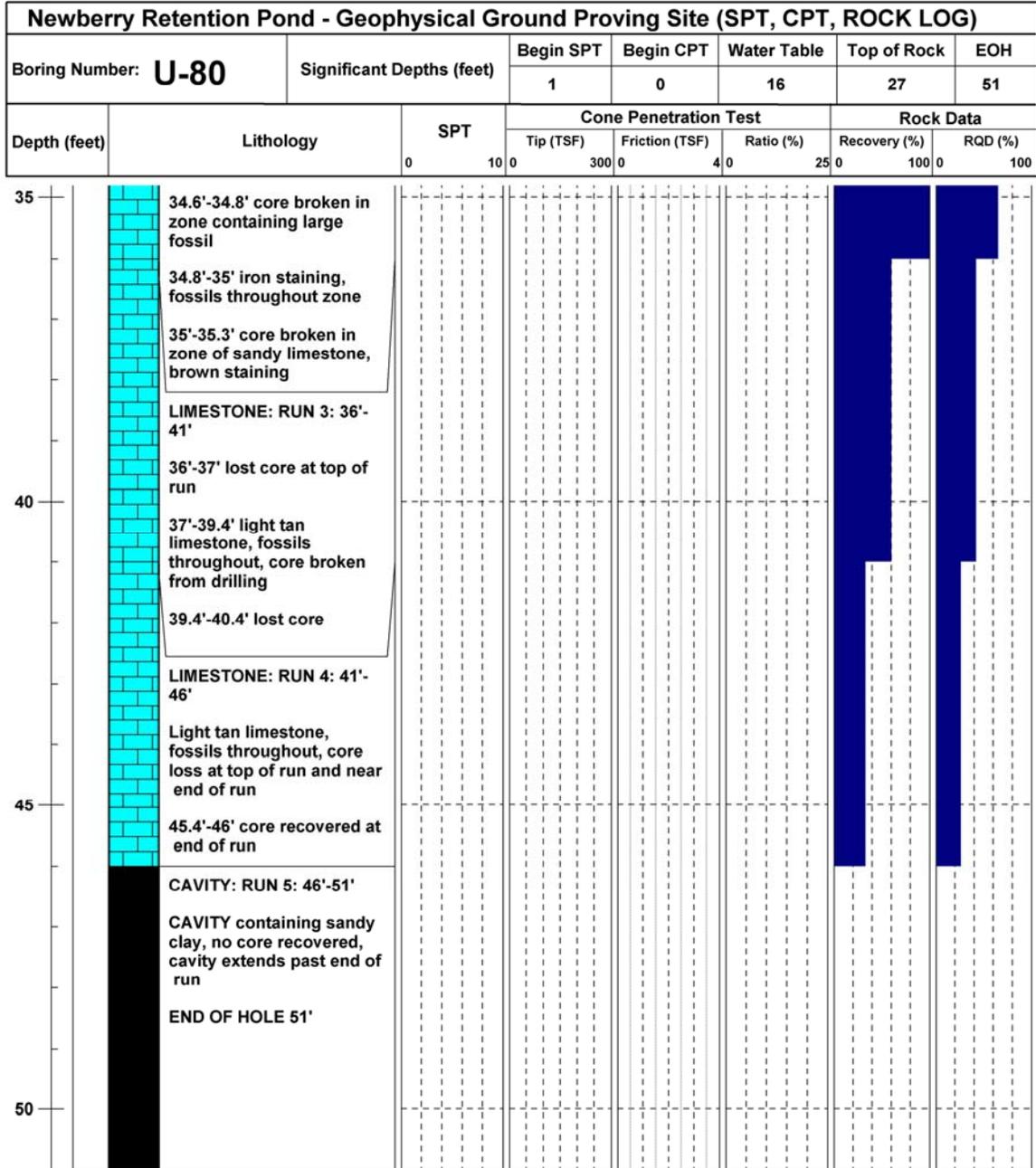


Figure B-10 Continued

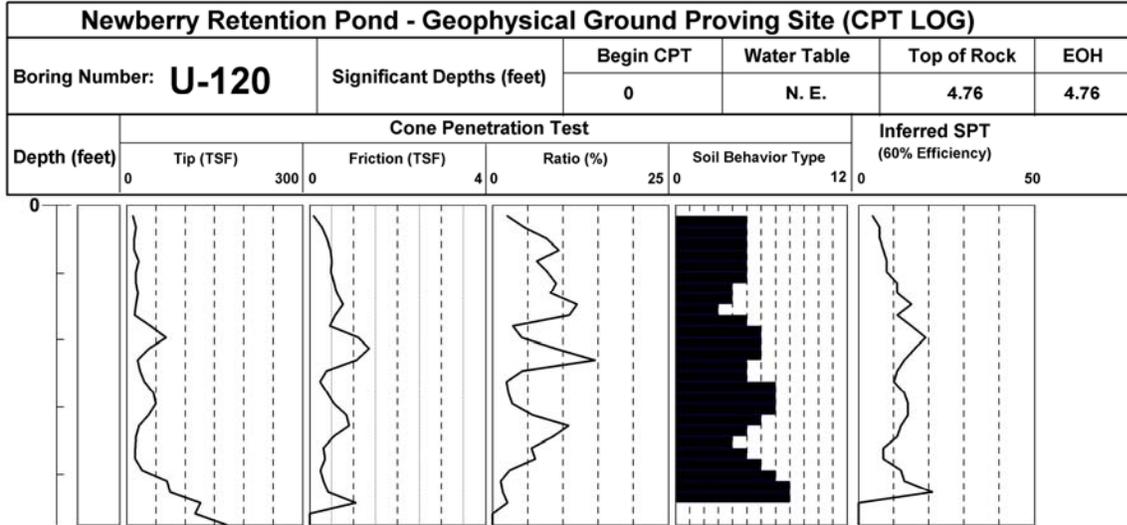


Figure B-11 Intrusive testing data from U Line, station 36.6 m

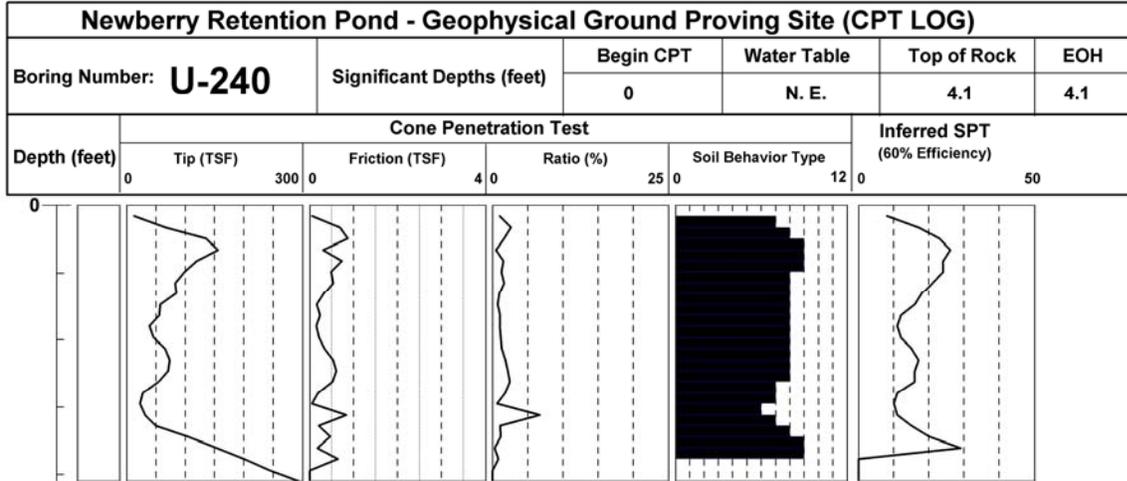


Figure B-12 Intrusive testing data from U Line, station 73.2 m

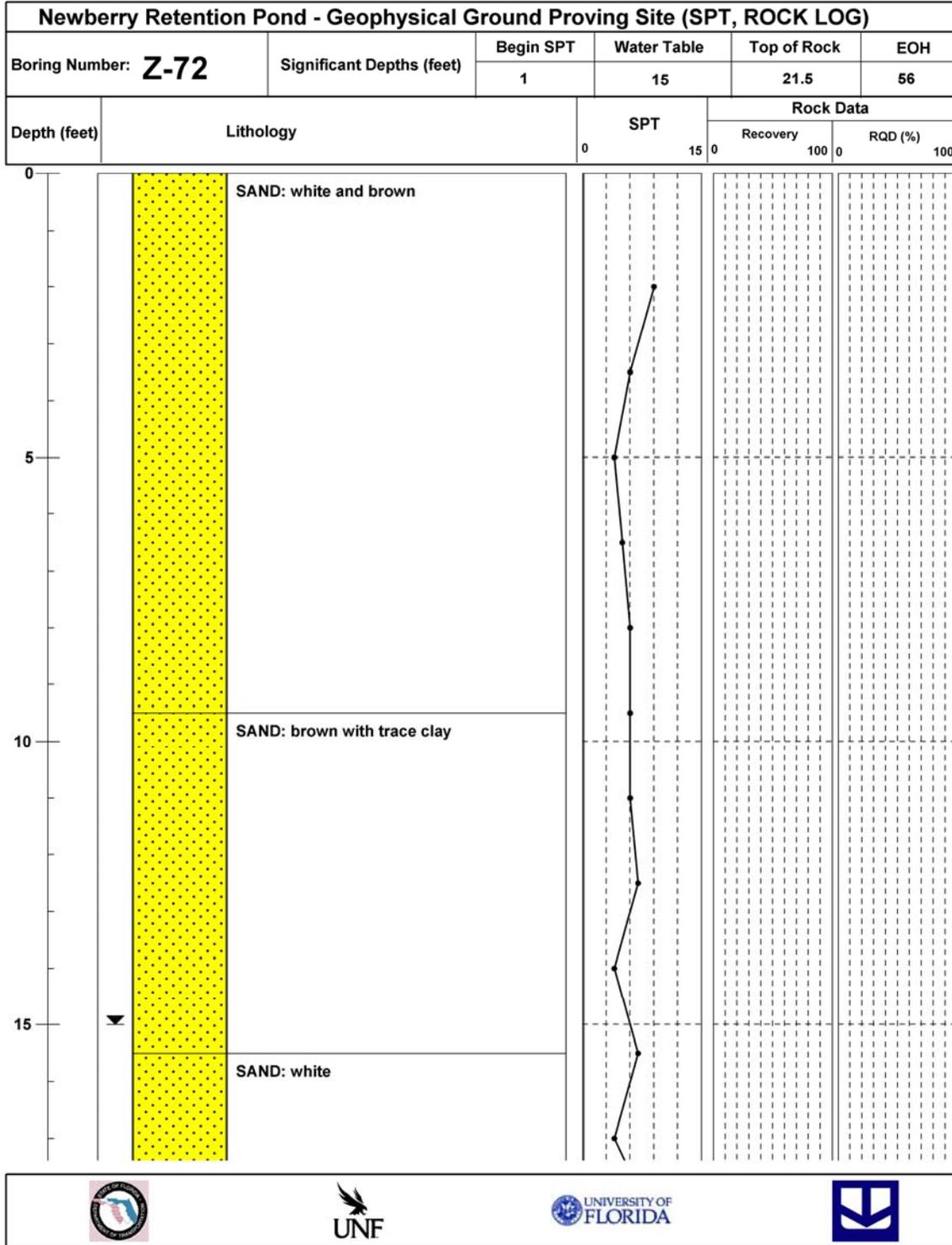


Figure B-13 Intrusive testing data from Z Line, station 21.9 m

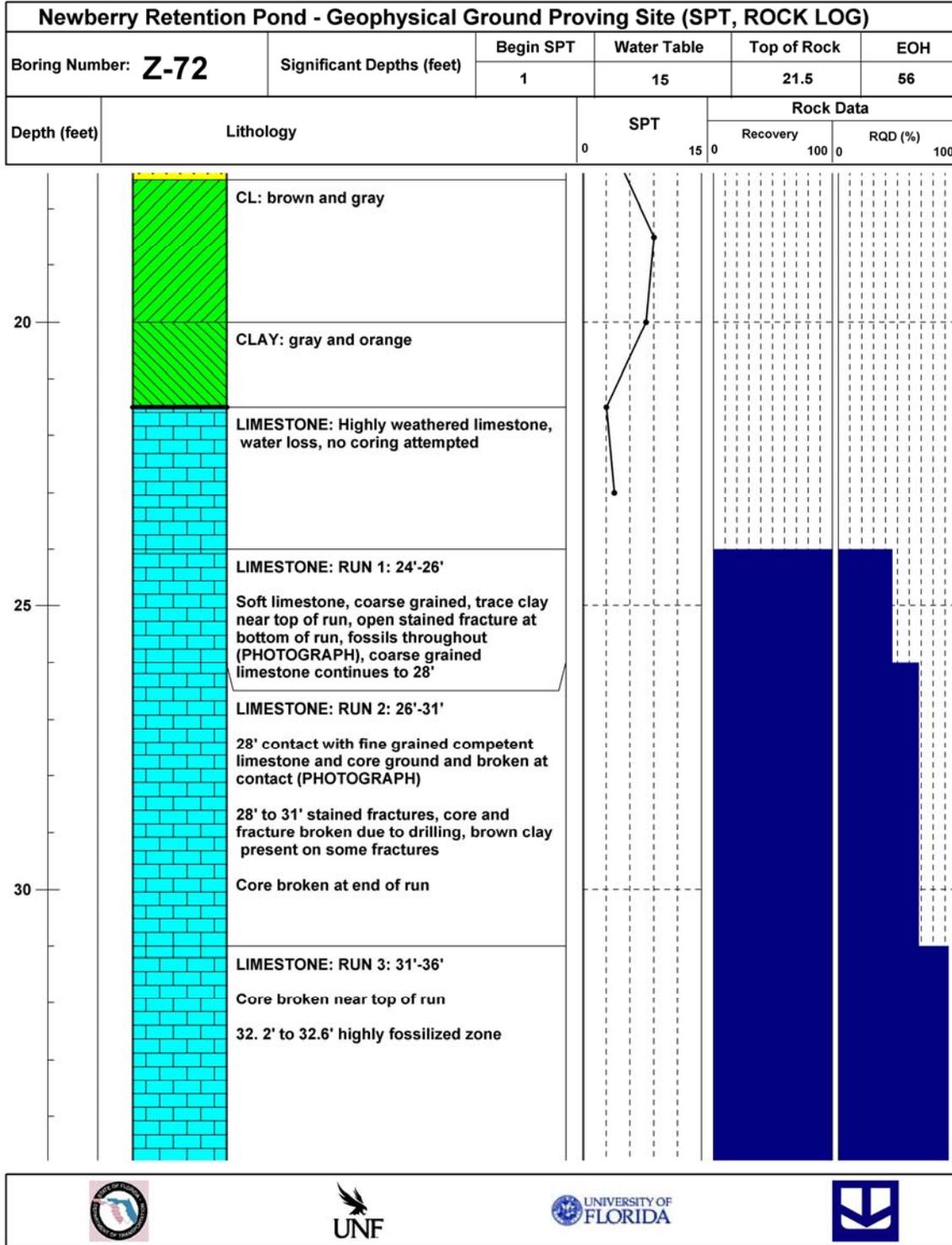


Figure B-13 Continued

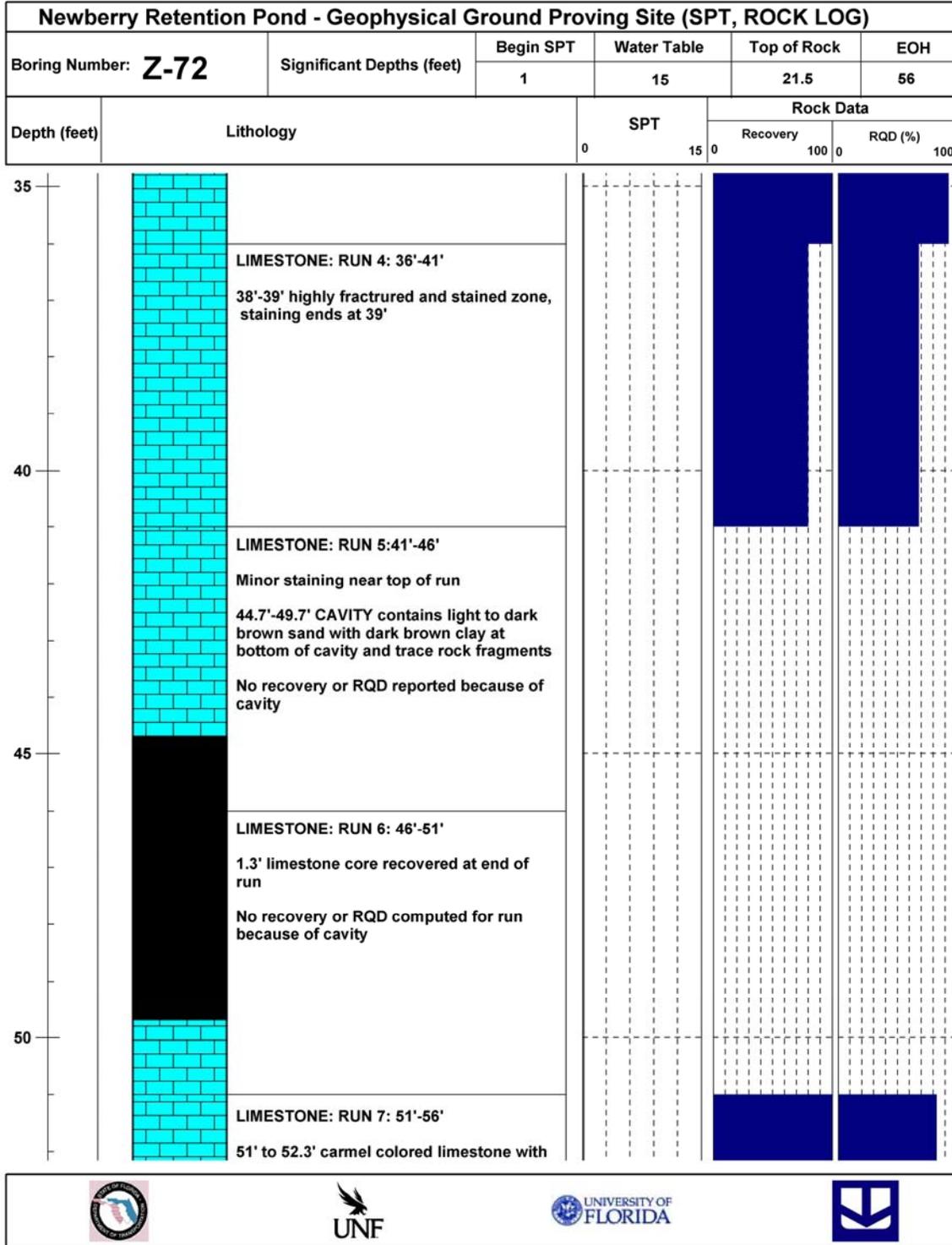


Figure B-13 Continued

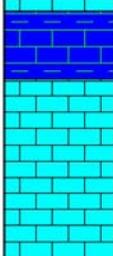
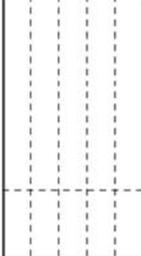
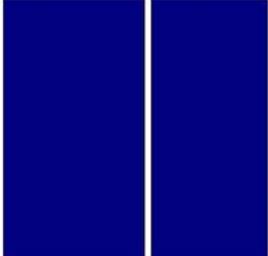
Newberry Retention Pond - Geophysical Ground Proving Site (SPT, ROCK LOG)					
Boring Number: Z-72	Significant Depths (feet)	Begin SPT	Water Table	Top of Rock	EOH
		1	15	21.5	56
Depth (feet)	Lithology	SPT		Rock Data	
		0	15	Recovery	RQD (%)
		0	15	100	100
55	 <p>stained fracture at end</p> <p>52.3' to 53.3' limestone with very thin dark brown clay layers and highly weathered zones (PHOTOGRAPH)</p> <p>53.3' to 56' tan to white fine grained limestone with healed fractures at end of run</p> <p>END OF HOLE 56'</p>				



Figure B-13 Continued

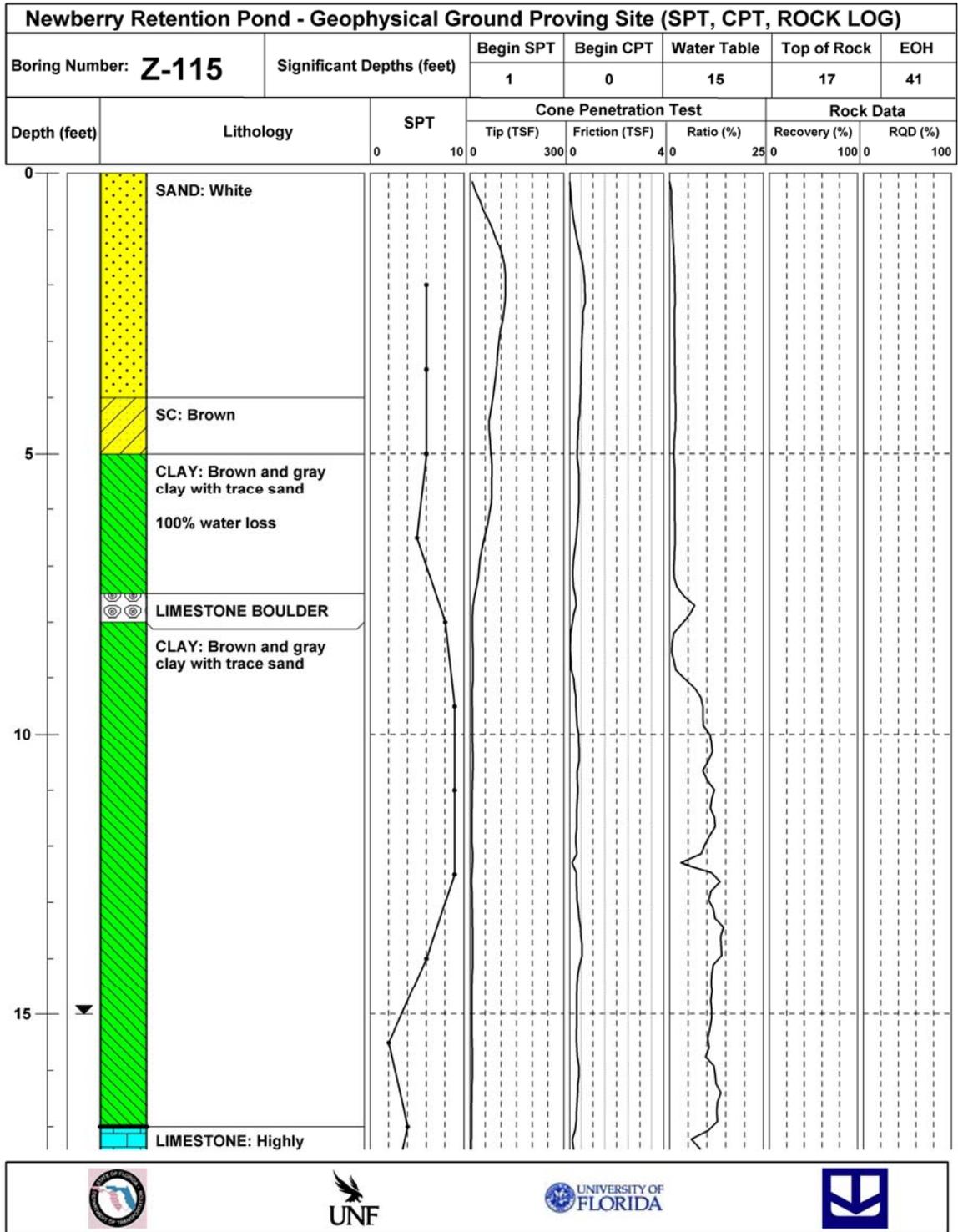


Figure B-14 Intrusive testing data from Z Line, station 35.0 m

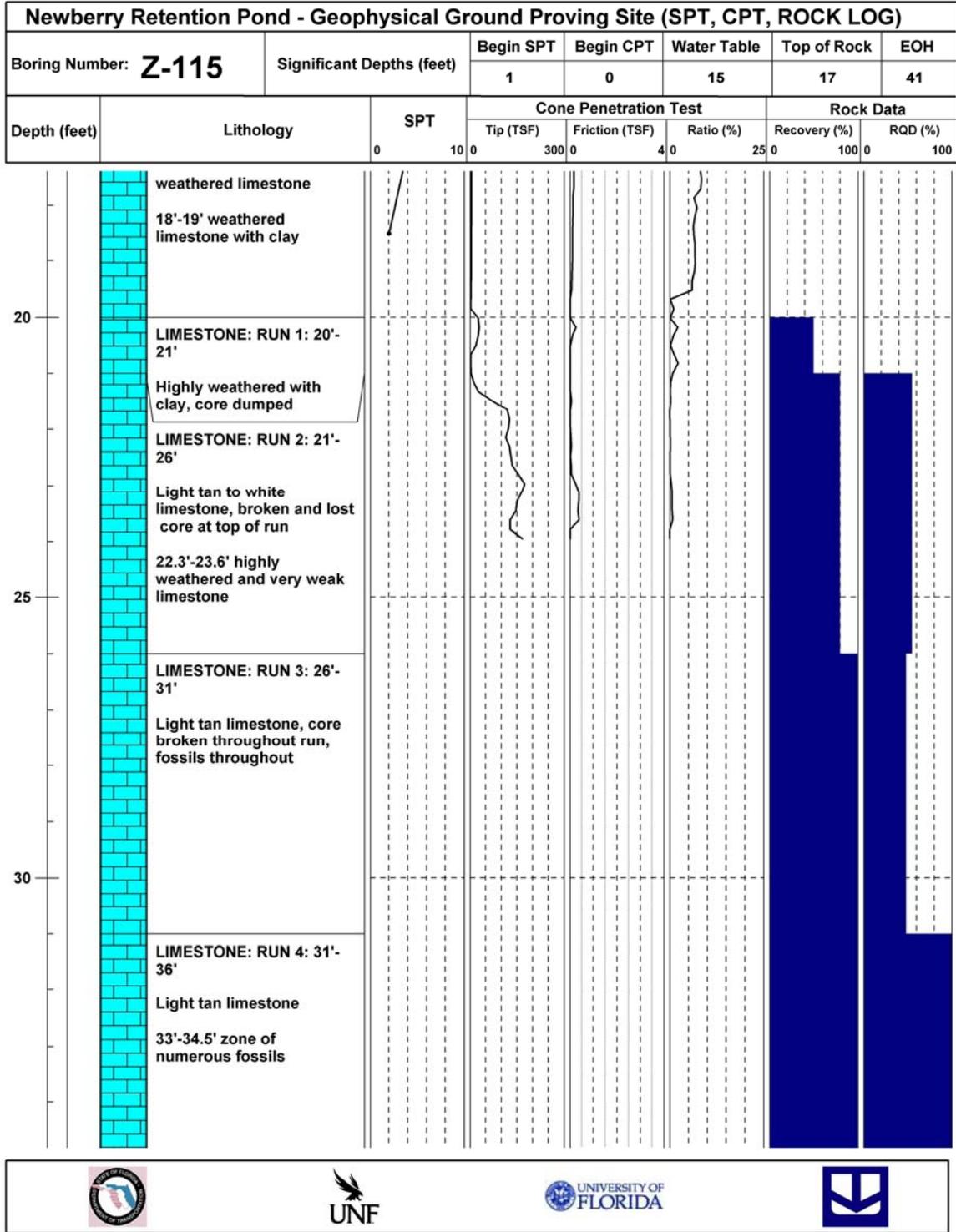


Figure B-14 Continued

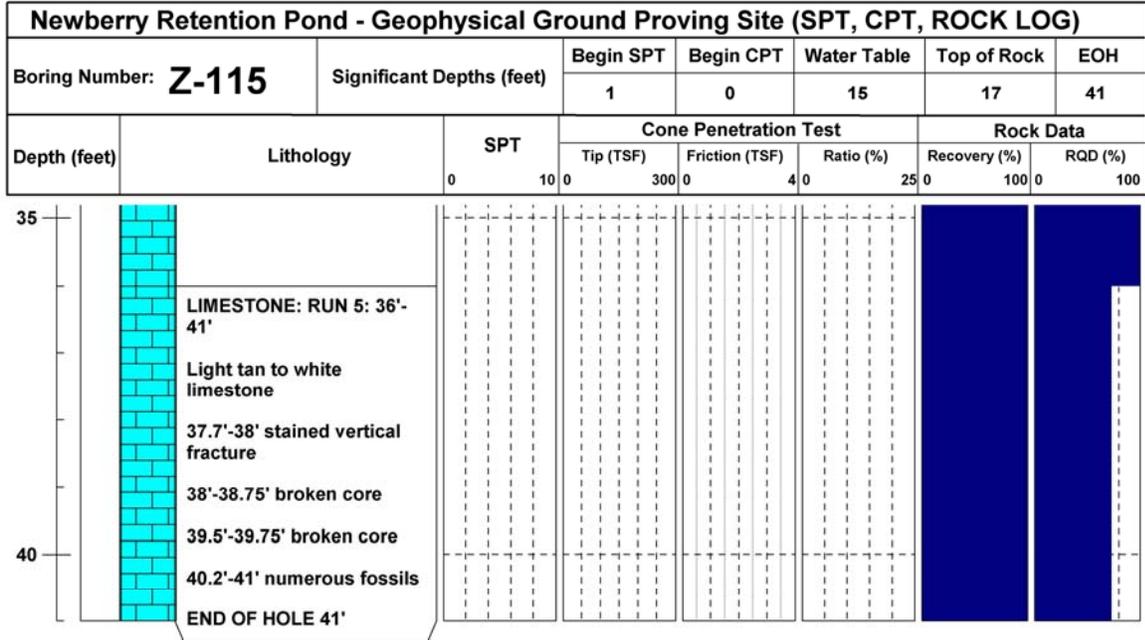


Figure B-14 Continued

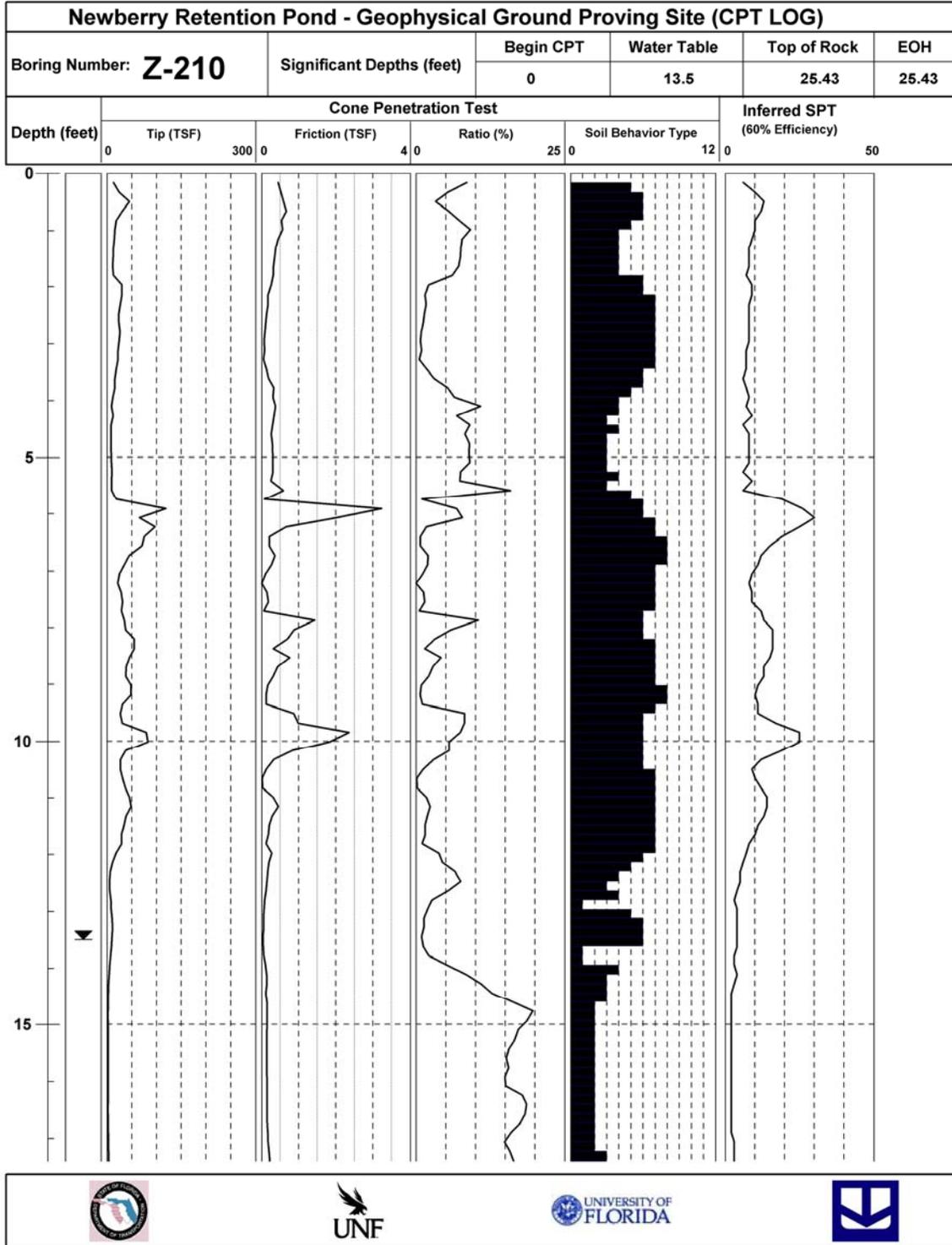


Figure B-15 Intrusive testing data from Z Line, station 64.0 m

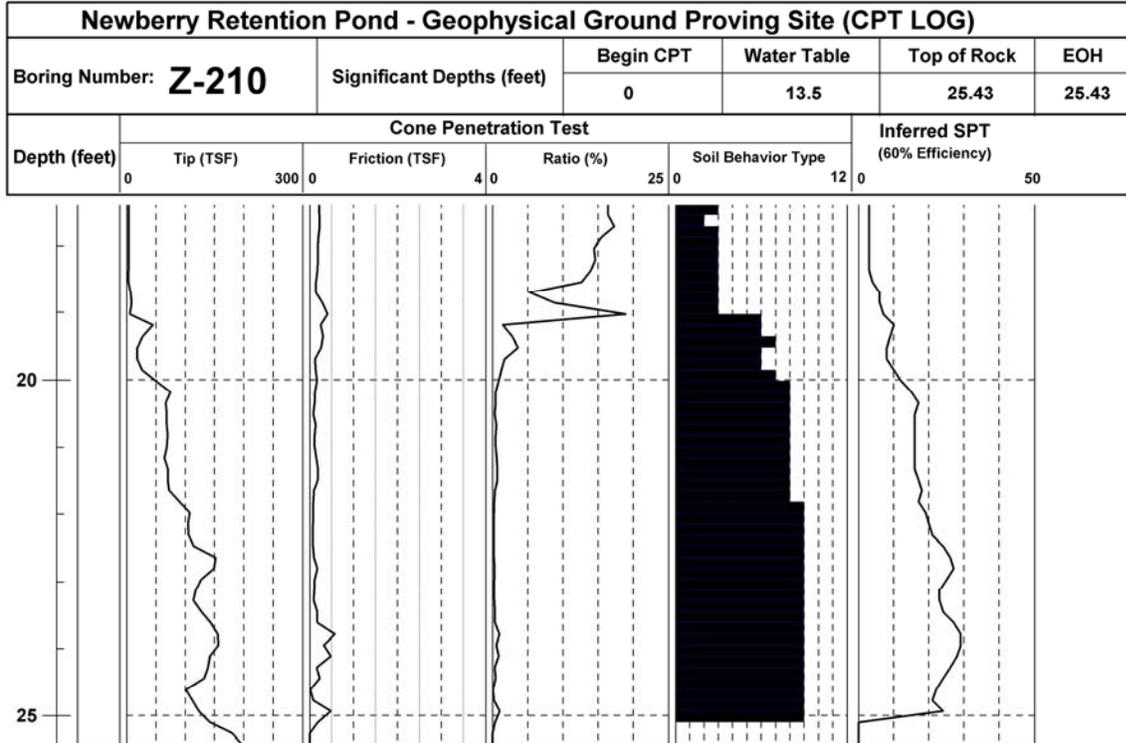


Figure B-15 Continued

APPENDIX C
 COMPARISON OF P-WAVE VELOCITY TOMOGRAMS TO TOP OF BEDROCK
 DEPTHS ENCOUNTERED THROUGH INTRUSIVE TESTING

The yellow rectangles indicate locations of intrusive testing, with the bottom end representing the depth at which bedrock was encountered.

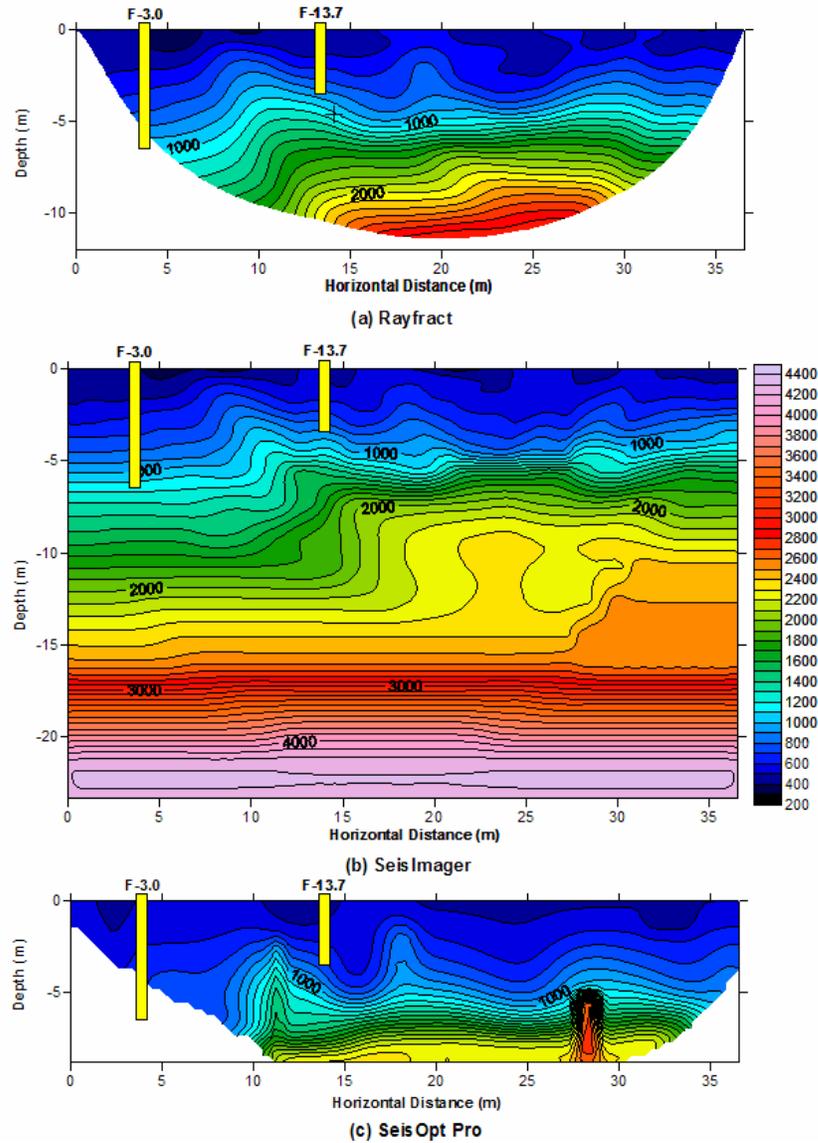


Figure C-1 Top of bedrock location from intrusive testing for F Line, station 0-36.6 m.
 (a) Rayfract, (b) SeisImager, and (c) SeisOpt Pro.

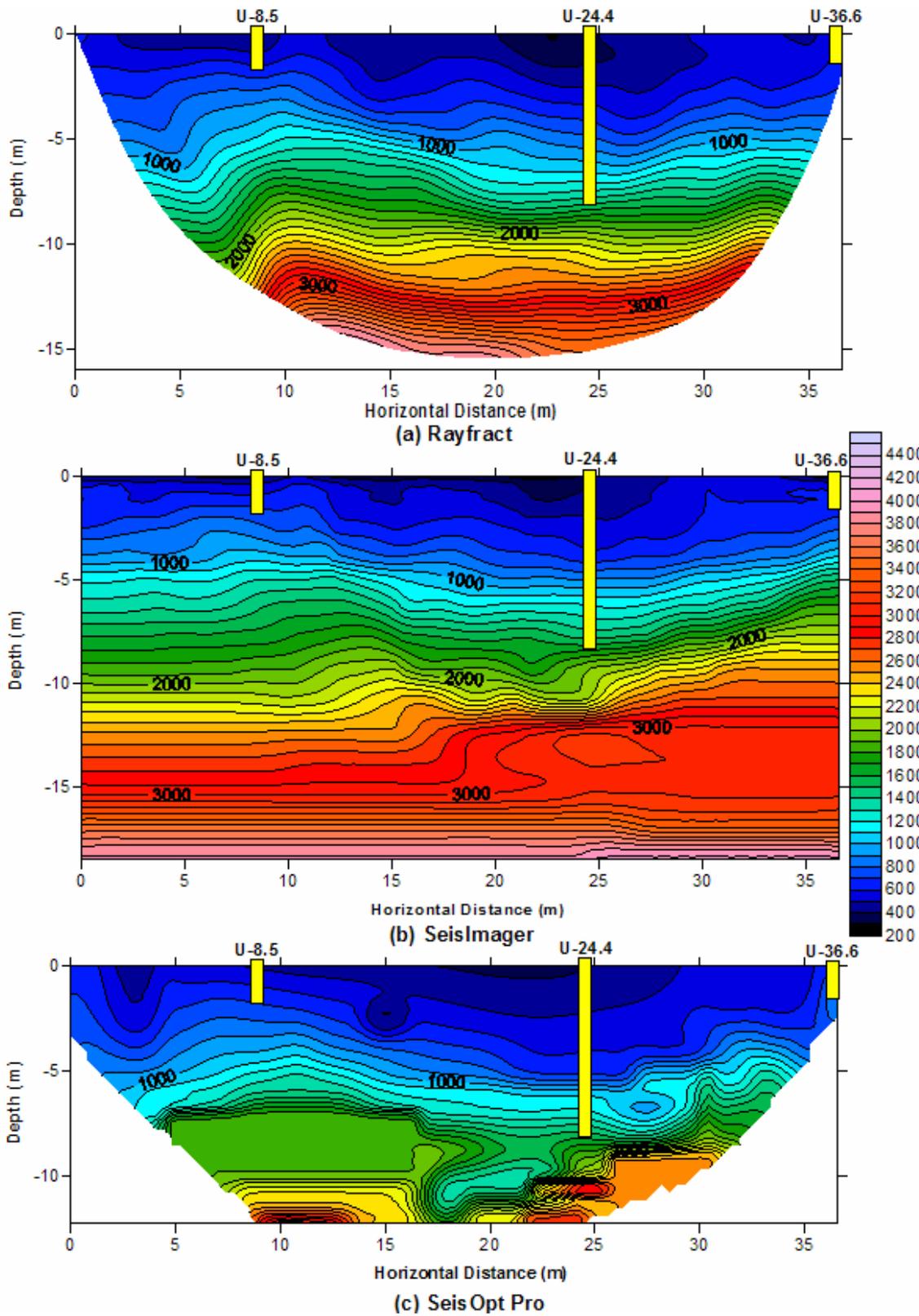
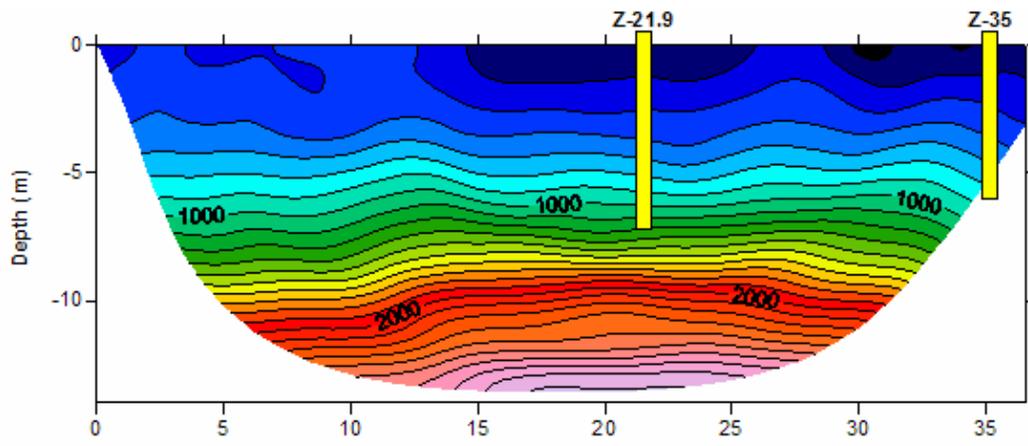
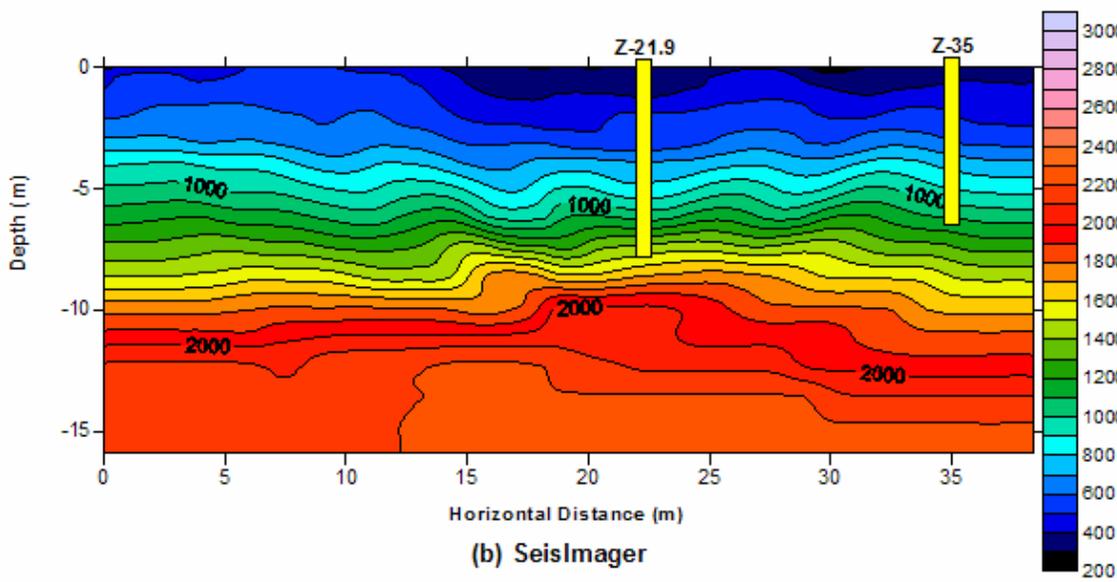


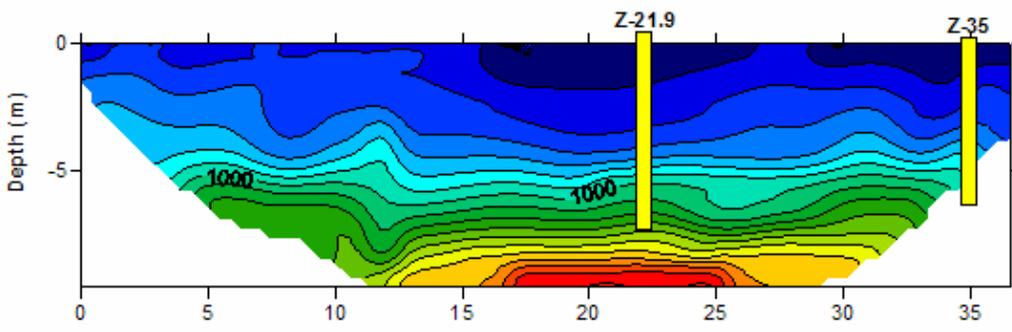
Figure C-2 Top of bedrock location from intrusive testing for U Line, station 0-36.6 m. (a) Rayfract, (b) SeisImager, and (c) SeisOpt Pro.



(a) Rayfract

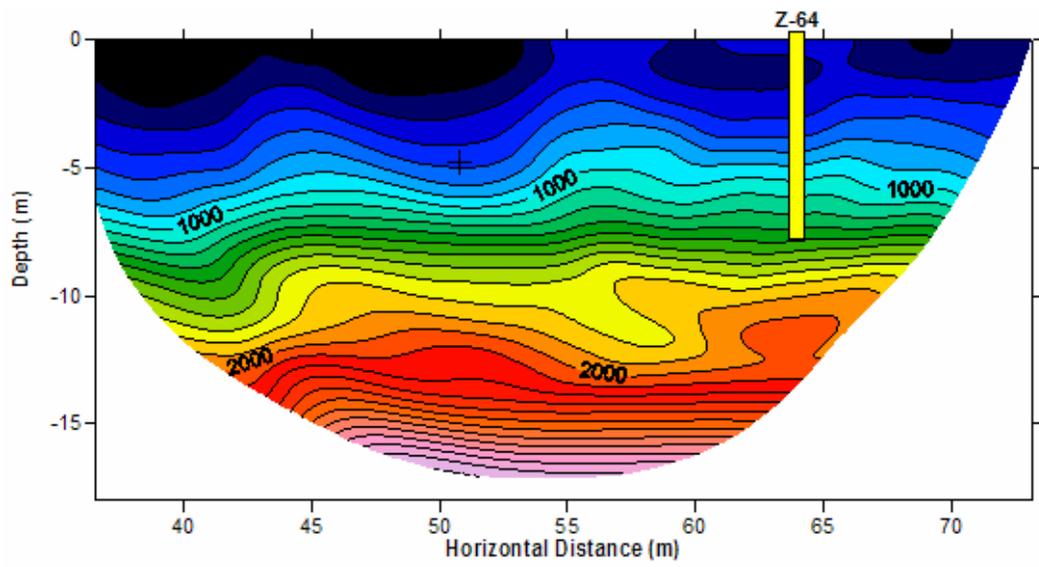


(b) SeisImager

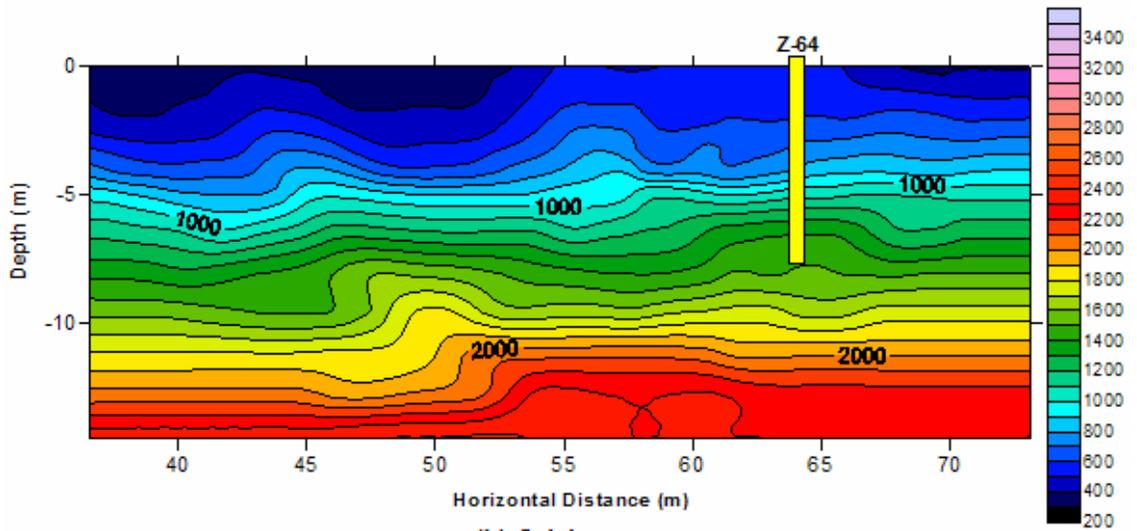


(c) SeisOpt Pro

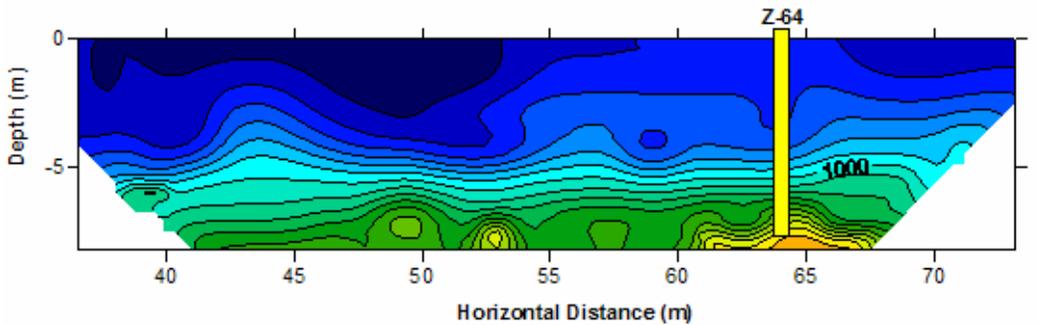
Figure C-3 Top of bedrock location from intrusive testing for Z Line, station 0-38.4 m. (a) Rayfract, (b) SeisImager, and (c) SeisOpt Pro.



(a) Rayfract



(b) SeisImager



(c) SeisOpt Pro

Figure C-4 Top of bedrock location from intrusive testing for Z Line, station 36.6-73.2 m. (a) Rayfract, (b) SeisImager, and (c) SeisOpt Pro.

APPENDIX D
CLOSE CONTOUR P-WAVE TOMOGRAM INTRUSIVE DATA COMPARISON

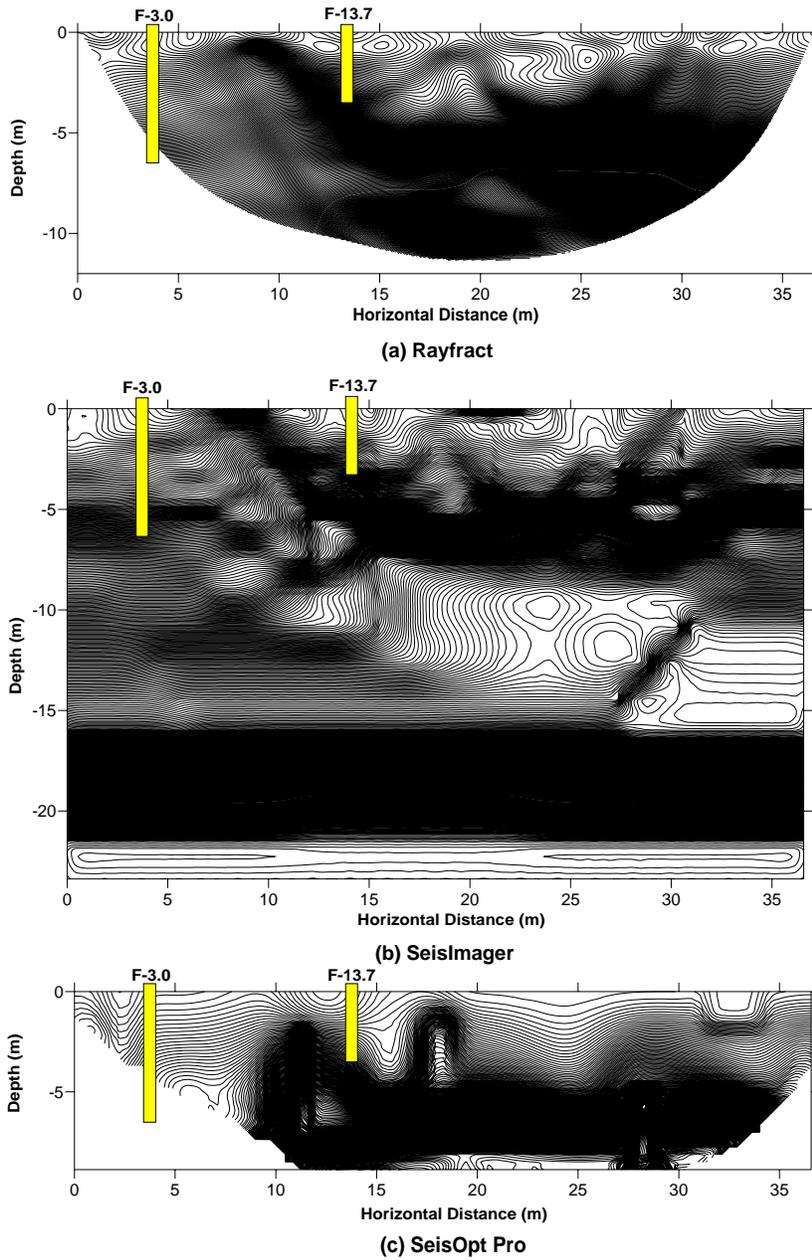


Figure D-1 Estimated top of bedrock from intrusive testing overlain onto 10 m/s contour interval tomograms produced for the F line 36.6-73.2 m. (a) Rayfract, (b) SeisImager, and (c) SeisOpt Pro.

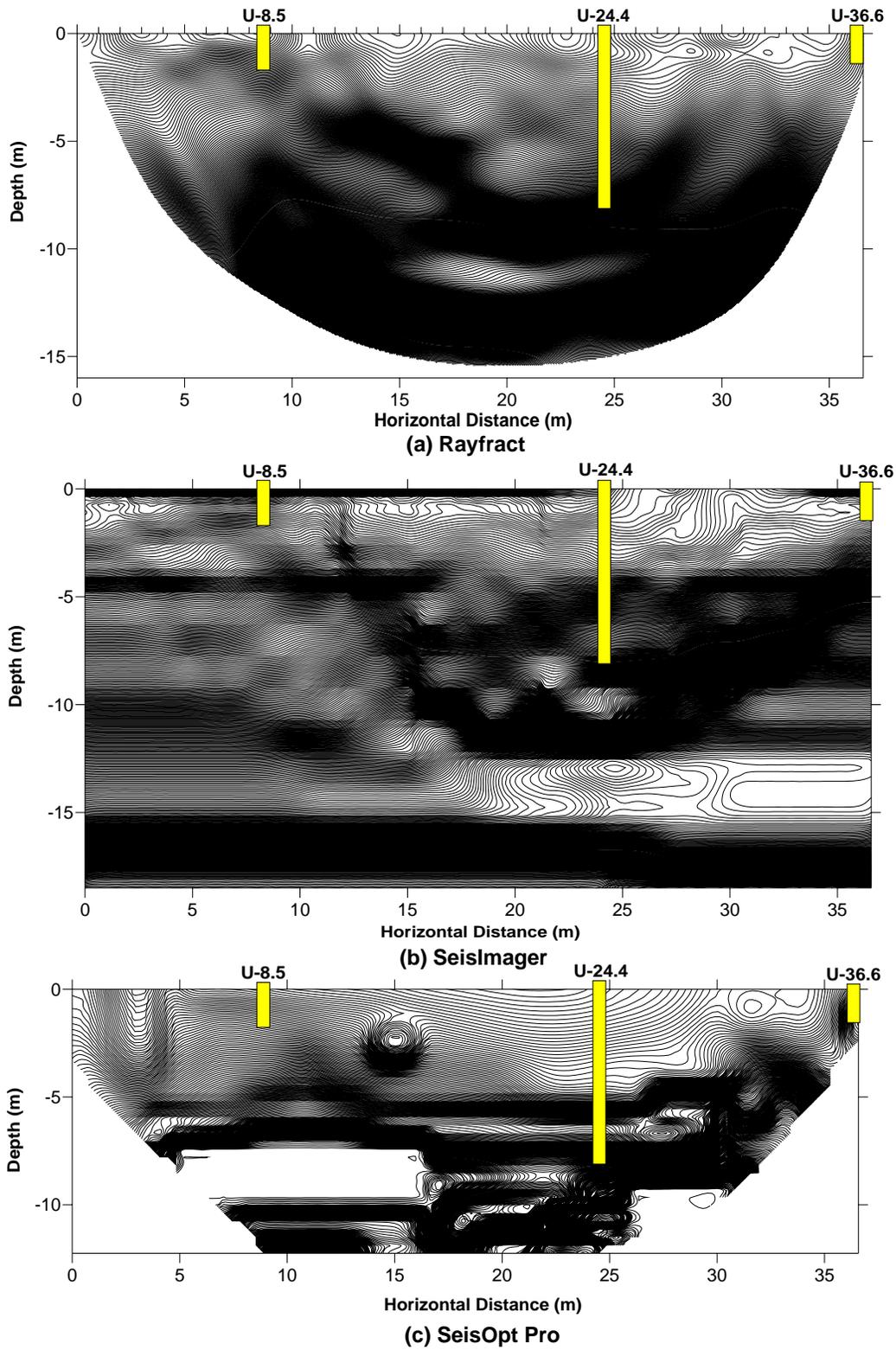


Figure D-2 Estimated top of bedrock from intrusive testing overlain onto 10 m/s contour interval tomograms produced for the U line 0-36.6 m. (a) Rayfract, (b) SeisImager, and (c) SeisOpt Pro.

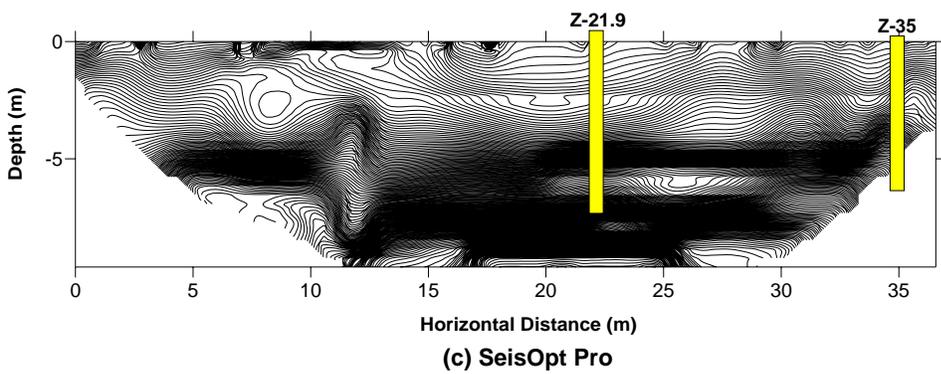
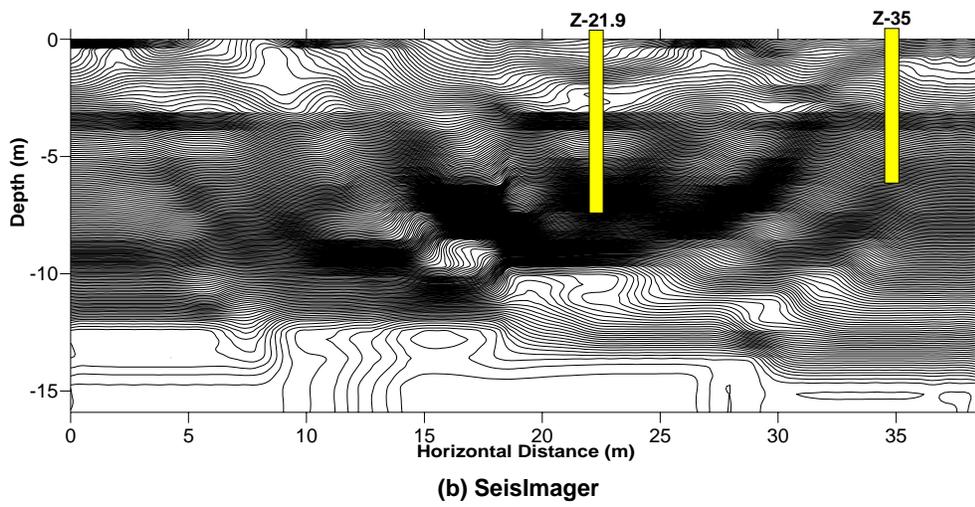
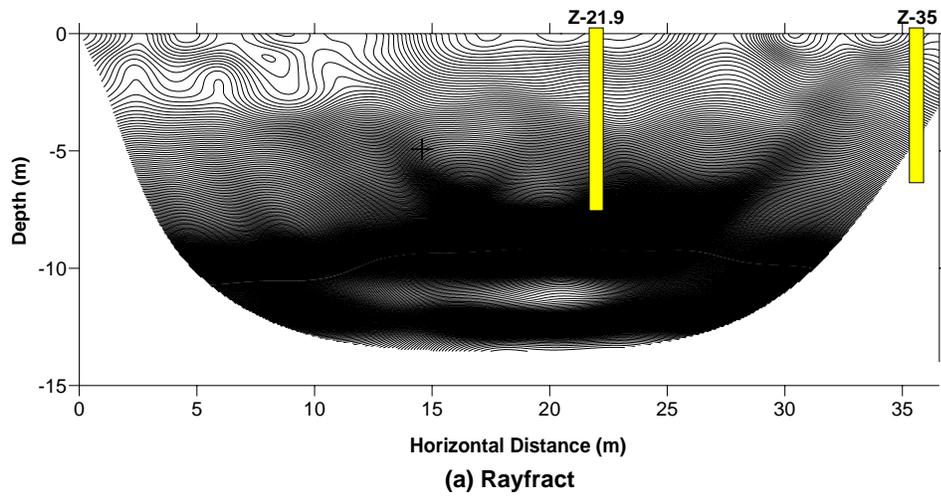
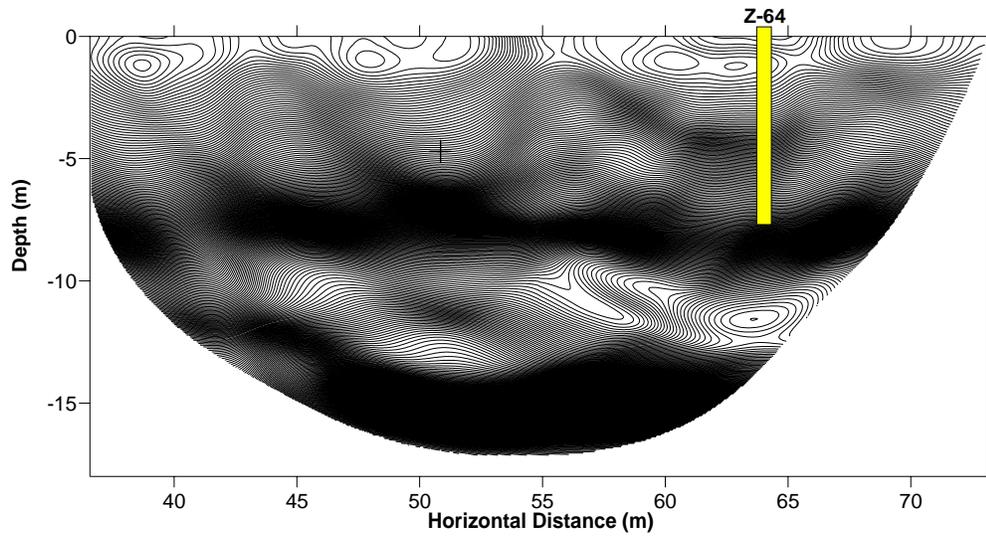
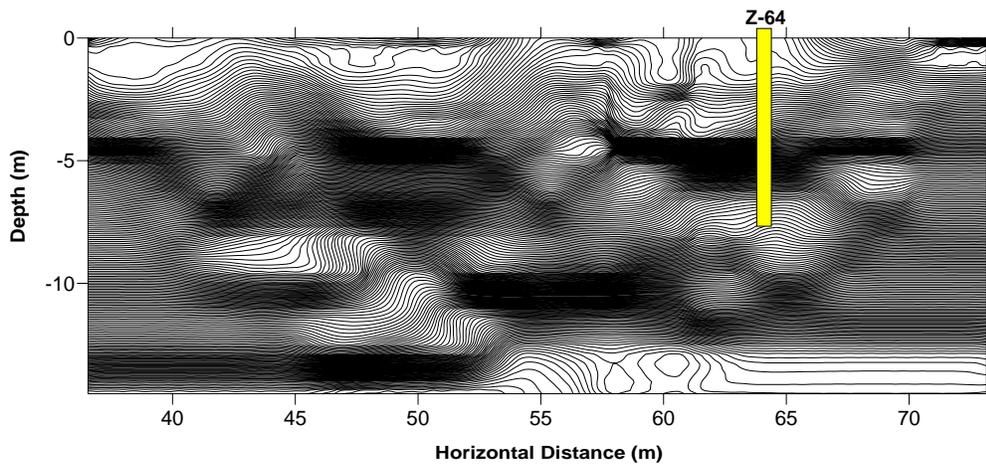


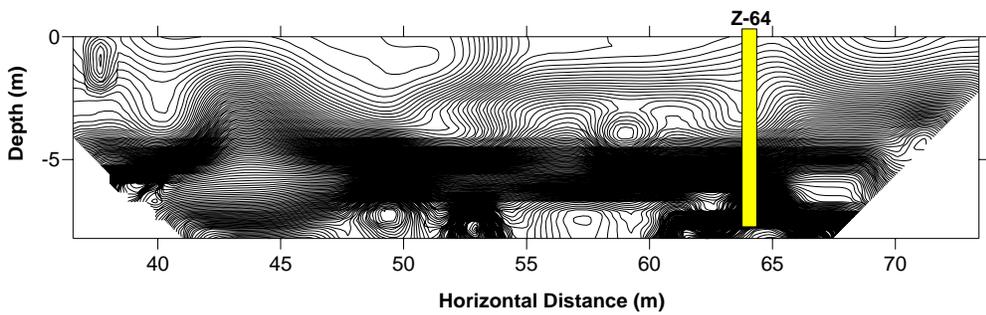
Figure D-3 Estimated top of bedrock from intrusive testing overlain onto 10 m/s contour interval tomograms produced for the Z line 0-38.4 m. (a) Rayfract, (b) SeisImager, and (c) SeisOpt Pro.



(a) Rayfract



(b) SeisImager



(c) SeisOpt Pro

Figure D-4 Estimated top of bedrock from intrusive testing overlain onto 10 m/s contour interval tomograms produced for the Z line 36.6-73.2 m. (a) Rayfract, (b) SeisImager, and (c) SeisOpt Pro

APPENDIX E
RAYTRACING DIAGRAMS FOR TOMOGRAMS

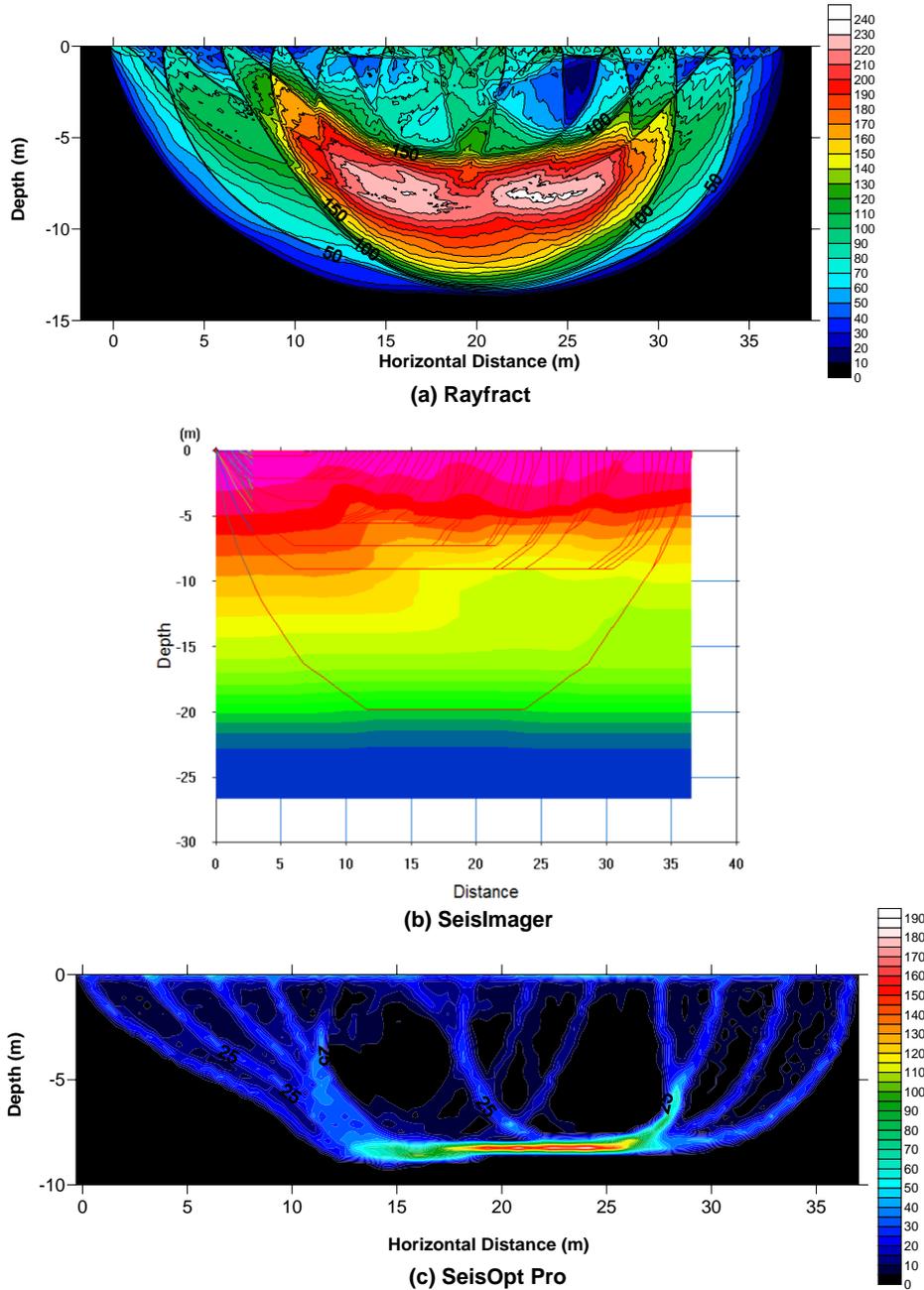
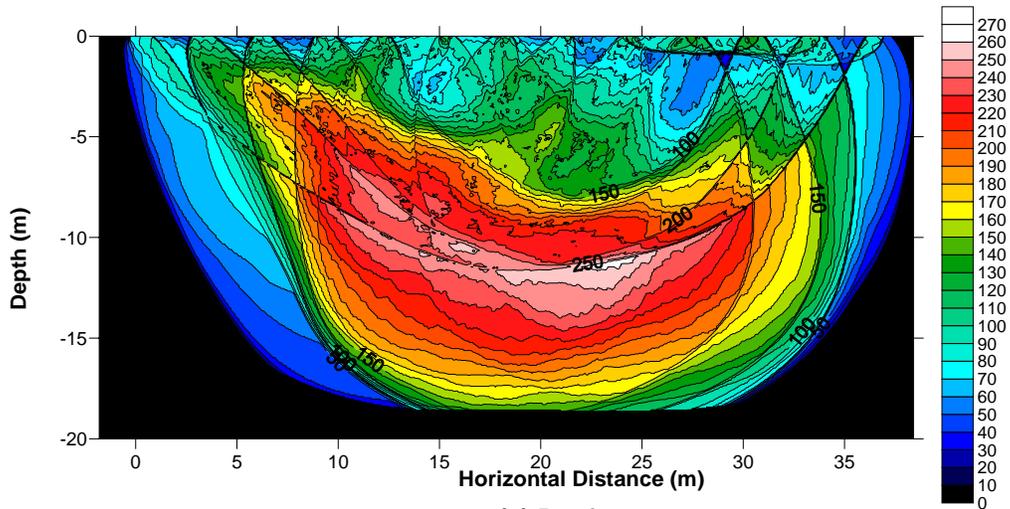
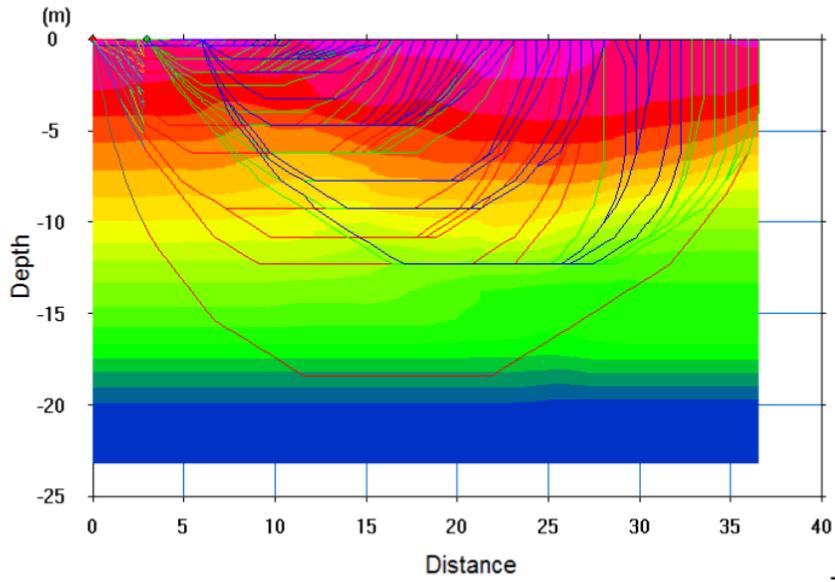


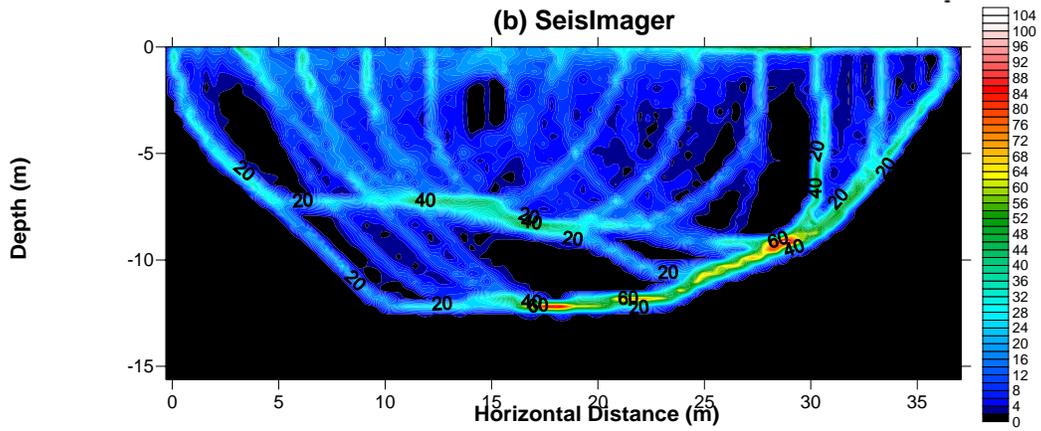
Figure E-1 Raytracing diagram for F Line, station 0-36.6 m. (a) Rayfract, (b) SeisImager, and (c) SeisOpt Pro.



(a) Rayfract



(b) SeisImager



(c) SeisOpt Pro

Figure E-2 Raytracing diagram for U Line, station 0-36.6 m. (a) Rayfract, (b) SeisImager, and (c) SeisOpt Pro.

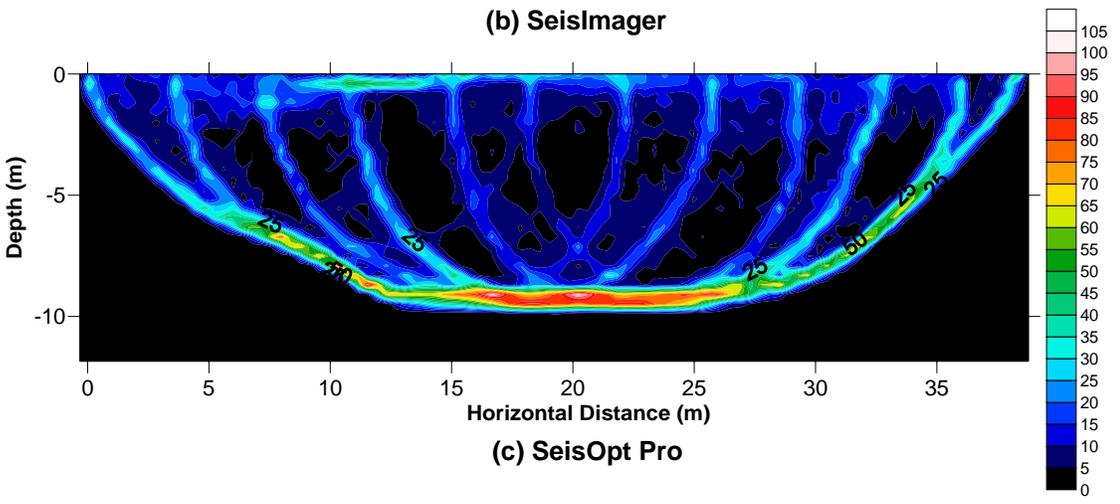
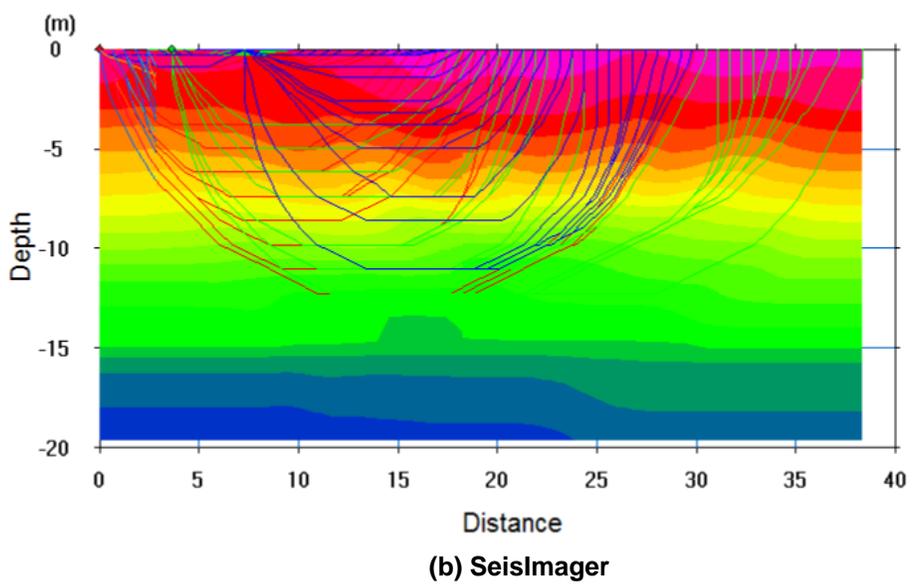
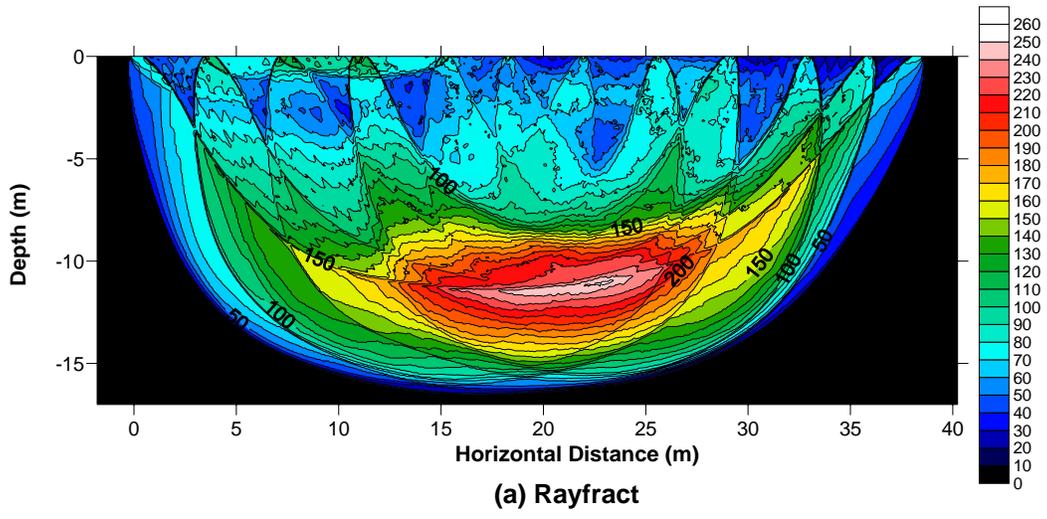
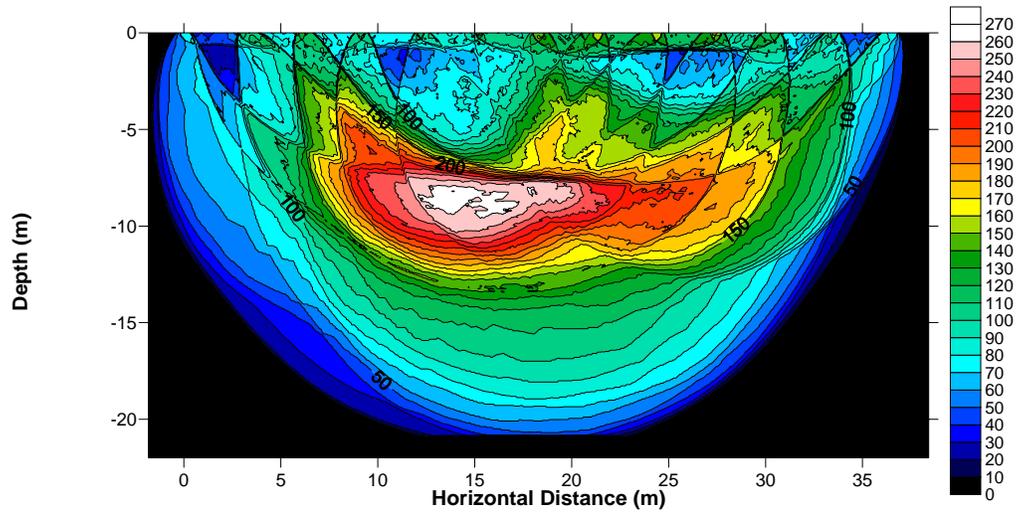
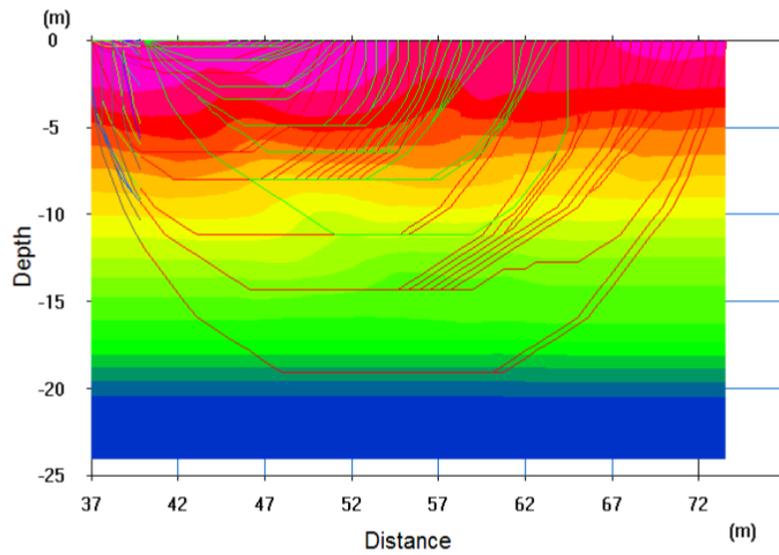


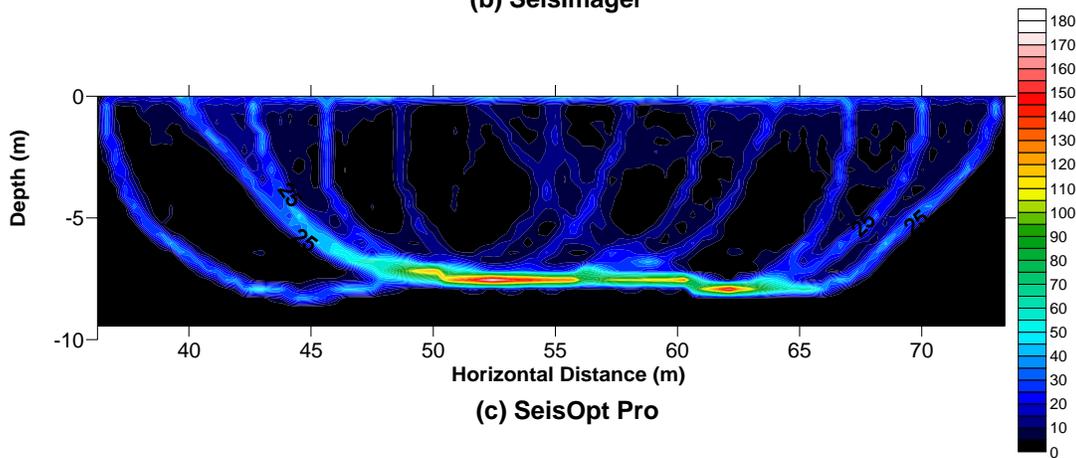
Figure E-3 Raytracing diagram for Z Line, station 0-38.4 m. (a) Rayfract, (b) SeisImager, and (c) SeisOpt Pro.



(a) Rayfract



(b) SeisImager



(c) SeisOpt Pro

Figure E-4 Raytracing diagram for Z Line, station 36.6-73.2 m. (a) Rayfract, (b) SeisImager, and (c) SeisOpt Pro

LIST OF REFERENCES

- Campbell, K. M. and Scott, T. M. (1991), "Radon Potential Study, Alachua County, Florida: Near-Surface Stratigraphy and Results of Drilling," Florida Geological Survey Open File Report Number 41, 15 pp.
- Carpenter, P. J., Higuera-Diaz, I. C., Thompson, M. D., Atre, S., and Mandell, W. (2003), "Accuracy of Seismic Refraction Tomography Codes at Karst Sites," *Geophysical Site Characterization: Seeing Beneath the Surface, Proceedings of a Symposium on the Application of Geophysics to Engineering and Environmental Problems*, San Antonio, Texas, April 6-10, pp. 832-840.
- Cramer, B.J., and Hiltunen, D.R. (2004), "Investigation of Bridge Foundation Sites in Karst Terrane Via Seismic Refraction Tomography," *83rd Annual Meeting Compendium of Papers CD-ROM*, Transportation Research Board, Washington, D.C., January 11-15.
- Florida Department of Transportation, (2004) "Soils and Foundations Handbook," FDOT Homepage, <http://www.dot.state.fl.us/Structures/Manuals/SFH.04-22-2004.pdf>, (Accessed September 2006).
- Geo-Services International Limited, Geo-Services International Limited Homepage, (1999) <http://www.geophysics.co.uk/mets3.html#srp>, (Accessed August 2006).
- Golden Software, Inc., (2003), *Surfer version 8.04 Users Manual and Software for Windows*.
- Hayashi, K. and Takahashi, T. (2001), "High Resolution Seismic Refraction Method Using Surface and Borehole Data for Site Characterization of Rocks," *International Journal of Rock Mechanics and Mining Sciences*, Vol. 38, pp. 807-813.
- Hiltunen, D.R., Hudyma, N., Quigley, T.P., and Samakur, C. (2007), "Ground Proving Three Seismic Refraction Tomography Programs," (Accepted for Publication), *Transportation Research Record: Journal of the Transportation Research Board, Washington, D.C.*
- Hudyma, N., Hiltunen, D.R., and Samakur, C. (2007), "Variability of Karstic Limestone Quantified Through Compressional Wave Velocity Measurements," (Accepted for Publication), *Proceedings of GeoDenver 2007, New Peaks in Geotechnics*, American Society of Civil Engineers, Denver, CO, February 18-21.
- Intelligent Resources Inc., (2006), *Rayfract Version 2.64 Users Manual and Software for Windows*.
- Moser, T. J. (1991), "Shortest Path Calculation of Seismic Rays," *Geophysics*, Vol. 56, No. 1, January, pp. 59-67.
- Optim LLC, (2004), *SeisOpt Pro Version 3.0 Users Manual and Software for Windows*.

- Oyo Corporation, (2001), *SeisImager Users Manual and 2D Refraction Analysis Software for Windows*.
- Pullammanappallil, S. K. and Louie, J. N. (1994), "A Generalized Simulated-Annealing Optimization for Inversion of First-Arrival Times," *Bulletin of the Seismological Society of America*, Vol. 84, No. 5, October, pp. 1397-1409.
- Qin, F., Luo, Y., Olsen, K., Cai, W., and Schuster, G. T. (1992), "Finite-Difference Solution of the Eikonal Equation," *Geophysics*, Vol. 57, pp. 478-487.
- Randazzo, A.F., (1997), "The sedimentary platform of Florida: Mesozoic to Cenozoic", in *The Geology of Florida* (ed. Randazzo, A.F. and Jones, D.S.), University of Florida Press, Gainesville.
- Redpath, B.B. (1973), "Seismic Refraction Exploration for Engineering Site Investigations," *Technical Report TR E-73-4*, U.S. Army Engineer Waterways Experiment Station Explosive Excavation Research Laboratory, Livermore, California, May.
- Schuster, G. T. and Quintus-Bosz, A. (1993), "Wavepath Eikonal Traveltime Inversion: Theory," *Geophysics*, Vol. 58, No. 9, September, pp. 1314-1323.
- Scott, T. M. (2001), "Text to Accompany the Geologic Map of Florida," *Florida Geological Survey Open File Report Number 80*, 28 pp.
- Sheehan, J.R., Doll, W.E., and Mandell, W.A. (2003), "Evaluation of Refraction Tomography Codes for Near-Surface Applications," Submitted for Publication in *Proceedings of 73rd Annual Meeting of Society of Exploration Geophysicists*, Dallas, Texas, October 26-31.
- Sheehan, J., Doll, W., Watson, D.B. and Mandell, W. (2005a), "Application of Seismic Refraction Tomography to Karst Cavities," *U.S. Geological Survey Karst Interest Group Proceedings. Rapid City, South Dakota, September 12-15*, pp. 29-33.
- Sheehan, J.R., Doll, W.E., and Mandell, W.A. (2005b), "An Evaluation of Methods and Available Software for Seismic Refraction Tomography Analysis," *Journal of Environmental and Engineering Geophysics*, Vol. 10, No. 1, March, pp. 21-34.
- Tihansky, A.B. (1999), "Sinkholes, West-Central Florida: A link between surface water and ground water," *U.S. Geological Survey Circular 1182*, pp. 121-140.
- Vidale, J. E. (1988), "Finite Difference Calculation of Travel Times," *Bulletin of the Seismological Society of America*, Vol. 78, pp. 2062-2076.
- Williams, K.E., Nicol, D. and Randazzo, A.F. , (1977), "The Geology of the Western Part of Alachua County, Florida" *Florida Geological Survey Report of Investigations No. 85*.
- Woodward, M.J., (1992), "Wave-equation Tomography," *Society of Exploration Geophysicists, Geophysics*, Vol. 57, No.1, pp. 15-26.

Zhang, J. and Toksoz, M.N., (1998), "Nonlinear Refraction Traveltime Tomography," *Society of Exploration Geophysicists, Geophysics*, Vol. 63, No.5, pp. 1726-1737.

BIOGRAPHICAL SKETCH

Timothy Patrick Quigley was born on June 18, 1980 in East Meadow, NY and remained there until he graduated from East Meadow High School in 1998. He enrolled in college at North Carolina State University in Raleigh, NC, and graduated with a Bachelors of Science in Civil Engineering in May of 2003. After working in the university's Co-Op program for a semester as an undergraduate for a materials testing firm he realized the importance of work experience for a geotechnical engineer. With that he decided that it would be most beneficial to gain a few years of work experience before continuing on with graduate studies.

He moved to Lakeland, FL to work for a geotechnical and materials testing engineering consulting firm for the next two years. He enrolled at the University of Florida in Gainesville, FL in August of 2005 where he worked as a graduate research assistant under Dr. Dennis Hiltunen. He completed his studies in December of 2006, graduating with a Master of Engineering degree and is employed at a geotechnical engineering consulting firm in North Carolina.